UNIVERSITY OF OKLAHOMA

GRADUATE COLLEGE

NEUROIMAGING BIOMARKERS FOR NONINVASIVE BRAIN STIMULATION IN MAL DE DÉBARQUEMENT SYNDROME

A DISSERTATION

SUBMITTED TO THE GRADUATE FACULTY

in partial fulfillment of the requirements for the

Degree of

DOCTOR OF PHILOSOPHY

By

YAFEN CHEN
Norman, Oklahoma
2021

NEUROIMAGING BIOMARKERS FOR NONINVASIVE BRAIN STIMULATION IN MAL DE DÉBARQUEMENT SYNDROME

A DISSERTATION APPROVED FOR THE
STEPHENSON SCHOOL OF BIOMEDICAL ENGINEERING

BY THE COMMITTEE CONSISTING OF

Dr. Han Yuan, Chair

Dr. Christian Lemon

Dr. Yoon-Hee Cha

Dr. Jerzy Bodurka

Dr. Lei Ding

Acknowledgements

I would like to thank my advisor Dr. Han Yuan and the rest of my committee for their comments, feedback, and guidance along my program. Thanks to Dr. Han Yuan and Dr. Yoon-Hee Cha who shared with me their insights and supported me significantly through my work. Thanks to Dr. Jerzy Bodurka, Dr. Christian Lemon and Dr. Lei Ding for all your input in my dissertation work.

My gratitude also goes to my labmates and colleagues, Dr. Guofa Shou, Yuxuan Chen, Fan Zhang, Julia Tang and many others who I have worked with. I enjoyed our friendship, and I am deeply thankful for all your company.

This dissertation is also dedicated to my family members, most importantly, my beloved grandmother. Without you, I would not have started this journey and continued to firmly march on. I also appreciate the company of my little brother Xingtao and little sister Guannan. You always bring the bright side of life to me and energize me even across the Pacific Ocean.

The work in the dissertation was supported by NSF RII Track-2 #1539068, the Institute for Biomedical Engineering Science and Technology at The University of Oklahoma, Laureate Institute for Brain Research, the William K. Warren Foundation, an equipment grant from the MdDS Balance Disorders Foundation, NIH/NIGMS P20 GM121312, and the Springbank Foundation.

Contents

List of Tables

List of Figures

Acronyms

ATP: adenosine triphosphate

AFNI: analysis of functional neuroimages

BOLD: blood-oxygenation-level-dependent

df: degree of freedom

DMN: default mode network

DLPFC: dorsolateral prefrontal cortex

EEG: electroencephalogram

tECS: transcranial electric current stimulation

EPI: echo-planar imaging

EC: entorhinal cortex

FDG-PET: fluorodeoxyglucose positron emission tomography

FDR: false discovery rate

fMRI: functional magnetic resonance imaging

FN: false negative

FOV: field of view

FP: false positive

GLM: general linear model

HRF: hemodynamic response function

IAF: individual alpha frequency

ICA: independent component analysis

ICPC: independent component phase coherence

IPL: inferior parietal lobule

LDA: linear discriminate analyses

LOOCV: leave-one-out cross validation

MT MdDS: motion triggered MdDS

MDD: major depressive disorder

MdDS: Mal de Debarquement Syndrome

MFG: medial frontal gyrus

MNE: minimum norm estimation

MPRAGE: magnetization-prepared rapid gradient-echo

MTs: motor thresholds

MTG: middle temporal gyrus

OCD: obsessive-compulsive disorder

RSFC: resting state functional connectivity

rTMS: repetitive transcranial magnetic stimulation

ROI: region of interest

SPM: Statistical Parametric Mapping

tACS: transcranial alternating current stimulation

TI: inversion time

TN: true negative

TP: true positive

TR/TE: repetition time/echo time

VAS: visual analogue scale

Abstract

This dissertation summarizes my work to identify biomarkers for neuromodulation treatment in Mal de Débarquement Syndrome (MdDS) using resting state EEG and fMRI. Biomarkers that are associated with the symptom changes after stimulations can potentially guide development and selection of effective treatment, therefore expediting the process of patients getting access to beneficial treatment. I have developed a data-driven method to extract and quantify the functional connectivity of resting-state brain networks as biomarkers. Through simultaneously acquired resting-state EEG and fMRI, I have identified response biomarkers at the network level across three different protocols (i.e., 10-Hz/1-Hz repetitive transcranial magnetic stimulation (rTMS), continuous theta burst stimulation (cTBS) and transcranial alternating current stimulation (tACS)). Specifically, my work have revealed that the visual network and the default mode network were clinically relevant to the symptom changes and potentially important indicators for optimizing the stimulation target.

I have also integrated simultaneous EEG and fMRI data to demonstrate the validity of EEG-network-based biomarkers. The EEG-informed fMRI has shown consistent synchronization with EEG networks in response to the repetitive transcranial magnetic stimulation. Furthermore, the entorhinal-cortex-seeded fMRI connectivity revealed that the stimulation-related changes in the left precuneus and cingulate gyrus have normalized the pathological differences in MdDS patients when compared with healthy controls. This part of analysis also has suggested the mechanism of noninvasive brain stimulation via modifying the connectivity patterns in disease-related networks.

Finally, I explored the feasibility of customizing the stimulation parameters in cTBS and tACS based on the imaging biomarkers. Through classifying targets into optimal vs. non-optimal, my analysis revealed that the transient EEG after a single, try-out administration of cTBS stimulation can signify the optimal stimulation targets. Furthermore, the response biomarkers showed distinct patterns that are sensitive to various tACS stimulation parameters, including frequencies and phases. Especially, the tACS based on the prior knowledge of individual alpha frequency is most effective in reducing symptoms, which again emphasized the importance of stimulation paradigm tailored to individuals.

Overall, the findings of my dissertation work have demonstrated the merit of multi-modal neuroimaging in noninvasive brain stimulation, in identifying the response biomarkers and understanding the mechanism of treatment. The integration of neuroimaging with stimulation will be able to optimize the individual treatment effect via personalizing the brain stimulation through a biomarker-based, closed-loop approach.

1. Chapter 1: Introduction

1.1 Neuroimaging

The rise of noninvasive brain imaging opens the door for flexible and tolerable experiment designs in human participants to probe the brain organizations and neuron communication mechanism. It has been used in a variety of investigations to visualize the brain in behavioral tasks and resting states in both healthy and diseased conditions. It has also been combined with external brain modulation tools, such as all types of brain stimulation protocols, to provide insight on how the modulation tool interacts with the brain and therefore unveil the potential applications of neuromodulation tools in brain disorders. The first known electrophysiological recording in humans was pioneered by a German psychiatrist Hans Berger in 1924 (Zeidman et al., 2014). Electroencephalography (EEG) is able to record the electrical activity originated from the brain cortex and propagating to the human scalp (**Fig. 1-1**). Specifically, it is known to record the post-synaptic signals and composed of accumulated electrical activations from populations of neurons (Nunez and Srinivasan, 2006). By the virtue of a near-source, quasi-static electromagnetic field, the EEG measures the electric signals related to populational neuronal activities at a superior spatial resolution of milliseconds. In application, EEG have several clinical indications (Kreuzer, 2017; Macdonell et al., 1988). For example, it is an essential monitor tool for epilepsy as it presents critical information about epileptiform discharge and provides great sensitivity in spotting any sudden changes in the brain. It has also been combined with a vast of biomedical engineering methods to extend its capability in investigating neurological or psychiatric disorders (Billeci et al.,

2013) (Noachtar and Rémi, 2009), such as Autism- Spectrum Disorders, and depression (Whitton et al., 2018).

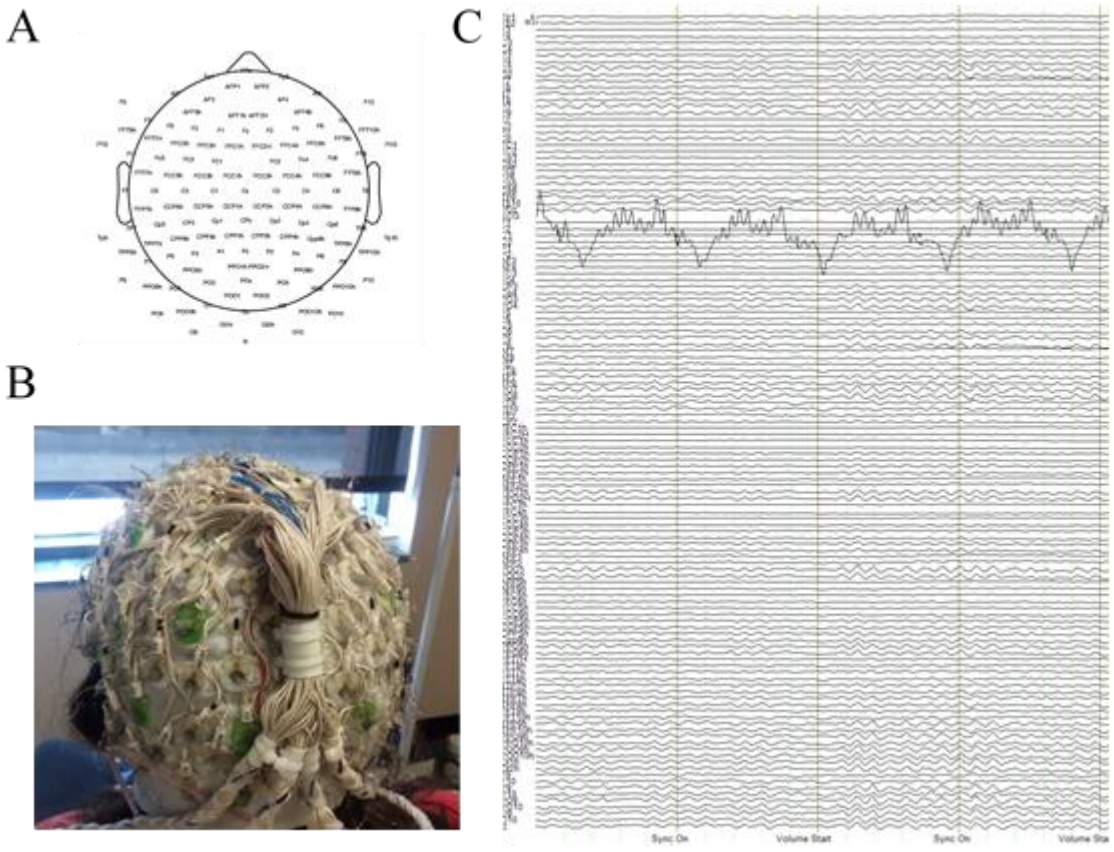

Figure 1-1: Demonstration of high-density EEG montage in (A), EEG cap in (B), EEG waveforms in (C) during recordings.

Functional magnetic resonance imaging (fMRI) is another revolutionary imaging tool, which records the blood-oxygen-level-dependent signals (BOLD) and known for its excellent spatial resolution in measuring the region-confined activities in the brain tissue. The basis of fMRI relies on the neurons' metabolism (Logothetis, 2008). As adenosine triphosphate (ATP) is consumed when neurons generate and propagate signals, supplementing energy for the neurons requires oxygen exchange through blood vessels (Logothetis, 2008). Therefore, an increased level of neuron activations demands large oxygen input and leads to a local increase of deoxygenated hemoglobin [Hb], which

constitutes the primary detection measure of fMRI (Glover, 2011). As Hb is not related to the electrophysiological information transmission directly, fMRI is considered an indirect measure of brain activities. Nevertheless, its emergence quickly dominated the neuroscience community. The investigation into default mode network (Raichle, 2015; Raichle et al., 2001a) using fMRI has shown tremendous value for studying the brain as an organization of wired-up networks between isolated regions in brain disorders. Increasingly, with the growing capability of computer computation and the popularity of the concept of big data, more sophisticated statistical methods have been used to infer the brain fMRI data in a more complex way (Fox and Raichle, 2007; Hutchison et al., 2013; Li et al., 2019).

A critical application of neuroimaging in the brain research field is to develop clinically relevant biomarkers to deepen the understanding of disorder pathology (Greicius, 2008; Zhang and Raichle, 2010), as well as facilitate therapy responses (Brakowski et al., 2017; Horn and Fox, 2020). For example, numerous studies have recognized that many brain disorders are not solely caused by one isolated brain area but instead result from dysfunctional brain networks or dysconnectivity among segregated brain regions (Fox et al., 2012a). These neuroimaging features related to the disorder mechanisms could contribute significantly to the early diagnosis of these disorders. Early diagnosis and intervention make it possible to achieve a better therapeutic effect than after symptoms manifest.

1.2 Noninvasive brain stimulation

Due to the low response rate of pharmacological treatment in many neurological and psychiatric disorders the intrinsic dysfunction of brain network being increasingly

indicated as the potential cause of these diseases by imaging biomarkers, brain stimulation has gained wide attention to act as a tool for manipulating brain synchronization to assist the pharmacological treatment or serve as an alternative (Fox et al., 2012b; Siddiqi et al., 2020). Repetitive transcranial magnetic stimulation (rTMS) is one of the most popular noninvasive brain stimulation techniques and has been approved by the FDA, after many clinical trials and sufficient study of the possible adverse effects for use in depression, obsessive-compulsive disorder (OCD), migraine (Chail et al., 2018). In the typical setting of rTMS, a coil, usually in the shape of a figure eight is energized to generate the magnetic field (Fox et al., 2012a). According to the Maxwell-Faraday equation, the current generated by the magnetic field can penetrate the skull and scalp with effective intensity to depolarize or hyperpolarize the neurons at that site. This depolarization or hyperpolarization of neurons affects the electricity propagation cascade and consequently impacts the wired-up network of the brain that connects local and remote regions. Because of its ability to impact the brain network connectivity in a controlled manner, rTMS is regarded as a useful therapeutic tool. However, the responses to the rTMS in patients are susceptible to individual heterogeneity (Kar, 2019). Therefore, visualizing the underlying brain responses using fMRI and EEG or any other imaging tools may benefit our comprehension of neuromodulation mechanism. The combined investigation of neuroimaging and rTMS is a natural progression as it may tell us what rTMS physically does to the brain. Additionally, by revealing alterations in the brain through imaging after rTMS and corresponding clinical responses, the investigation could also elucidate the mechanism of rTMS in improving or worsening the symptoms as well as the pathological nature of the disease.

Compared with rTMS, transcranial alternating electric stimulation (tECS) requires a cheaper, more portable set up and can directly modulate the brain oscillations through external frequencies; it facilitates probing the causal link between brain oscillations and their cognitive functions (Feurra et al., 2011). tECS is composed of three different current conditions, alternating current (AC), direct current (DC) and random noise (RN) stimulation (Paulus, 2011). Among these, tACS (electrodes illustration in **Fig. 1-2**) is used primarily to entrain the brain in a frequency-specific manner and can be applied as a sinusoidal, rectangular or even more complex waveform. Mostly commonly, tACS is to entrain the brain using the external periodic current wave (Helfrich et al., 2014b). Similar to rTMS, tACS is reported to augment or decrease the brain synchronization to impact the cognitive function if applied with appropriate parameters (Paulus, 2011), and it is a promising tool to benefit any disorders that exhibit brain network dysfunction as the underlying cause. Because of the strong influence of tACS on cortical oscillators, tACS might contribute significantly to the treatment of neurological or psychiatric disorders related to disturbed neural oscillations. Specifically, tACS is shown to modulate the brain in a frequency-specific manner (Feurra et al., 2011) and might perform differently based on the priori brain states (Neuling et al., 2013; Ruhnau et al., 2016).

Figure 1-2: tACS uses bandage to hold sponge electrodes in place and electrodes cables connect to a portable stimulator (out of image).

1.3 Mal de Débarquement Syndrome

Mal de Débarquement Syndrome (MdDS) is a motion perception disorder caused by entrainment to background motion (Cha, 2009; Hain et al., 1999). The symptoms of MdDS are manifested as a bobbing, rocking or swaying perception (Cha, 2009), but other symptoms such as headache, fatigue, visual motion intolerance, and tinnitus suggest that it involves more brain networks than just the vestibular system. This disease has two subtypes, the first is usually triggered by the exposure of prolonged periods of low-frequency, low-amplitude oscillating motion such as sea travel or airborne travel, also termed as motion triggered (MT) MdDS the other subtype is less common, in which symptoms can arise spontaneously or with other triggers (e.g., surgery, childbirth, etc.) (Cha, 2015; Cha, 2009). In this dissertation work, we only looked at MT MdDS, which we will refer to simply as MdDS. Indeed, there are no peripheral vestibular deficits in MdDS (Cha, 2009). Due to the limited literature on MdDS, little is known on its pathophysiology and its subtypes. A PET and fMRI study (Cha et al., 2012) has revealed

the abnormal connectivity and metabolism of MdDS compared with healthy controls. Therefore, neurulation approaches, such as repetitive transcranial magnetic stimulation (rTMS), has been experimentally investigated in the treatment of MdDS (Cha et al., 2016b; Dell'Osso et al., 2009). Prior neuroimaging and noninvasive brain stimulation studies on MdDS have indicated that both long range fronto-parietal connectivity as well as as corticolimbic connectivity with the entorhinal cortext are related to symptom status (Cha et al., 2018; Cha et al., 2012; Chen et al., 2019; Ding et al., 2014; Yuan et al., 2017). The first neuroimaging study on MdDS using fluorodeoxyglucose positron emission tomography (FDG-PET) showed that there is hypermetabolism in the left entorhinal cortex and amygdala along with increased connectivity to posterior parietal and occipital cortex (Cha et al., 2012). Using funcitonal magnetic resonance imaging (fMRI), reduction in resting state functional connectivity measured between the entorhinal cortex and the inferior parietal and precuneus regions corresponding to the default mode network (DMN) has been shown after repetitive transcranial magnetic stimulation (rTMS) of the dorsolateral prefrontal cortex (DLPFC) (Yuan et al., 2017). The resting state network connectivity measured by electroencephalography (EEG) also showed reduction in the medial frontal gyrus (MFG) and inferior pareital lobule (IPL) as part of the default mode network, which also were correlated with the fMRI connectivity changes to the default mode network (Chen et al., 2019). Morever, measurements of independent component phase coherence (ICPC), an EEG marker of synchronicity, have shown reductions in synchrony as a function of symptom status (Cha et al., 2018; Ding et al., 2014).

1.4 Simultaneous EEG and fMRI

fMRI measuring the blood oxygen level-dependent (BOLD) signal reflects human brain activity indirectly (Logothetis et al., 2001). Despite its limited temporal resolution at the level of seconds, fMRI has been proven to be a useful neuroimaging modality in studying brain activation and more recently, brain synchrony between regional areas (Biswal et al., 1995). In contrast to fMRI, EEG measures neuronal currents on a millisecond scale with the ability to detect current sources at the cortical level after addressing the so-called "inverse problem" (Grech et al., 2008). In light of complementary features of EEG and fMRI, researchers have been able to combine those modalities (Mulert et al., 2004; Ritter and Villringer, 2006) and prospectively link the signals characterized by fMRI to phenomena revealed by EEG (Perry and Bentin, 2009; Yuan et al., 2016). This multimodal approach has been suggested to overcome the spatial resolution limitations of EEG and the temporal resolution limitations of fMRI. Furthermore, it has the advantage of translating fMRI-based imaging to EEG-based imaging, which is portable and adaptable to versatile recording environments, such as those done simultaneously with TMS (Ilmoniemi and Kičić, 2009).

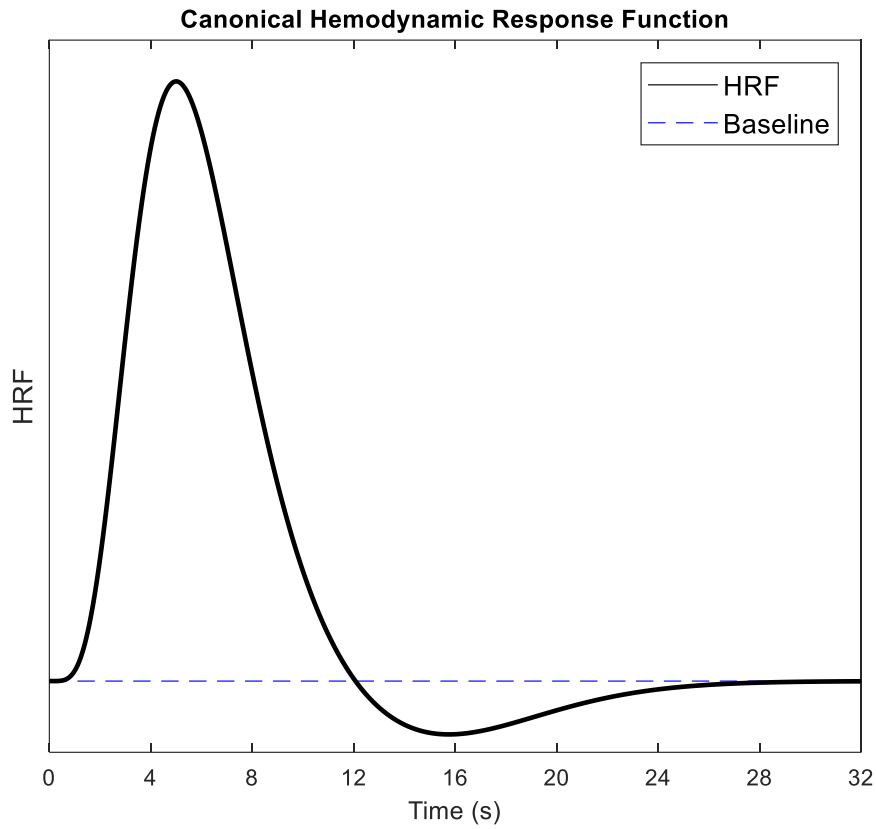

Figure 1-3: Canonical hemodynamic response function waveform used in general fMRI analyses (Penny et al., 2011).

A popular way to associate EEG and fMRI is to compute the EEG- informed fMRI model. In this approach, the high temporal resolution time courses from EEG are input as the regressors and fed into the general linear model (GLM) of fMRI. Computing regressors from EEG concerns the hemodynamic response delay in fMRI and therefore requires the convolution with hemodynamic response function (HRF) to offset the delays between two signals. HRF describes the impulse response function towards external stimulations in fMRI. It was originally defined as boxcar-shape form (Keilholz et al., 2004; Pelled et al., 2007), but later is commonly formulated as a parameterized double-gamma function (Lindquist et al., 2009). The canonical HRF **Fig. 1-3** was a HRF of a double-gamma function, using the implementation of a widely used fMRI analysis

toolbox Statistical Parametric Mapping (SPM) (Penny et al., 2011) and proposed by other scientists (Penny et al., 2011; Yu et al., 2012). In addition to convolution with HRF, the fed in EEG data have been explored in a few other formats, including simple clean EEG, or more recently in literature, clustering derived microstates, ICA derived microstates (Abreu et al., 2018) and microstates of specific frequency (Schwab et al., 2015). This type of analysis utilizes whole brain EEG channels and allows mapping of scalp EEG signals to the fMRI volume structures by correlating their temporal signals. Notably, this type of analysis heavily relies on the choice of HRF and it remains to be seen if there is a more appropriate response function. fMRI can be used to inform EEG as well though less common. This type of analysis mostly focuses on increasing the estimation of source localization and therefore improve the EEG spatial accuracy (Lei et al., 2015).

1.5 Outline of this dissertation

In this dissertation work, I have thoroughly explored neuroimaging biomarkers for rTMS and tACS as intervening protocols in MdDS. In the simultaneous EEG and fMRI data acquired in patients before and after the stimulation treatment, I have found significant imaging biomarkers that shed light on the pathological mechanism of MdDS as well as the treatment mechanism of brain stimulations. I also investigated the possibility of using transient EEG to guide the customized protocol for an individual patient. By combining EEG with fMRI, I for the first time have demonstrated that EEG and fMRI are imaging biomarkers in MdDS, and that EEG serves as the electrophysiological correlate of fMRI.

The primary contribution of my dissertation is to develop the response and predictive biomarkers in EEG and fMRI to assist the decision-making of using

noninvasive brain stimulation in MdDS. The imaging features prevalent in positive responders could guide the future protocol design with the aim of imitating the beneficial brain responses. This part is elaborated in **Chapters 2 and 3**.

The second contribution is to elucidate the mechanism of noninvasive brain stimulation in rectifying the abnormal connectivity in the DMN network. Through the comparison with healthy participants, we can see the therapeutic effect of brain stimulations by normalizing the disease-related connectivity. This part is elaborated in **Chapter 4**.

The final contribution of my dissertation is to demonstrate the feasibility of using closed-loop EEG features to guide noninvasive brain stimulation application. In cTBS and tACS, I have found the stimulation parameters, such as target sites and frequencies, customized to each individual could benefit the patients more. This part is elaborated in **Chapter 5**.

2. Chapter 2: ICA-Based EEG Networks Are Modulated by Noninvasive Brain Stimulation

Three cohorts of MdDS patients have participated in this study. The utilized brain stimulations evolved from traditional 10-Hz/1-Hz rTMS to cTBS and tACS. We moved from the a traditional, FDA-approved protocol of 10-Hz/1-Hz rTMS towards cTBS as the cTBS stimulations can be delivered in a more rapid manner (40 seconds in cTBS vs. 30-minutes in 10-Hz/1-Hz rTMS), and can generate longer stimulation effects (Huang et al., 2005). tACS was used because it was more friendly to be a home-based therapy, while rTMS/cTBS as on-site treatment demands travelling which might aggravate MdDS symptoms. Given our previous investigations in fMRI and PET (Cha et al., 2012; Yuan et al., 2017), our goal was to identify EEG features that could differentiate positive responders from the negative or neutral responders. Across three different treatment protocols, we examined EEG data and identified both response and predictive EEG biomarkers in rTMS and cTBS.

2.1 rTMS protocols

2.1.1 Demographics

The details of the study are published in (Chen et al., 2019). Study procedures were completed according to Declaration of Helsinki guidelines and approved through Western IRB (www.wirb.com). Participants provided written informed consent and were recruited under ClinicalTrials.gov study NCT02470377. This study used rTMS in an off-label manner. Twenty individuals diagnosed with MdDS were included in this study. All participants provided written informed consent. The mean age of the participants was 52.9 ± 12.6 years, ranging from 28 to 76 years. The duration of illness had a mean of 35.2

± 24.2 months, median 30 months, and a range of 8–96 months. All participants were female, which was consistent with the high prevalence of female sex in MdDS (Cha, 2009). Participants were included if they had: 1) persistent oscillating vertigo after disembarking from sea, air and land-based travel that started within two days of disembarkation, 2) symptoms lasting at least 6 months, and 3) were evaluated by an experienced neurologist or otolaryngologist and were found to have no other cause for symptoms. In general, we recruited a medically refractory group that had failed vestibular therapy and at least two medication trials. Individuals were excluded if they: 1) had contraindications to undergoing rTMS or EEG/fMRI, such as medications known to reduce seizure threshold, 2) were pregnant or planned to be in the course of the study, 3) had an unclear trigger for their symptoms, 4) were incapable of completing all study-related testing, or 5) had an unstable medical or psychiatric condition such as a history of bipolar disorder or psychosis.

2.1.2 Concurrent MR-EEG acquisition

EEG were simultaneously recorded with fMRI on day 1 before the treatment and day 5 after treatment as the treatment protocol took 5 days. All EEGs were recorded through a 126-channel cap by using a BrainAmp amplifier (Brain Products GmbH, Munich, Germany). Sintered Ag/AgCl ring electrodes were mounted into the scalp cap according to the standard 10-5 system. Ten kiloohm was the impedance upper limit for all EEG electrodes. In the first 10 participants of the group, EEGs were acquired separately from fMRI at a sampling frequency of 1000Hz while they were seated in a recliner and instructed to keep still with eyes closed during recording, which lasted 5 min (i.e., first group). In the second 10 participants, resting-state EEG was simultaneously

obtained with fMRI at a sampling frequency of 5000Hz for a period of 6min and 10 sec (i.e., second group). The SyncBox device (Brain Products GmbH) was used to synchronize the internal sampling clock of the EEG amplifier with the MRI scanner 10MHz master clock signal.

2.1.3 rTMS sessions

In the first protocol on MdDS patients, both 1Hz inhibitory and 10Hz excitatory stimulation were administered to each participant at about the same time each day over five consecutive days. The Localite TMS Navigator® frameless stereotaxy system was used to determine the center of DLPFC as the location of the anterior portion of the middle frontal gyrus. rTMS was administered with the Magventure MagPro X100 stimulator with a cooled figure-of-eight coil (**Fig. 2-1**) in biphasic mode with the handle back at a 45° angle relative to the midsagittal plane. The motor thresholds (MTs) for each motor hand cortex were determined each day for each participant. The hand knob landmark (Yousry et al., 1997) was identified by the neuronavigation system and MTs were confirmed by evoking 50 uV motor potential responses from the contralateral abductor pollicis brevis muscle. rTMS sessions were composed of 1 Hz stimulation over right DLPFC at 110% of right MT for 1200 pulses (20 mins) and followed by 10Hz stimulation over left DLPFC at 110% of left MT for 2000 pulses (25 mins). The 10 Hz protocol was administered as 26 seconds rest following trains of 40 pulses over 4 seconds.

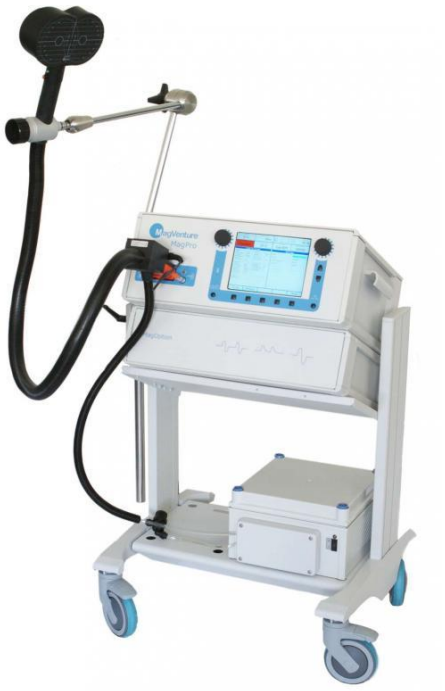

Figure 2-1: rTMS device from MagVenture, with a stand to hold the stimulator and a coil to deliver the stimulation (picture copyright by https://www.magventure.com/us).

2.1.4 Visual analogue scale (VAS)

A visual analogue scale (VAS) of 0-100 was employed to evaluate the participants' symptoms in which 0 indicated a symptom-free state while 100 represented dizziness so severe that standing was not possible. The VAS reporting for each participant was done before and after the five rTMS sessions. The differences between VAS scores before and after rTMS were calculated and participants were categorized as follows: those whose score increased by 10 points or more were considered to be negative responders; those whose scores decreased by 10 or more were considered to be positive responders; and those whose scores changed between -10 and 10 were considered to be neutral responders.

2.1.5 EEG analysis

The pipeline of EEG analysis is shown in **Fig. 2-2**. Data were removed of various environmental and physiological artifacts, including the MR gradient artifacts (in BrainVision Analyzer 2.1), the cardioballistic artifacts (in BrainVision Analyzer 2.1), the muscle and ocular movement related artifact (using ICA in MATLAB 2016a). Bad channels with excessive artifacts were discarded via visual check (less than 1% on all data) and the removed channel would be interpolated by averaging its nearby four channels. Filtering of high pass at 0.5 Hz, low pass at 70 Hz and notch between 59-61Hz was applied. EEG raw data were down-sampled to the microstate to retain the EEG data at a higher signal-to-noise ratio (Lehmann et al., 1987; Yuan et al., 2016). Boundary element models for all participants were built based on individual structural MRI data in FreeSurfer (https://surfer.nmr.mgh.harvard.edu/). Individual digitization files of genuine electrode location were co-registered to the model scalp (two of all datasets used the standard digitization file due to the bad quality of the original files). Physiological source imaging was used to back project the EEG measurement on the scalp to the cortex for each individual by a minimum norm method (Dale and Sereno, 1993b; Hämäläinen and Ilmoniemi, 1994) (see the following section for more details on source analysis). The spatial distributions of sources estimation of the 20 participants were then aligned to a standard head cortex for further analysis in MATLAB 2016a. Absolute value of source data were temporally concatenated across participants and went through temporal independent component analysis (ICA) using the infomax ICA algorithm implemented in the EEGLAB toolbox (http:// sccn.ucsd.edu/eeglab). A total of 30 ICs was calculated. The number of IC was chosen based on our previous investigation which yielded a

reasonable cross-modal consistency between EEG and fMRI networks (Yuan et al., 2016). The EEG networks were compared with template fMRI networks derived from a large cohort of healthy individuals by Yeo et al. (Yeo et al., 2011) (i.e. the "Yeo 7 network" parcellation). Spatial correlation coefficients with Yeo template networks were calculated and the IC with the highest spatial correlation was chosen as the match for a network. Six EEG networks were identified, including the default mode network, the visual network, the frontoparietal network, the sensorimotor network, the limbic network, and the dorsal attention network.

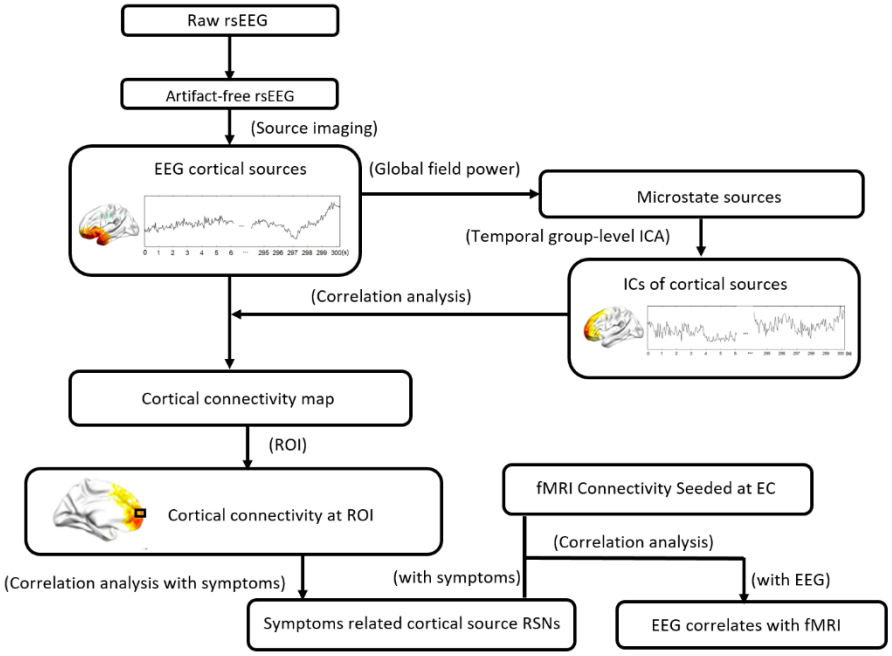

Figure 2-2: After preprocessing, resting state EEG (rsEEG) data were projected onto cortical surfaces through source imaging. Microstates on source signals were extracted, concatenated and subject to group-level independent component analysis (ICA) performed. Cortical connectivity was calculated as the correlation between time courses of cortical sources and independent components (ICs). Connectivity values were extracted from regions of interest (ROI) and compared between pre-TMS and post-TMS sessions with regard to symptom changes. EEG-based networks were also compared with the fMRI connectivity seeded at the entorhinal cortex (EC) (Chen et al., 2019).

The EEG connectivity map of each IC was then calculated as the Pearson correlation between the time course of each temporal IC and the time courses of source dipoles on the cortical surface area for each subject. For statistical analyses, Pearson correlation coefficients on each map were converted to z scores by Fisher's z transform. Pre- and post-TMS EEG connectivity maps were computed separately. The pre-TMS connectivity map is also referred to as the "baseline" connectivity map. "Post-minus-pre-connectivity" maps represent the connectivity changes after rTMS, which was calculated by subtracting the pre-TMS map from the post-TMS map for individuals.

The modulation on EEG networks was further examined with regard to symptom changes. We first defined regions of interests (ROI) based on the pre-TMS maps. Cortical surface area within a radius of 6 mm centered at the maximum of the IC map was drawn as an ROI (Sridharan et al., 2008). The ROIs' center coordinates are listed in **Table 1**. Connectivity values, i.e., z scores, within an ROI were extracted and averaged for each ROI. We then tested the relationship between EEG connectivity changes and symptom changes characterized by the VAS measurement. For example, a positive correlation coefficient signified a decrease in EEG connectivity related to a decrease of VAS scores. Similarly, if the connectivity increased when VAS scores increased, this would also be represented by a positive correlation coefficient. If connectivity increased while VAS decreased, or vice versa, the correlation coefficient would be negative. The method of controlling the False Discovery Rate (FDR) by (Benjamini and Yekutieli, 2001) was employed for addressing the multiple comparison problem. The symbol q denotes the corrected p value. Furthermore, to test whether the difference in connectivity was significant within each responder group, we performed a paired, two-tailed t-tests on the

post-TMS and pre-TMS z-scores and the two-sample t-tests were employed for comparing connectivity of different groups.

2.1.6 Electrophysiological source imaging

For EEG source analyses, we used individual physical forward models linking the source dipoles to scalp EEG measurements. The forward model was constructed as a 3-layer boundary element model composed of scalp, skull and brain based on triangular elements. Each layer was given its own conductivity value (Zhang et al., 2006). Structural MRIs were implemented and employed to generate the geometric models individually. Briefly, the forward model can be expressed in a linear equation as follows:

$$\mathbf{\Phi} = \mathbf{A} * \mathbf{S} + \mathbf{N} \qquad \mathbf{1}$$

where Φ is a matrix of the measured EEG, S is the unknown matrix of amplitudes of the source dipoles over time, and A is the gain matrix. N is a vector specifying the noise at each electrode.

There are a variety of linear inverse operators of the forward model. We used the minimum norm estimation (MNE) method (Dale and Sereno, 1993b; Hämäläinen and Ilmoniemi, 1994). The linear inverse operator for this method is expressed by:

$$\boldsymbol{W = RA^T(ARA^T + C)^{-1}} \qquad \mathbf{2}$$

where C and R are covariance matrices of the noise and sources, respectively. Taken together, the minimum norm estimate of S, i.e. S' is computed as:

$$\mathbf{S'} = \mathbf{W} * \mathbf{\Phi} \qquad \mathbf{3}$$

2.1.7 Results

All 20 participants finished the rTMS protocol and imaging sessions. The symptom score changes from Day 1 to Day 5 were evenly spread across the 20 participants. Six out of the 20 participants reported decreased symptoms after the

treatment (VAS changes: -32.50 ± 17.56, "positive responders"), six of the participants felt slightly worse (VAS changes: +11.67 ± 3.73, "negative responders"), and the remaining eight participants reported unchanged symptoms (VAS changes: -1.38 ± 2.39 of VAS, "neutral responders"). For each cohort (1st and 2nd), the distribution of responses was identical: 30% positive, 30% negative and 40% neutral.

Table 2-1: Regions of Interest in EEG networks matched to templates RSNs (Chen et al., 2019).

Identified Network	Region of Interest	MNI Coordinates (mm)		
		X	Y	Z
Default Mode	lMFG	-20.26	57.80	1.819
Visual	rFG	28.42	-92.86	-12.55
Frontoparietal	rMFG	37.93	42.16	22.27
Motor	lPG	-57.80	-16.15	34.33
Limbic	rMTG	47.94	3.968	-33.87
Dorsal Attention	lP	-8.610	-72.18	49.07

lFG: left Fusiform Gyrus, rPG: right Precentral Gyrus, lP: left Precuneus, rMFG: right Middle Frontal Gyrus, lMFG: left Medial Frontal Gyrus, rMTG: right Middle Temporal Gyrus.

Since our previous PET and fMRI studies have indicated an important role of DMN in differentiating individuals with MdDS from the healthy controls as well as being related to the symptom changes (Yuan et al., 2017), we first focused our investigation on the DMN. From EEG source data, one network was identified as the match to the DMN of Yeo template (**Fig. 2-3A**). Connectivity values within ROIs from the DMN were extracted from all individual pre- and post- rTMS images. Results revealed a significant correlation coefficient ($r = 0.54$, $q < 0.05$, **Fig. 2-3C**), between the difference in

connectivity values and the changes in symptoms after rTMS. Specifically, a positive correlation indicated that greater symptom reduction was associated with a stronger decrease in connectivity within the DMN. The connectivity within the DMN in the positive subgroup was effectively reduced after TMS (paired *t* test, t(5) = -2.54, p = 0.05, **Fig**. **2-3D**). In comparison with the negative subgroup, the reduction of connectivity in the positive responders was significantly lower (unpaired *t* test, t(10) = -2.80, p = 0.02, **Fig**. **2-3D**).

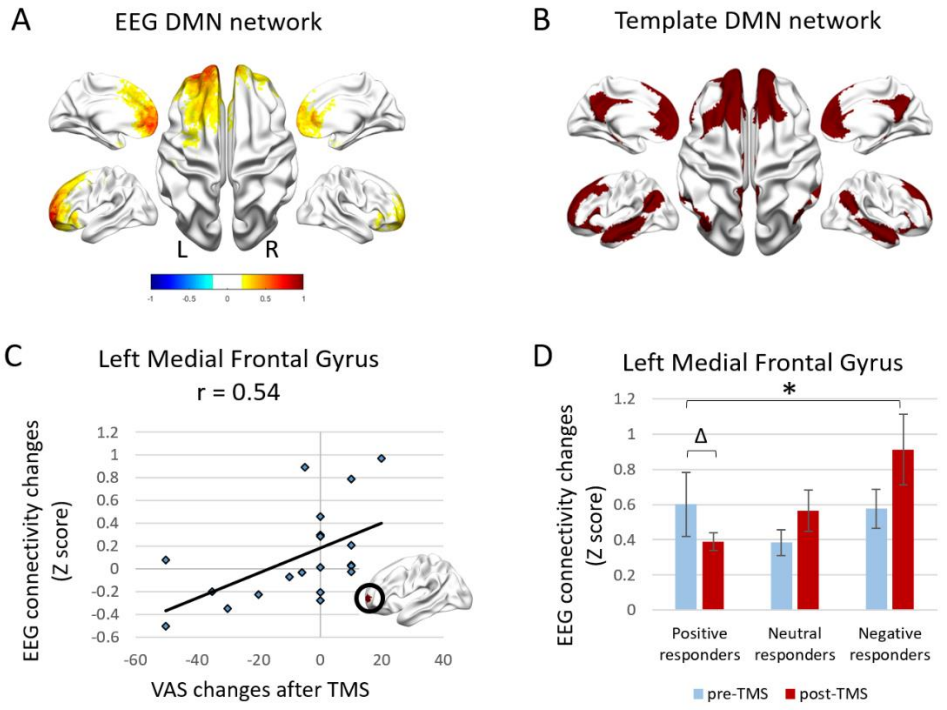

Figure 2-3: Connectivity changes before and after rTMS in the Default Mode Network correlate with symptom changes. The default mode network was identified in EEG (A), which matched the fMRI template (B) by Yeo et al. (2011). The connectivity changes extracted from the ROI in the left medial frontal gyrus were positively correlated with symptom changes shown in (C) ($q < 0.05$). Pre- and post-TMS values are shown in (D) for the subgroups of positive, neutral and negative responders, separately. * indicates significant between-group comparisons (positive responders vs. negative responders, unpaired t test: t(10) = -2.80, p = 0.02). Δ indicates significant within-group comparison (paired t test, t(5) = -2.54, p = 0.05) (Chen et al., 2019).

We then extended our analysis to all the EEG networks identified in our procedure. A total of six networks matched the Yeo template networks (Yeo et al., 2011), i.e. the visual, motor, dorsal attention, limbic, frontoparietal, and default mode networks, with spatial correlations ranging from 0.21 to 0.45 (with mean ± std = 0.32 ± 0.091). **Table 2-1** lists coordinates of the center of ROIs in all identified networks. Among the five EEG networks beside DMN, correlation analyses between ROI connectivity changes and VAS changes drew our attention to the visual network (**Fig. 2-4A**) and the limbic network (**Fig. 2-5A**). Similar to the DMN, modulations seen in the visual network across individuals were positively correlated with symptom changes (**Fig. 2-4C**, r = 0.52, $q<0.05$). However, a reversed correlation was identified in the ROI of the limbic network, i.e., the right middle temporal gyrus, in which a greater reduction of symptoms was associated with an increase in connectivity (**Fig. 2-5C**, r = -0.61, $q<0.05$). In the sub-group of positive responders, the increase in EEG connectivity only approached significance ($t(5) = 2.45$, $p = 0.06$, **Fig. 2-5D**), yet appeared to be higher than the changes in negative responders ($t(10) = 2.49$, $p = 0.03$, **Fig. 2-5D**).

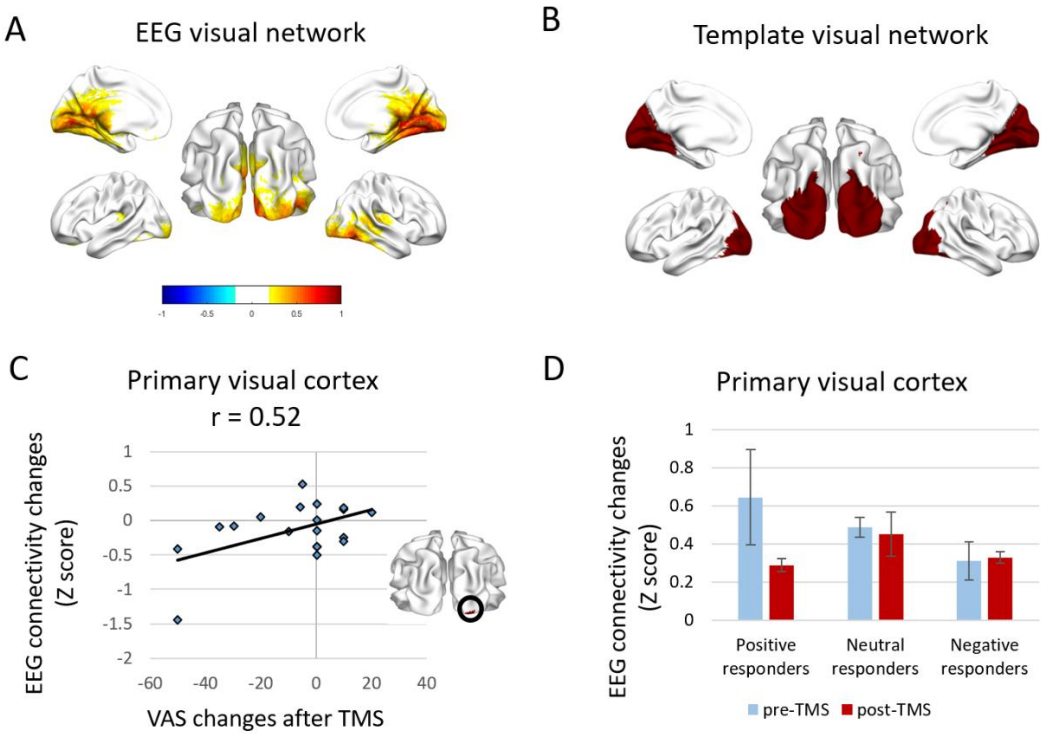

Figure 2-4: Connectivity changes before and after rTMS in the visual network are correlated with symptom changes. A visual network was identified in EEG (A), which matched the fMRI template (B) by Yeo et al. (2011). The connectivity changes extracted from the ROI in the primary visual cortex were positively correlated with symptom changes as shown in (C) ($q < 0.05$). Pre- and post-TMS values are shown in (D) for the subgroups of positive, neutral and negative responders, separately. Δ indicates areas of difference of between post- and pre-TMS connectivity values that approached significance. None of the between-group or within group comparison was significant (Chen et al., 2019).

Finally, we investigated whether the baseline EEG connectivity of several networks is predictive of the symptom changes after rTMS. First, the primary visual network was found to have a predictive effect ($r = -0.53$, $q<0.05$, **Fig. 2-6**), indicating high baseline connectivity predicts better treatment response. In the prediction analysis, we also extended our examination to include other EEG networks than the six template matches. The baseline connectivity of the ROIs for the DMN and the limbic network are shown in **Fig. 2-7 and 2-8**; the data did not reach significance. Nonetheless, in the left medial frontal gyrus, the majority of the participants' baseline connectivity followed a

similar descending trend (i.e., higher baseline connectivity associated with greater symptom reduction, r = -0.25).

2.1.8 Discussion

This study investigated the modulation effects of rTMS on brain networks using multimodal neuroimaging data, i.e., EEG and fMRI. In a group of MdDS participants, we were able to identify resting state networks based on EEG data that were matched to six fMRI template networks. The connectivity changes of the EEG networks were positively correlated with symptom change in the left medial frontal gyrus and in the primary visual cortex. In addition, such changes obtained by EEG were also correlated to fMRI-measured connectivity changes involving deeper subcortical structures, particularly in a network that includes the entorhinal cortex, the precuneus and right inferior parietal lobule, all of which are nodes of the default mode network. Furthermore, baseline EEG connectivity values in primary visual cortex and right inferior parietal lobule were found to predict symptom changes induced by rTMS, with particularly high baseline connectivity predictive of reduction of symptoms.

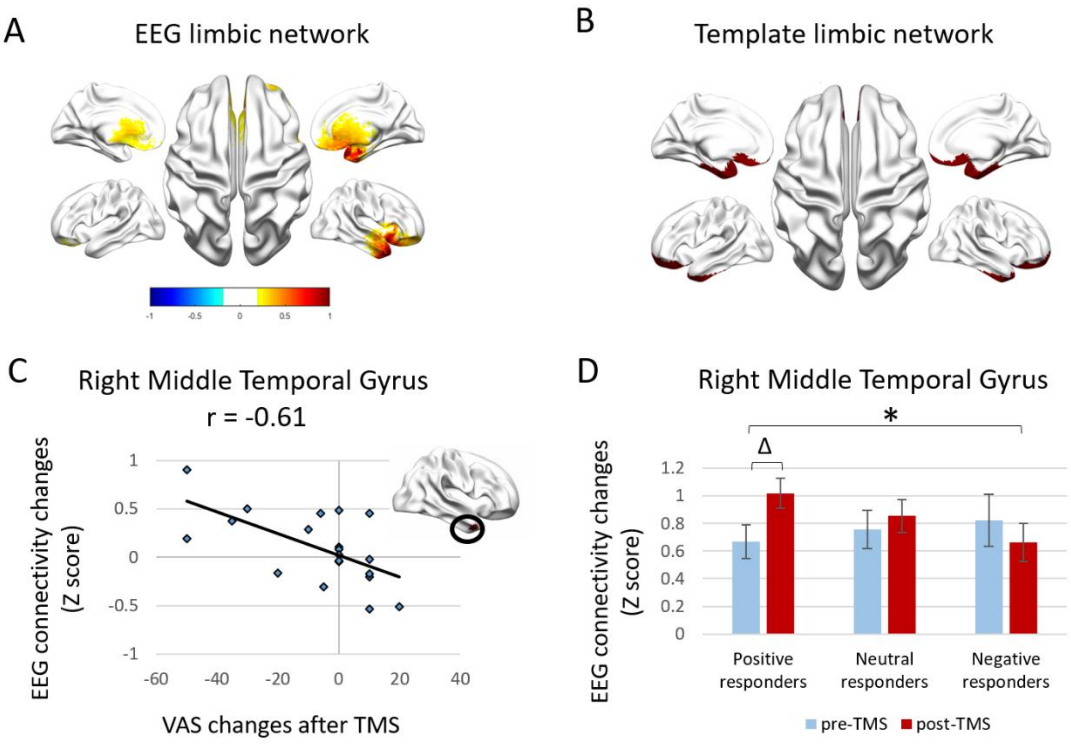

Figure 2-5: Connectivity changes before and after rTMS in the limbic network are correlated with symptom changes. A limbic network was identified in EEG (A), which matched the fMRI template (B) by Yeo et al. (2011). The connectivity changes extracted from the ROI in the middle temporal gyrus were positively correlated with symptom changes as shown in (C) ($q < 0.05$). Pre- and post-TMS values are shown in (D) for the subgroups of positive, neutral, and negative responders, separately. * indicates significant between-group comparisons (positive responders vs. negative responders, unpaired t test: $t(10) = 2.49$, $p = 0.03$). Δ indicates within-group comparisons that approached significance (paired t test, $t(5) = 2.45$, $p = 0.06$) (Chen et al., 2019).

The rTMS protocol employed in the current study targeted both left DLPFC and right DLPFC since our pilot studies of these two targets had previously demonstrated efficacy in relieving symptoms in some individuals with MdDS (Cha et al., 2013; Cha et al., 2016b). Network analysis of EEG data revealed a positive correlation between modulation in connectivity and changes in symptoms. Particularly, in the sub-group of positive responders to rTMS, reduction of symptoms was associated with a reduction of connectivity values. In the visual cortex, functional connectivity decreased after rTMS

on average and consistently in each positive responder. Notably, the visual cortex has been reported to possess higher connectivity with the entorhinal cortex in MdDS in a PET/fMRI study (Cha et al., 2012). This suggests that one of the therapeutic mechanisms of rTMS in MdDS is to normalize hyper connectivity in visual networks. In a prior investigation (Cha et al., 2018; Ding et al., 2014) a decrease of EEG connectivity was represented by a decrease in post-TMS neural synchrony of the posterior parietal and occipital areas. This decrease in synchrony was associated with an improvement in symptoms of MdDS, which are consistent with our findings in the visual cortex.

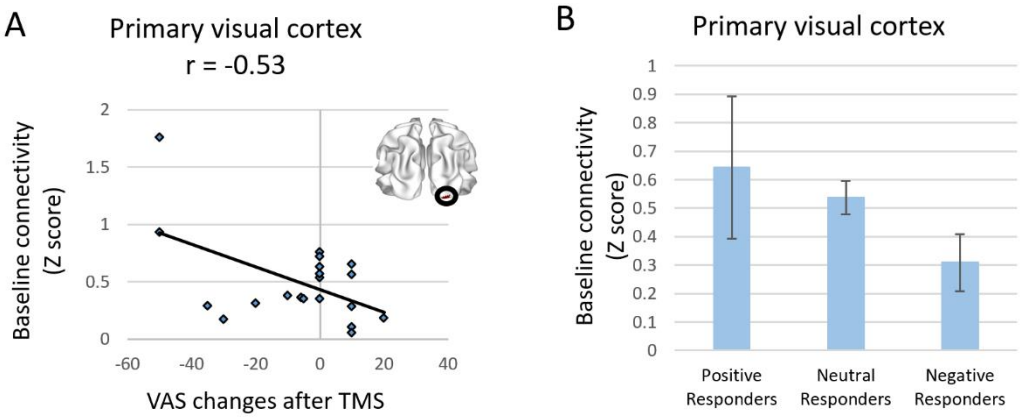

Figure 2-6: Baseline connectivity in EEG visual network is related to symptom improvement. Pre-TMS connectivity extracted from the ROI in the primary visual cortex is correlated with symptom changes, as shown in (A). The average connectivity values in the subgroups of the positive, neutral, and negative responders are shown in (B). None of the between-group or within group comparisons were significant (Chen et al., 2019).

Other studies have investigated rTMS effects on brain networks such as in major depressive disorder (MDD). (DeGiorgio et al., 2014) used 10-Hz rTMS targeting the left DLPFC in depression patients and imaged them before and after stimulation. They found that connectivity in the DMN was reduced significantly towards the lower connectivity level of healthy controls in treatment responders. Patients' symptom reduction was

observed to be related to decreased connectivity within the DMN in a study by (Philip et al., 2018) in which 5-Hz TMS was given to the participants. Those results suggest that one mechanistic role of rTMS in decreasing depressive symptoms is via the normalization of the hyper connectivity in DMN. Considering that the left medial frontal gyrus is a key node within the DMN (Yeo et al., 2011), our observation of the positive correlation between in DMN desynchronization and symptom improvement in MdDS emphasizes the important role of DMN in treating disorders characterized by abnormal function. In MdDS, desynchronization of visual cortex connectivity is also related to symptom improvement after rTMS implicating some disorder specific effects that layer upon perhaps more general signatures of maladaptive brain states.

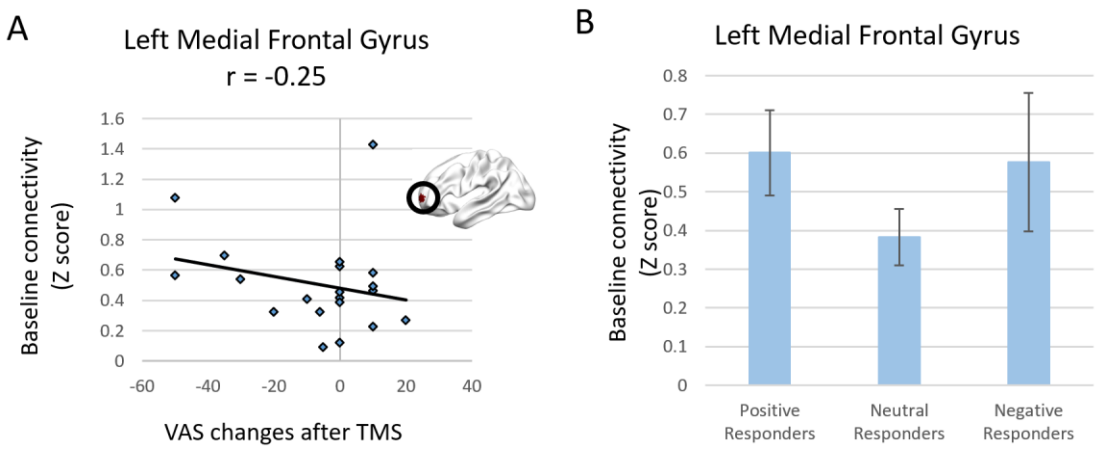

Figure 2-7: Baseline connectivity in EEG default mode network. Pre-TMS connectivity extracted from the ROI in the left medial frontal gyrus did not reach a significant correlation with symptom changes ($p > 0.05$) (Chen et al., 2019).

Furthermore, our baseline analysis showed that, on average, positive responders had higher pre-TMS connectivity over visual cortex as shown in **Fig. 2-6**. The connectivity between entorhinal cortex and motion processing areas such as the temporal and posterior occipital areas was found to be higher than in healthy controls (Cha et al., 2012). Those with higher baseline connectivity in visual areas may have had more room

to change than those with lower connectivity. In a parallel fMRI study, Yuan et al. (Yuan et al., 2017) also reported that higher fMRI baseline connectivity between the rTMS targets (DLPFC) and entorhinal cortex (also a part of DMN) correlated with better treatment response. Higher RSFC was found to be critical in predicting positive treatment effects in other studies employing rTMS. In a study utilizing rTMS at DLPFC to treat patients with major depression, (DeGiorgio et al., 2014) identified higher baseline RSFC in the positive response group compared to the poor response group. As a follow-up study, Avissar et al. (Avissar et al., 2017) reported that rTMS response could be predicted by higher RSFC in DLPFC-to-striatum in a larger subject study. Baeken et al., (Baeken et al., 2017) investigated theta burst stimulation effects on MDD subjects comparing their baseline connectivity with healthy controls, and found that baseline RSFC between subgenual anterior cingulate and medial orbitofrontal cortex could distinguish responders from non-responders. Together, these findings support the prospect that measurements of RSFC before treatment could potentially be used to predict treatment responses in MdDS, MDD, and other disorders. The current study shows that EEG can serve as a complementary modality in predicting treatment responses.

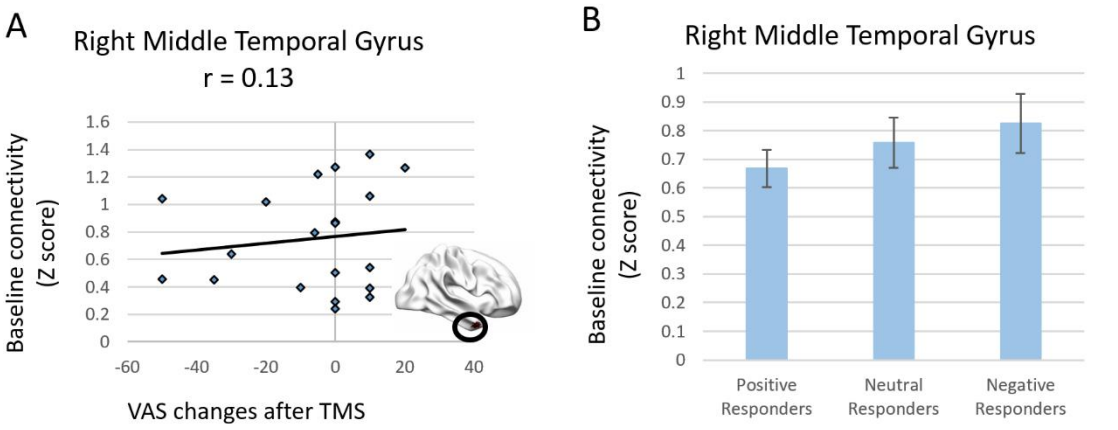

Figure 2-8: Baseline connectivity in EEG limbic network. Pre-TMS connectivity extracted from the ROI in the right middle temporal gyrus did not reach significant correlation with symptom changes ($p > 0.05$) (Chen et al., 2019).

2.2 cTBS protocol

The details of the study are described in the article (Chen et al., Under Review). In the rTMS protocol, we targeted bilateral DLPFC with 1Hz right-sided and 10Hz left-sided stimulation and about 30% of participants improved within the 5-day course of the repetitive stimulations. A critical challenge was to design a more effective protocol that can achieve higher response rate and greater symptom improvement. The DLPFC protocol motivated our current study to consider a more intensive form of stimuli, i.e. continuous theta burst stimulation (cTBS) in which trains of gamma frequency stimulation (50 Hz) are given at theta frequency (5 Hz) intervals (Cha et al., 2019). This form of stimulation more closely models the theta-gamma coupling of cortico-cortico communication. The more rapid stimulation parameters and generally longer stimulation effects compared to standard pulsed stimulation have led to increasing numbers of therapeutic trials of theta burst stimulation for various clinical conditions (Di Lorenzo et al., 2020; Li et al., 2018; Schwippel et al., 2019; Zhao et al., 2020). Notably, cTBS has been deemed as a non-inferior protocol to 10Hz stimulation over DLPFC for depression (Dhami et al., 2019). In our latest study of MdDS (Cha et al., 2019), the cTBS protocol led to doubling of the response rate compared to the DLPFC protocol allowing a broader distribution of positive clinical effects on which to draw correlations to symptom improvement. On a similar base of 24 starting participants, 16 individuals, as opposed to 7 individuals, reported at least a 10-point reduction in symptom severity of oscillating vertigo on a visual analogue scale of 0-100. A key remaining question in the cTBS study is whether any changes in neural circuits were related to the symptom changes in MdDS

patients after completion of the stimulation. Such knowledge of biomarkers is critical for establishing the neuromodulation mechanism of cTBS and for further individualized tailoring of the protocol.

2.2.1 Demographics

The study was performed at the Laureate Institute for Brian Research in Tulsa, OK. Study procedures were implemented in accordance to Declaration of Helsinki guidelines and approved through Western IRB (www.wirb.com). Participants gave written informed consent and were recruited under ClinicalTrials.gov study NCT02470377. Twenty-four individuals diagnosed with MdDS were recruited in this study, while one did not complete the data recording. The mean age at the time of the study was 51.46 ± 11.75 years, median of 53.5 years, and a range of 30 – 70 years. The duration of illness had a mean of 25.29 ±20.92 months, median 17 months, and a range of 7 – 104 months. The inclusion and exclusion criteria were the same as in **Chapter 2.1.1**.

2.2.2 Concurrent MR-EEG acquisition

EEG was collected following the same procedures as in DLPFC protocol. Before and after cTBS protocol, MR-EEG were recorded through a 126-channel cap using BrainAmp MR Plus amplifiers (Brain Products GmbH, Munich, Germany) with sintered Ag/AgCl ring electrodes following the standard 10-5 system. Ten KΩ was the impedance upper limit for all EEG electrodes. Sampling rate was 5000 Hz. Participants lied down in the MRI machine and were instructed to keep still with eyes closed during the 6-min resting state recording. The SyncBox device (Brain Products GmbH) was used to

synchronize the internal sampling clock of the EEG amplifier with the MRI scanner 10 MHz master clock signal.

2.2.3 cTBS sessions

In this protocol of continuous theta burst stimulation (cTBS), the stimulation frequency elevated to 50 Hz and delivered as a triplet burst repeated at 5 Hz (Huang et al., 2005) which gave a total 600 pulses in about 40 seconds. cTBS was administered using the same device as rTMS. cTBS sites were composed of posterior regions and randomized across patients among occipital cortex (45%), cerebellar vermis (42%), lateral cerebellar hemisphere (40%). Individual MRI data were acquired for use in neuronavigation during the delivery of pulses to identify each target. The targeting sites were designed so to take into account the stimulation target as a critical factor for beneficial outcomes. The stimulation intensity was given to patients at a low level initially and increased to the maximum of tolerated level after they habituated.

2.2.4 MR-EEG analysis

Simultaneous MR-EEG data at resting state were acquired before and after stimulation (day 1 and day 5, respectively). The MR-EEG data were cleaned of various environmental and physiological artifacts, including the MR gradient, cardioballistic, muscle, and ocular movement related artifacts. Specifically, the gradient artifact and cardioballistic artifacts were removed in Brain Vision Analyzer 2.1 based on average artifact subtraction (Allen et al., 2000). Additionally, artifact residuals were removed through independent component analysis (ICA) in MATLAB 2017b. Bad channels with excessive artifacts were discarded via visual check and replaced by an average of its nearby four channels. The percentage of bad epochs ranged from 0 - 5% and was not

significantly different between pre and post cTBS sessions (paired t-test, $p > 0.1$). High-pass filtering at 0.5 Hz, low-pass filtering at 70 Hz and notch filtering between 59-61Hz were applied. All channels were re-referenced to the common average.

For EEG source reconstruction, individual MRI data were utilized to project scalp EEG measurements to cortical sources. Boundary element models for all participants were built based on individual structural MRI data segmented by FreeSurfer (https://surfer.nmr.mgh.harvard.edu/). The head model was constructed as a 3-layer boundary element model: scalp, skull, and brain based on triangular elements. Each layer was given its own conductivity value (Zhang et al., 2006). Individual digitization files of genuine electrode location were co-registered to the scalp model. EEG source imaging was used to calculate the current dipoles on the cortex for each individual by a minimum norm method (Dale and Sereno, 1993a; Hämäläinen and Ilmoniemi, 1994).

To perform the group level analysis, individual head models were registered to the standard FreeSurfer "fsaverage" subject (Fischl et al., 1999). Continuous source data were down-sampled to the microstate to retain data at a higher signal-to-noise ratio (Lehmann et al., 1987; Yuan et al., 2016). Absolute values of source data were then temporally concatenated across patients and a temporal ICA, i.e. the infomax ICA algorithm implemented in the EEGLAB toolbox (http:// sccn.ucsd.edu/eeglab), was performed to reconstruct the EEG networks at the group level (Chen et al., 2019; Yuan et al., 2016). Because the patients in the current study turned out to be predominantly responders, we derived the projecting matrix based on responders only but applied the reconstruction of network connectivity to all patients. As comparison, we also ran the ICA analysis on all patients. A total of 25 ICs was calculated. The number of IC was

chosen based on our prior investigations, which yielded cross-modal consistency between EEG and fMRI networks (Yuan et al., 2016).

Individuals' cortical connectivity of the EEG network was then calculated based on the group-level ICA analysis. In particular, the projecting matrix was applied to individual patients' continuous source matrices to calculate the time series of the EEG networks. Then, in every patient, Pearson correlation coefficient between the time course of each network and the time course of each source dipole on the cortical surface was calculated, resulting in a map of correlation coefficients as the EEG connectivity map. Pre- and post-cTBS EEG connectivity maps were computed separately from data on day 1 and day 5 respectively. The pre-cTBS connectivity map is also referred to as the "baseline" connectivity map. "Post-minus-pre-connectivity" maps represent the connectivity changes after cTBS, which were calculated by subtracting the pre-cTBS map from the post-cTBS map for each participant.

In the current study, the visual network and the default mode network were primarily examined, as informed by our prior investigations of repetitive TMS at the DLPFC sites (Chen et al., 2019). To identify the visual network, spatial correlation coefficients between the Yeo template of the visual network (Yeo et al., 2011) and all EEG network maps was calculated and the one with the highest spatial correlation was chosen as the EEG visual network. Similarly, a match for the Yeo template of default mode network was identified and termed as the EEG DMN. The significance of spatial matching was assessed by a bootstrap approach based on the null distribution of spatial correlation values established in (Yuan et al., 2016). In addition, we also searched all other EEG networks for any symptom-related changes. Two additional EEG networks

that present singular nodes of the default mode network, i.e. the left and right inferior parietal lobules (IPL), were manually selected as sub-networks of DMN.

2.2.5 Results

A total of 24 patients were recruited to participate in the cTBS study and 23 patients have completed the data recording protocol. 16 out of the 23 participants were responders because they showed improved symptoms of more than 10 points (VAS changes: average -37.70 ± 16.30 points, range -88 to -15) and the other 7 were non-responders (VAS changes: average 0.71± 7.12 points, range -8 to 15), as shown in **Fig. 2-9**. Compared with our previous study of rTMS at the DLPFC site (Chen et al., 2019), more patients in the current protocol were responders (i.e. 69.6%) and the improvement was overall greater in responders (compared to VAS reduction of -32.50 ± 17.56 in DLPFC protocol). The regions of interest in identified networks are listed in **Table 2-2.**

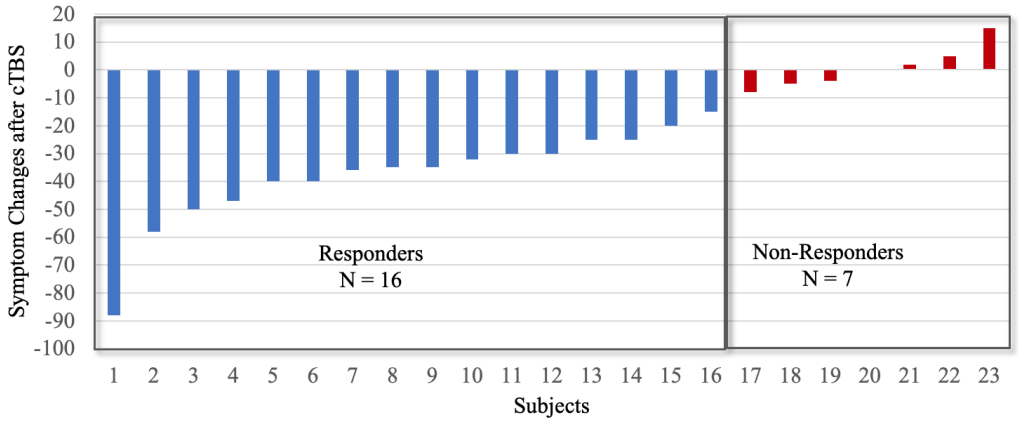

Figure 2-9: Clinical responses. The VAS changes of 16 responders are in blue and 7 non-responders in red (Chen et al., Under Review).

Since our prior work have shown that rTMS modulation on EEG visual network and DMN were associated with symptom changes (Chen et al., 2019; Yuan et al., 2017), our current investigation focused on the visual network and DMN. Through a group-level network analysis and a template matching approach, EEG visual network on the posterior

brain regions was identified (**Fig**. **2-10A**) with a spatial correlation of 0.61 with Yeo template of visual network ($p < 0.01$) (Yeo et al., 2011). Meanwhile, EEG DMN that was primarily composed of the medial frontal gyrus and medial prefrontal cortex was identified (**Fig**. **2-11A**) with a spatial correlation of 0.31 with Yeo template of DMN ($p < 0.05$). Furthermore, two EEG networks were manually selected, such that they respectively constitute the left and right inferior parietal lobules as two key regions of DMN (shown in **Fig. 2-12A and 2-13A**), even though they were not identified as a significant spatial match with the Yeo template. Table 1 lists coordinates of the center of ROIs in these four selected networks.

Then we assessed whether the modulatory effect to these EEG networks were associated with individuals' symptom responses on day 5. Considering that this cohort of patients are primarily positive responders, we first tested the normality of VAS and EEG connectivity changes by using a Kolmogorov–Smirnov test, which indicated that the tested values were from a normal distribution. A positive correlation was consistently identified between the VAS changes and EEG connectivity changes in the visual network (**Fig. 2-10C**: $r = 0.43$, $p = 0.04$) as well as the left and right IPL sub-networks of DMN (right IPL in **Fig 2-13A**: $r = 0.60$, $p = 0.002$; left IPL in **Fig 2-12A**: $r = 0.41$, $p = 0.05$). The positive correlation indicated that greater symptom reduction was associated with a stronger decrease in connectivity. However, in the medial frontal gyrus of the EEG DMN, the EEG connectivity changes were not related to the symptom responses ($r = 0.19$, $p > 0.1$).

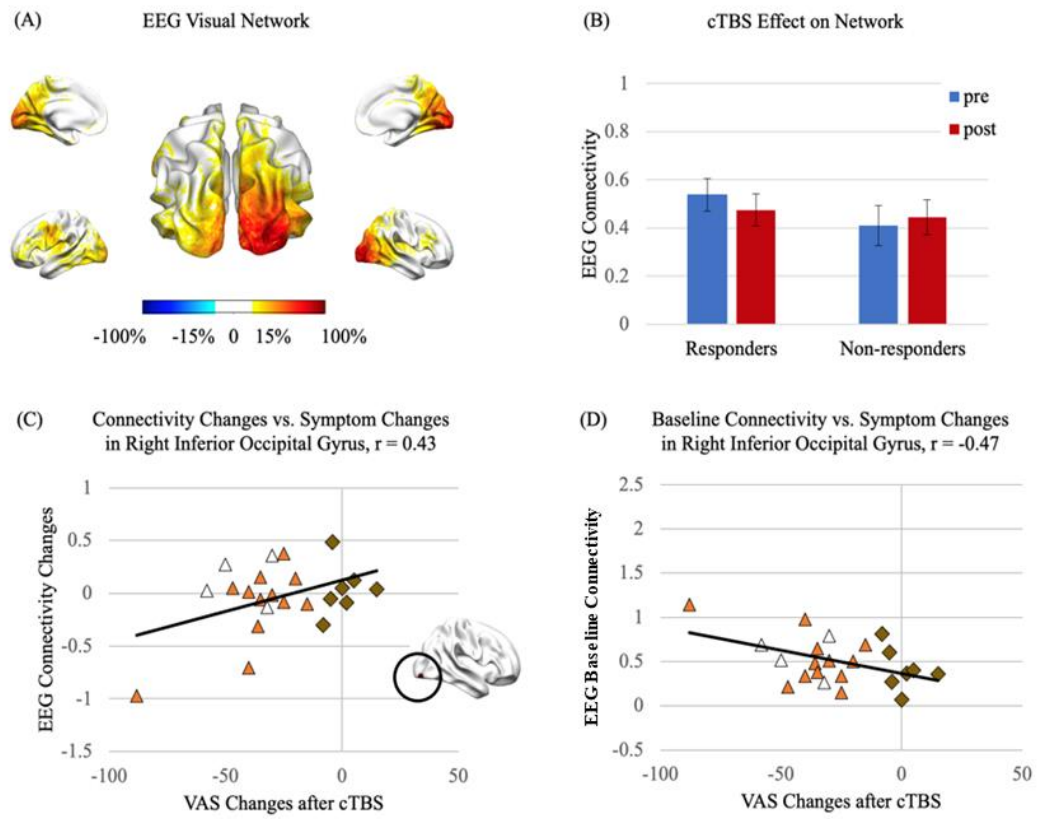

Figure 2-10: EEG visual network and ROI analysis in right inferior occipital gyrus (IOG). (A) the identified EEG visual network centered in the right IOG. (B) shows the contrast (post-treatment vs. pre-treatment) of EEG for responders and non-responders. Connectivity changes (C) as well as the baseline connectivity (D) are associated with treatment responses (Chen et al., Under Review).

We also assessed the within-group and between-group changes of EEG connectivity on day 5. Analysis showed that in the responders, the post-stimulation changes of the left MFG region were lower than those in the non-responders (**Fig. 2-11B**: $p = 0.02$). Within-group assessment further revealed that responders' decrease of EEG network connectivity in the left MFG approached significance ($p = 0.1$), whereas non-responders' increase was significant in the medial frontal gyrus ($p = 0.003$). In addition, regarding the network changes in the right IPL, the responders showed approaching-significance difference than the non-responders (**Fig. 2-13B**: $p = 0.1$). Interestingly,

regarding both left MFG and right IPL, the effect appears in opposite directions among the two response types: whereas stimulation decreased the connectivity in responders, it increased the connectivity in non-responders.

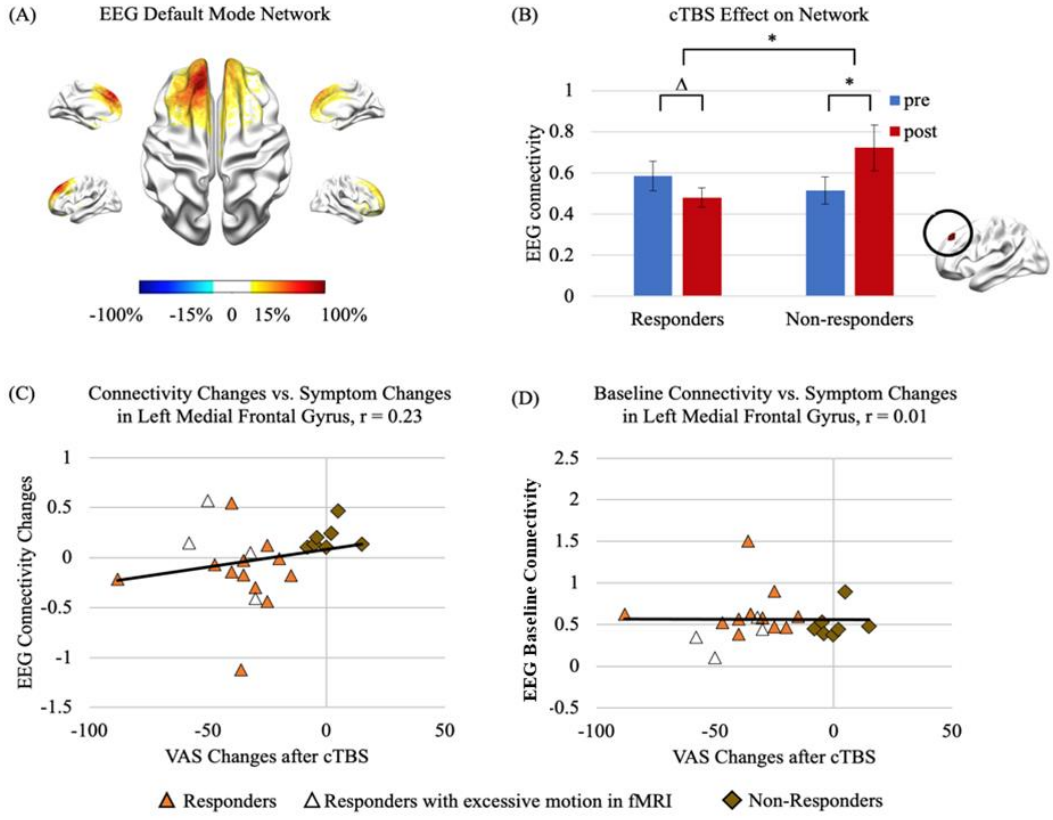

Figure 2-11: EEG DMN network and ROI analysis in left medial frontal gyrus. (A) shows the identified EEG network that includes the left medial frontal gyrus. (B) shows the contrast (post-treatment vs. pre-treatment) of EEG for responders and non-responders. * Indicates significance at $p < 0.05$. Δ Indicates approaching significance at $p < 0.1$ (Chen et al., Under Review).

In addition, we assessed whether the pre-stimulation connectivity of each EEG network on day 1 was associated with individuals' symptom responses on day 5, in order to investigate a predictive role of baseline status. Our analysis revealed that the baseline connectivity is a consistent predictor: network connectivity values in three regions negatively correlated with patients' symptom responses (visual cortex in **Fig. 2-10D**, r =

-0.47, p = 0.02; left IPL in **Fig. 2-12D**: r = -0.55, p = 0.006; right IPL in **Fig. 2-13D**, r = -0.61, p = 0.002). Notably, a negative association indicates that higher baseline connectivity predicted greater reduction of symptoms after cTBS. However, in the medial frontal gyrus of the EEG DMN, the baseline connectivity values were not found to relate to the symptom responses.

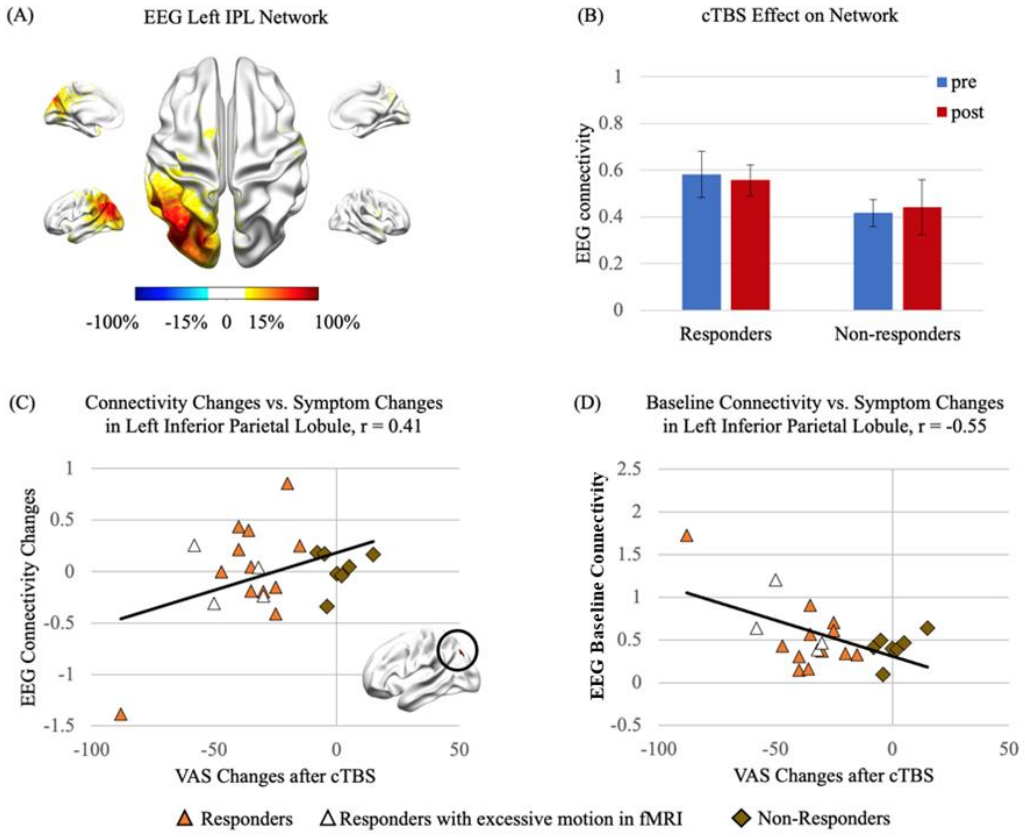

Figure 2-12: EEG network and ROI analysis in left inferior parietal lobule. (A) shows the identified EEG network that includes the left inferior parietal lobule. (B) shows the contrast (post-treatment vs. pre-treatment) of EEG for both responders and non-responders. Connectivity changes (C) as well as the baseline connectivity (D) are associated with treatment responses (Chen et al., Under Review).

2.2.6 Discussion

The current study is a follow-up study of Chen et al. (Chen et al., 2019) in which we investigated resting state brain network connectivity changes measured with EEG and

fMRI after repetitive stimulation of cTBS protocol. We have reconstructed resting state brain networks based on EEG source images and replicated the discovery of primary visual network and default mode network in a new cTBS protocol. This dataset of simultaneous EEG and fMRI acquisition also allowed us to demonstrate the association between EEG and fMRI networks. Our analysis has further shown that there is a positive relationship between symptom responses and connectivity changes and that baseline connectivity is inversely associated with the beneficial outcomes of cTBS, which was observed in the visual network as well as in regions belonging to the default mode network. We further determined that on the 2nd day try-out sessions of cTBS targets, the transient changes of EEG network connectivity induced by single administration of cTBS can be used to classify the optimal targets from non-optimal targets for repetitive stimulations.

Conventional rTMS for major depression disorder started with targeting left DLPFC using 10 Hz (O'Reardon et al., 2007). In the process of optimizing efficacy, a variety of approaches have searched for a better stimulation target, with the focus on identifying anatomical landmarks (Fitzgerald et al., 2009; Herbsman et al., 2009; Rusjan et al., 2010). Recently, a new targeting strategy was recommended based off its fMRI connectivity with the subgenual cingulate cortex – a key region in antidepressant studies (Fox et al., 2012a; Weigand et al., 2018). Importantly, the fMRI studies in depression indicated that functional connectivity that resides in large-scale neural circuits composed by several distant cortical, and sometime subcortical, structures are instrumental to the effect of rTMS (Drysdale et al., 2017; Fox et al., 2012a; Liston et al., 2014; Philip et al., 2018; Weigand et al., 2018). Similarly, in our rTMS study for MdDS, the results from

this current study and our previous work (Chen et al., 2019; Ding et al., 2014; Yuan et al., 2017) indicate that decrease in connectivity of both visual networks and posterior default mode network are related to symptom reduction in MdDS. Importantly, a unique design of our work is that we employed an iterative targeting strategy: first we determined what functional connectivity measurements correlated with symptom improvement after 10-Hz/1-Hz rTMS over DLFPC (Cha et al., 2016a; Chen et al., 2019; Yuan et al., 2017)) and then we adjusted the targets to posterior occipital/cerebellar regions in subsequent cTBS protocol (Cha et al., 2019). Compared with rTMS over DLPFC, cTBS over the dorsal occipital cortex and cerebellar vermis led to higher response rates. This may be due to better targeting (occipital/cerebellar vs. prefrontal), a higher frequency stimulation (cTBS vs. 10-Hz/1-Hz), or more intensive treatment (10-12 treatments vs. 5 treatments).

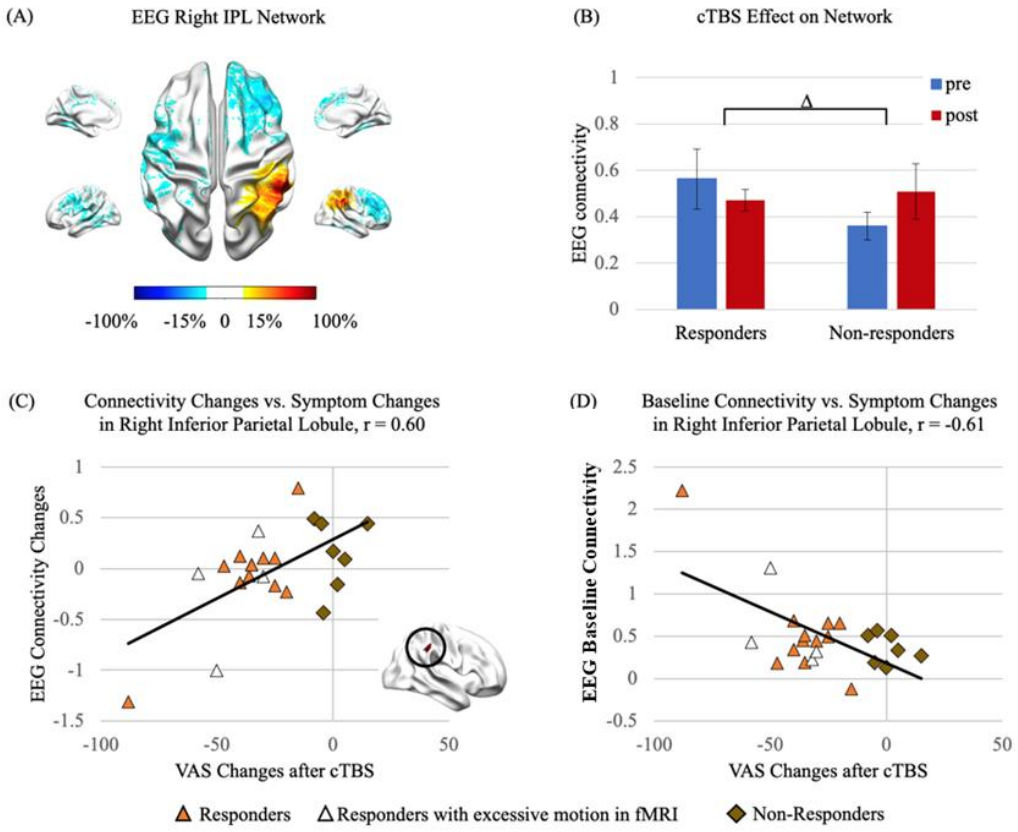

Figure 2-13: EEG network and ROI analysis in right inferior parietal lobule. (A) shows the identified EEG network that includes the right inferior parietal. (B) shows the contrast (post-treatment vs. pre-treatment) of EEG for both responders and non-responders. Connectivity changes (C) as well as the baseline connectivity (D) are associated with treatment responses. Δ indicates approaching significance at $p < 0.1$ (Chen et al., Under Review).

Our current study of multimodal imaging data before and after cTBS revealed the details of neuromodulatory effect on functional connectivity. One of the prominent symptoms in MdDS is the development of visually induced dizziness (e.g., watching action movies, playing video games) (Cha, 2009). In current analysis, one of the areas' functional connectivity correlated with symptom change is within the visual network, which was also disclosed previously (Chen et al., 2019). Comparing these two studies, despite two completely different stimulation protocols were utilized and that two non-overlapping cohorts of patients were examined, a common anatomical region in the visual

network - the right fusiform gyrus - was discovered, with a Euclidean distance of less than 10 mm. The identified region was in the parieto-occipital sulcus and in the vicinity of the area that was targeted by cTBS. This outcome emphasizes the robust role of visual network as a response biomarker in rTMS treatment for MdDS patients.

Table 2-2: Regions of interest in selected EEG resting-state networks (Chen et al., Under Review).

		MNI Coordinates (mm)		
EEG Networks	***Regions of Interest***	***X***	***Y***	***Z***
Default Mode Network	Left medial frontal gyrus	-15.06	42.13	40.53
	Left inferior parietal lobule	-33.81	-73.56	41.48
	Right inferior parietal lobule	54.10	-41.85	39.71
Visual Network	Right fusiform gyrus	36.22	-87.53	-12.03

In addition to the visual network, the connectivity changes over left and right IPL nodes also associate with the symptom's reductions, while the connectivity changes at the left MFG differed between responders and non-responders. These three regions are the key nodes of the default mode network, where the cTBS intended to intervene when the experiment was designed. The DMN has been considered to be a fundamental intrinsic network for normal mental functions and its dysfunction has been implicated in a variety of neurological disorders (Broyd et al., 2009), such as depression, schizophrenia etc. The DMN network is composed of several key nodes in the medial prefrontal cortex, posterior cingulate cortex/precuneus, the intraparietal sulcus, and the hippocampal formation,

which includes the entorhinal cortex (Buckner et al., 2008; Greicius et al., 2003). The DMN connection to the hippocampal formation flows through the entorhinal cortex (Ward et al., 2014). These hubs play critical roles in memory retrieval, navigation, internal mental monitoring and taking on the perspective of others (Buckner et al., 2008; Menon, 2015). In MdDS, the abnormal metabolic activities and functional connectives have been documented as compared with healthy individuals. The left entorhinal cortex, a pivotal part of the default mode network, has been shown to be the single cluster of hypermetabolism in PET study of MdDS (Cha et al., 2012). Later on, our multimodal imaging data of EEG and fMRI have shown that modulation of the connectivity in the default mode network in response to rTMS at DLPFC (Chen et al., 2019; Yuan et al., 2017). When DLPFC was stimulated, the stimulation did not lead to increased connectivity between the stimulation site and EC (Yuan et al., 2017), even though left prefrontal EC RSFC was shown to be lower in MdDS than in healthy controls (Cha et al., 2012). Instead, our data showed that stimulation at DLPFC played a modulatory role, resulting in decreases of functional connectivity between EC and multiples nodes of the default mode network – right inferior parietal lobule, precuneus and the other EC (Yuan et al., 2017). By using EEG network analysis, the current cTBS study again showed correlations between improvement in symptom severity and connectivity changes in multiples nodes of the default mode network – left medial frontal gyrus and bilateral inferior parietal lobules, which are consistent with previous findings despite of a completely different stimulation protocol. Especially in the left medial frontal gyrus, both the DLPFC and cTBS protocols have revealed a significant decrease of network-level connectivity in the positive responders, as compared to non-responders. However, even

though a prominent modulatory effect was evident in the left medial frontal gyrus, cTBS protocol did not reveal a linear correlation for its engagement in clinical responses, which was otherwise observed in DLPFC protocol. In addition, in posterior nodes of the DMN, correlation between connectivity and symptom changes were shown (**Fig. 2-12 and 2-13:** left and right IPL, respectively**)**. Considering that DMN generally encompasses both anterior and posterior hubs, our findings collectively indicate that cTBS to the occipital/cerebellar regions may exert stronger effects in local posterior regions than fronter regions**.**

2.3 tACS protocol

The details of the study are described in the article (Chen et al., In preparation). tACS modulates brain synchronizations by applying external current oscillations through sponge electrodes and employs a more portable and cheaper device than rTMS. From this point, it is an ideal alternative to rTMS and provides the possibility of a home-based therapy, which would be beneficial as travelling to the on-site treatment might aggravate the symptoms in MdDS. Thus, in our latest study of MdDS, we administered tACS on 24 patients. In light of our previous imaging studies regarding the clinical relevance of visual and default mode networks in MdDS, we had both front and parietal regions as the main stimulation targets.

2.3.1 Demographics

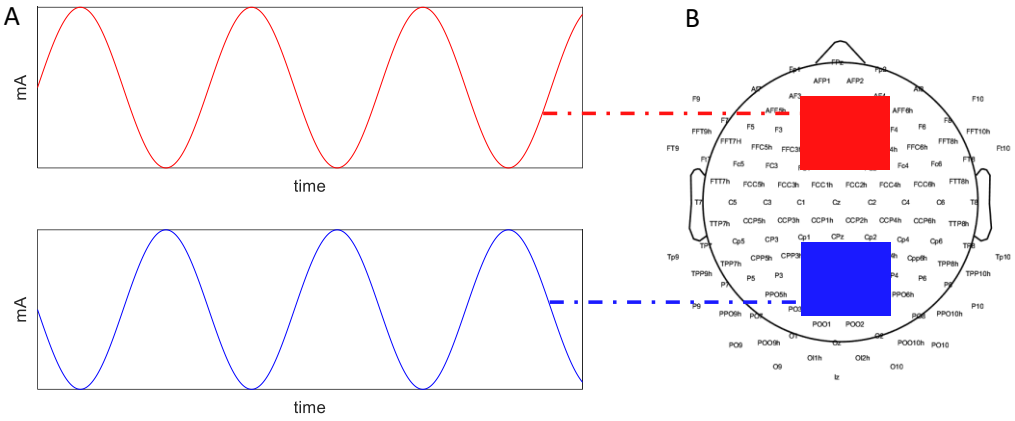

Figure 2-14: Anti-phase tACS set up. Red and blue sinusoidal waves are in opposite phases as shown in (A). Red and blue squares in (B) represent the sponge electrodes and its approximate locations on the scalp (Chen et al., In preparation).

The study was performed at the Laureate Institute for Brian Research in Tulsa, OK. Involved procedures follows the Declaration of Helsinki guidelines and approved by Western IRB (www.wirb.com). Twenty-four patients were recruited in this study with written informed consent provided but two were excluded due to missing data. The mean age of this cohort at the time of this study was 52.27 +/-11.67 and a range of 22 to 66 years. The duration of illness was of mean 39.32 +/- 54.45 and a range of 6 to 240 months. The inclusion and exclusion criteria were implemented the same as in **Chapter 2.1.1**.

2.3.2 Concurrent MR-EEG acquisition and tACS sessions

EEG and fMRI data were acquired following the same procedures as in cTBS protocol on Day 1 and 5. tACS was applied using the XCSITE 100 stimulator (Pulvinar Neuro LLC, Durham, NC). Since both in-phase and anti-phase at alpha frequency can reduce the motion illusion compared with control (40Hz) in a pilot study, this protocol employed three different tACS conditions: antiphase alpha-tACS, in-phase alpha-tACS and anti-phase gamma (40Hz). Two sponge electrodes (10 cm by 10 cm square shape)

were used and set on frontal and parietal regions (illustrated in **Fig. 2-14B**). the stimulation frequency was set at individual alpha frequency or slightly higher (rounding up to the nearest 0.5 Hz) through reading previously acquired EEG data. A return channel was placed on the left upper arm to allow the current circuit forms. The peak amplitude of the sinusoidal waveform was delivered over 20 minutes of 1 mA for anti-phase alpha-tACS and 2 mA for in-phase alpha-tACS. 22 individuals were stimulated, and the frequency varied from 10 Hz to 40 Hz (detailed stimulation parameters given in **Table 5-1**).

Patients were instructed to sit in a back supported chair, three phases of abovementioned conditions were administered in a randomized order and the most effective condition, as determined by the patient, was selected for use in the remaining sessions. On average, each patient received 10-12 sessions of tACS in the mornings over 3 days, and 60 mins break arranged in between sessions.

2.3.3 MR-EEG analysis

Resting state EEG data underwent preprocessing steps as described in **Chapter 2.1.5**, briefly, including removing heavy MR gradient artifact, cardio ballistic artifacts and the muscle/ocular movement artifact (ICA in MATLAB). The clean data then were down-sampled to 250 Hz. Filtering was applied as high pass of 0.5 Hz, low pass of 70Hz and band-stop between 59-61Hz. Group-level ICA was applied on concatenated source EEG data (from source imaging as in **Chapter 2.1.6**). The ICA derived networks were again used in analyzing this protocol, and detailed steps as in **Chapter 2.1.5**.

2.3.4 Results

The clinical responses in this protocol showed 12 patients improved while the rest 10 remained the same or got worse (**Fig. 2-15**), with an average VAS changes of -12.05+/-13.25 and range from -45 to 10. Notably, the reported VAS changes were based on the immediate effect after tACS protocol, we did not include out-lasting effect in the current analysis.

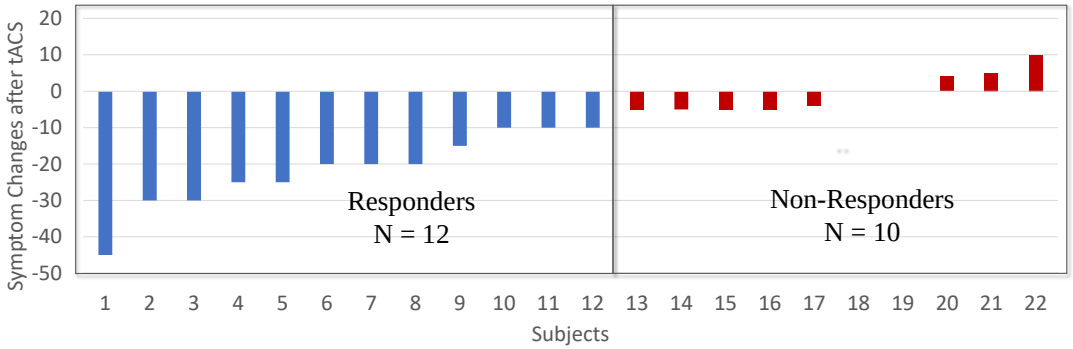

Figure 2-15: VAS changes across 22 patients in which 12 improved significantly and 10 remained the same or felt worse (Chen et al., In preparation).

We identified visual and default mode networks in this new protocol and found another one that was closely related to the clinical responses which enclosed parietal regions. In both the right medial frontal gyrus (**Fig. 2-16**) and the left cuneus (**Fig. 2-17**), we did not see any clinically relevant brain synchronizations from the seeded ROIs (circled out in **Fig. 2-14B and Fig. 2-15B**). But we did find the ROI (**Fig. 2-18B**) originating from the right cuneus displayed significant association with the clinical changes. However, it was negatively correlated with the clinical improvement and the positive responders and non-responders showed distinct directions of connectivity changes (**Fig. 2-18D**).

2.3.5 Discussion

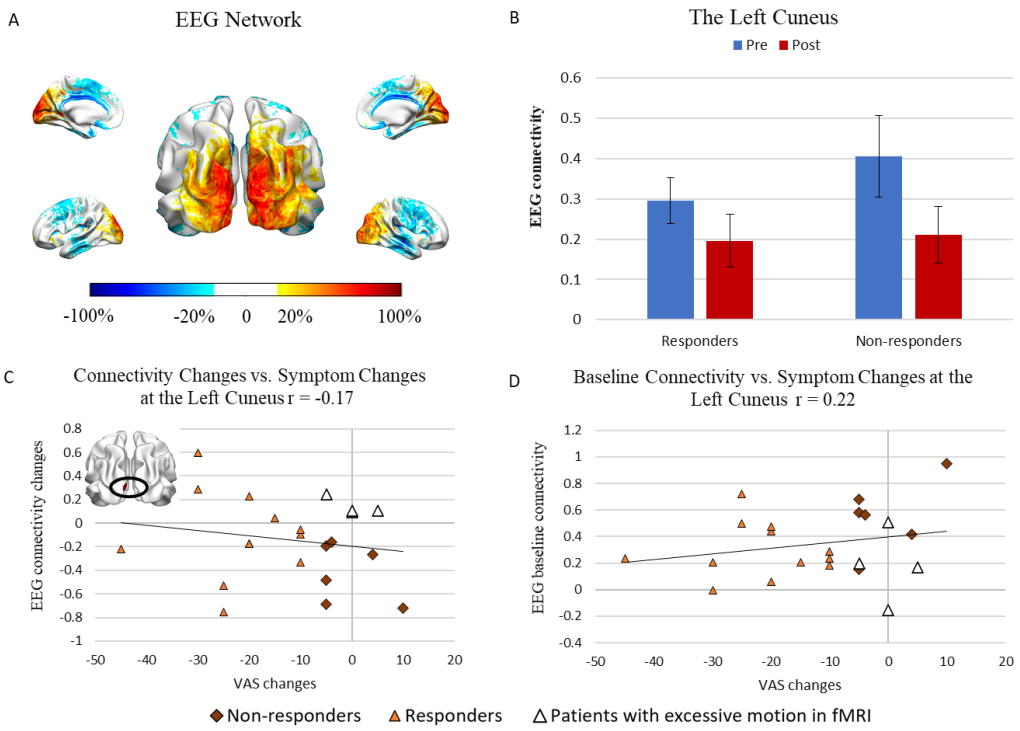

Figure 2-16: (A) shows the identified EEG network that consists of the left cuneus. The connectivity changes (C) as well as the baseline connectivity (D) are associated with the clinical responses. (B) shows the contrast (post-treatment vs. pre-treatment) of EEG for both responders and non-responders (Chen et al., In preparation).

tACS was employed here as an alternative to rTMS due not only to its potential as home-based therapy but also its capability of manipulating brain oscillations. Informed by our previous investigations in MdDS, we looked into both the left cuneus (**Fig. 2-16**) and right frontal medial gyrus (**Fig. 2-17**). We identified a new network ROI at the right cuneus which was clinically relevant. We failed to spot any significant network level connectivity changes in both visual and DMN. And the right cuneus displayed anti - correlation between EEG changes and VAS changes (**Fig. 2-18B**). This indicated the connectivity at the right cuneus increased more in the responders compared with non-responders (**Fig. 2-18D**) and differed from our reports in rTMS. This anti-correlation was

also spotted in the EC-based fMRI analysis of tACS at the left cingulate gyrus in **Chapter 4**. Notably, the parietal network encompassed massive surficial cortical areas with the maximum activation located on the right cuneus (**Table 3-2**). In light of its low spatial specificity compared to the DMN or visual network, this network synchronization might be contributed by extensive brain regions and therefore represented a broad effect of tACS on inter-connected sites which was seen more focalized in rTMS.

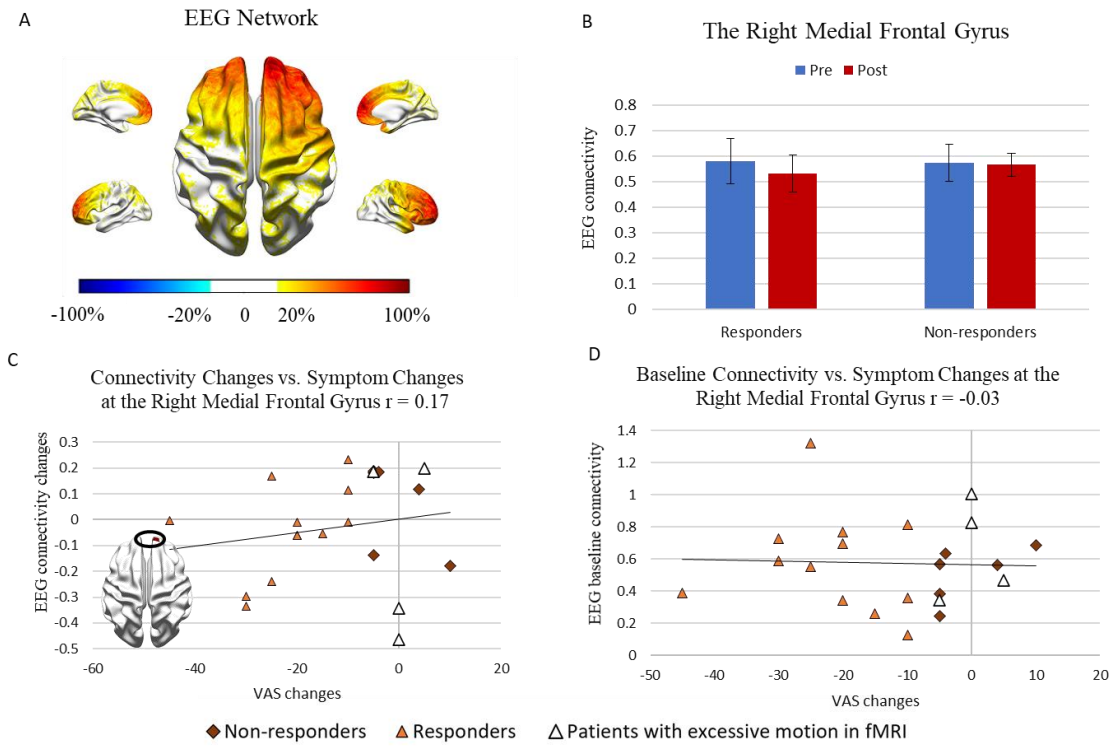

Figure 2-17: (A) shows the identified EEG network that consists of the medial frontal lobule. The connectivity changes (C) as well as the baseline connectivity (D) are associated with the clinical responses. (B) shows the contrast (post-treatment vs. pre-treatment) of EEG for both responders and non-responders (Chen et al., In preparation).

An important question to ask given 3 different protocols in MdDS was what a responsive brain would be like in EEG and fMRI. We were looking for converging evidence in abovementioned three protocols, but the answer seemed to be more complicated than we expected as it showed decrease connectivity in some of the networks

(**Chapters 2.1 and 2.2**) and also increased connectivity in here with variance across protocols. The community of neuroscience has strived to organize healthy brain as hierarchical networks to facilitate our understanding of healthy and provide reference for diseased groups (Vidaurre et al., 2017). But for most of the therapeutic tools, we did not have a full picture of whether the brain converged towards the healthy brain or achieving the efficacy by form a unique pattern (different than healthy) (Gudayol-Ferré et al., 2015) in a more complex way, for example, regarding the antidepressant effect in most of the depression studies, the normalization of brain connectivity towards the healthy was also accompanied by stubborn alterations not recovered by the treatment (Li et al., 2013; Liston et al., 2014). To answer this requires more efforts into the high-level imaging analysis of responders across different brain stimulation paradigms, in our case the patients who responded to the rTMS and tACS.

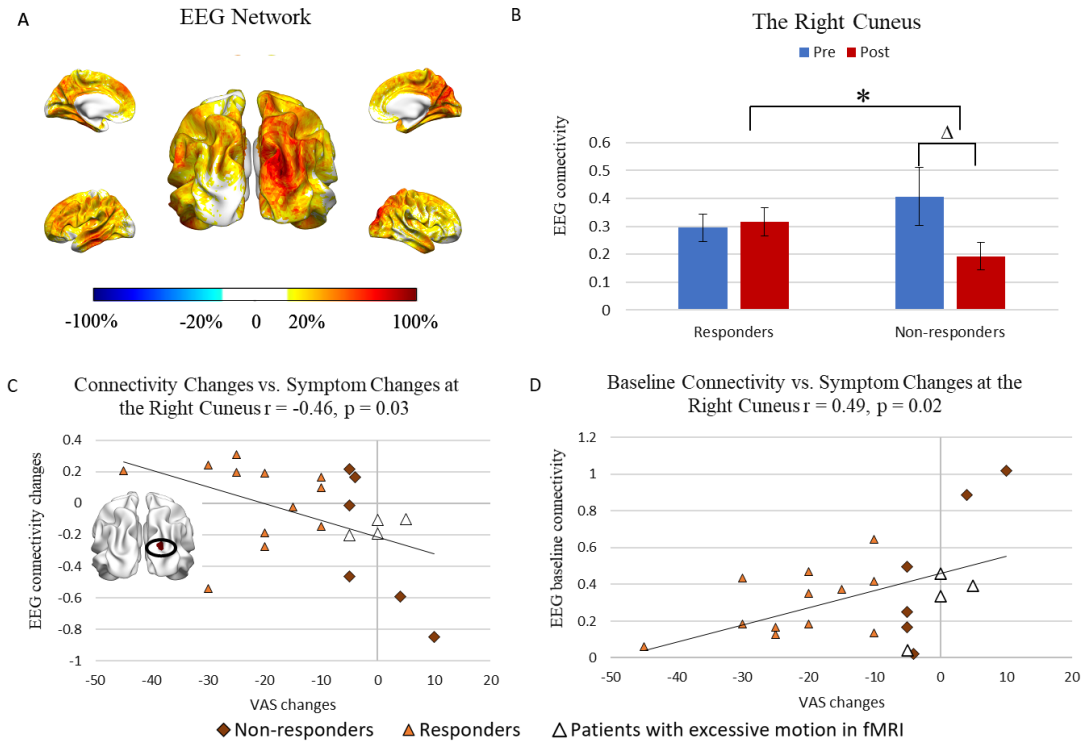

Figure 2-18: (A) shows the identified EEG network that consists of the right cuneus. The connectivity changes (C) as well as the baseline connectivity (D) are associated with the clinical responses. (B) shows the contrast (post-treatment vs. pre-treatment) of EEG for both responders and non-responders. * Indicates $p<0.05$ and Δ $p<0.1$ (Chen et al., In preparation).

To conclude, our EEG analysis on MdDS across treatment protocols revealed the response and predictive imaging biomarkers in visual and default mode networks in rTMS. We also identified the parietal network in tACS might contribute differently than visual or DMN. To further generalize the imaging biomarkers across these interference tools, in future study, we should integrate imaging analysis from a higher level in the responsive group.

3. Chapter 3: Cross-Modality Comparison in MdDS Using Simultaneous fMRI and EEG

In this chapter, I investigated the cross-modal association between EEG and fMRI. Since EEG sensors are placed at the scalp, the acquisition of EEG signal is concerned of limited sensitivity and specificity due to the volume conduction. Although in our study I have taken the electrophysiological source imaging approach to tackle such issues, in this chapter of my dissertation I further examined our simultaneous EEG and fMRI data to seek cross-modal validation for the constructed EEG networks. Initially, I compared the measures of EEG-network-level modulations from rTMS protocol with the connectivity changes of fMRI networks regarding a seed in the entorhinal cortex (**Chapter 3.1**). Although this analysis was able to assess the cross-model comparison of stimulation-related modulations at the network level, it did not address the spatial-temporal details in the networks probed by EEG or fMRI. Especially, a cortical region more superficial to the surface as measured by EEG has shown stimulation-related changes that covaried with fMRI connectivity involving a deep, subcortical area. Therefore, a more assumption-free way, to study to what extent the electrophysiological signals originated from neuronal populations would correlate with BOLD signals, is to compute EEG-informed fMRI through constructing the general linear model with EEG as regressors in cTBS and tACS (**Chapters 3.2 and 3.3**). This analysis allowed us to quantitatively assess the relationship between two modalities and even differentiate their own values in probing the brain. The integrated analysis of simultaneous EEG-fMRI data has yielded results that strongly attest to the association between EEG and fMRI.

Specifically, EEG activities in key regions of DMN have been found to correlate with fMRI activities from multiple regions that orchestrate DMN.

3.1 fMRI acquisition in DLPFC protocol

Both EEG and fMRI were performed on Day 1 and Day 5 with the rTMS sessions scheduled in the middle for each subject. Structural and resting state functional magnetic resonance images were collected using a General Electric Discovery MR750 whole body 3-Tesla MRI scanner (GE Healthcare, Milwaukee, WI). Whole brain resting-state fMRI data were acquired using the following parameters: FOV/slice = 240/2.9 mm, axial slices per volume = 34, acquisition matrix = 96×96, repetition time/echo time (TR/TE) = 2000/30 ms, SENSE acceleration factor R = 2 in the phase encoding (anterior-posterior) direction, flip angle = 90°, sampling bandwidth = 250 kHz. The EPI images were reconstructed into a 128×128 matrix, in which the resulting fMRI voxel volume was 1.875×1.875×2.9mm3. Additionally, simultaneous physiological pulse oximetry and respiration waveform recordings were obtained (with 40 Hz sampling) for each fMRI run. A photo-plethysmograph with an infrared emitter placed under the pad of the subject's left index finger was used for pulse oximetry while a pneumatic respiration belt was used for respiration measurements. The subject rested quietly with their eyes closed during the image acquisitions. A T1-weighted magnetization-prepared rapid gradient-echo (MPRAGE) sequence with sensitivity encoding was used to provide an anatomical reference for the fMRI analysis, which had the following parameters: FOV = 240 mm, axial slices per slab = 190, slice thickness = 0.9 mm, image matrix = 256×256, TR/TE = 5/2.012 ms, acceleration factor R = 2, flip angle = 8°, inversion time (TI) = 725 ms, sampling band-width = 31.2 kHz.

3.1.1 Resting state fMRI analysis

fMRI data were preprocessed to remove any artifacts according to the pipeline described in Yuan et al (Yuan et al., 2017). Specifically, major processing steps included respiration- and pulse-associated noise reduction, slice timing and rigid-body motion correction, spatial smoothing, and temporal filtering with a bandpass filter (0.005 - 0.1 Hz). Connectivity was calculated as the Pearson correlation between the seed region and the target regions. For further statistical analysis, Fisher transformation was employed to convert the correlation values into z-scores as the representation of resting state functional connectivity (RSFC). The seed region used was the left entorhinal cortex (EC), which has been found to be hypermetabolic in MdDS in a previous functional imaging study with fluorodeoxyglucose positron emission tomography (FDG-PET) (Cha et al., 2012). The coordinates of the individual EC locations were manually determined on high-solution structural MR images acquired in the coronal plane using anatomical guidelines by (Insausti et al., 1998). In order to assess the cross-modal relationship, fMRI connectivity was compared with the connectivity of EEG networks. Specifically, the fMRI connectivity between the seed at the left EC and the inferior parietal lobule, the precuneus and the right entorhinal cortex were considered, since the modulation of RSFC at those regions was indicative of the symptom changes after rTMS (Yuan et al., 2017).

3.1.2 Analysis to associate fMRI with EEG

Furthermore, we investigated the relationship of EEG connectivity to the fMRI findings (Yuan et al., 2017). Since the entorhinal cortex has been identified as a region with metabolic and functional connectivity abnormalities in MdDS, we hypothesized that modulation by rTMS should change network connectivity to the entorhinal cortex.

However, surface-based EEG cannot measure electrical signals originating from the entorhinal cortex directly. Thus, instead of examining the direct effect on the entorhinal cortex, we investigated whether modulation of superficial cortical regions with functional connectivity with the entorhinal cortex could be affected, possibly through a cortical-subcortical pathway. We propose that changes in connectivity revealed in EEG networks are related to changes in fMRI connectivity to the entorhinal cortex. Thus, in the analysis, we compared the connectivity values of EEG networks in ROIs to the connectivity values of fMRI seeded within the entorhinal cortex. Particularly, three cortical regions were considered based on our previous study (Yuan et al., 2017): the left precuneus, the right inferior parietal lobule and the right entorhinal cortex. We computed the Pearson correlation between fMRI and EEG connectivity changes with these regions; regression lines were drawn to indicate the correlation between those two modalities.

3.1.3 Results

Here we investigated the mechanism of rTMS modulation of EEG networks, and how they were related to fMRI connectivity seeded at the entorhinal cortex. Our rationale was that although EEG cannot directly measure electrical activity originating from deep limbic structures, EEG is able to detect network connectivity of superficial cortical areas co-modulated with those deep structures. Thus, we examined the cross-subject co-variation between the synchronization of EEG activities within a network (i.e., the EEG network connectivity) and the synchronization of fMRI activities between two regions (i.e., the fMRI RSFC). As shown in (**Fig. 3-1**), the analysis revealed that EEG

connectivity at the medial frontal gyrus within a DMN network co-varies with the RSFC between the entorhinal cortex and the right inferior parietal lobule ($r = 0.55$, $q < 0.05$).

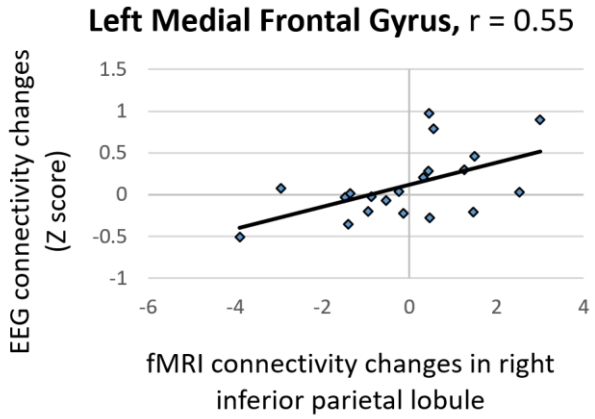

Figure 3-1: Association between fMRI connectivity and EEG connectivity. Changes in fMRI connectivity between nodes of the default mode network (i.e., the entorhinal cortex and inferior parietal lobule) are related to changes of the EEG network in the left medial frontal gyrus ($q < 0.05$) (Chen et al., 2019).

3.1.4 Discussion

Previous studies have revealed correspondence between fMRI and EEG resting state networks in both temporal (Britz et al., 2010; Yuan et al., 2012) and spatial domains (Yuan et al., 2016; Liu et al., 2017), mainly in healthy subjects. In our study, symptom-related EEG synchronization changes over medial frontal gyrus and visual areas complemented symptom-related RSFC changes shown by fMRI (Yuan et al., 2017). However, the regions that were found to be related to symptoms in EEG and fMRI did not completely overlap, i.e., EEG connectivity in visual cortex was shown to be related to RSFC in inferior parietal cortex in fMRI. The reason may be different methodologies of identifying networks in EEG and fMRI: EEG networks were defined using a data-driven approach whereas fMRI connectivity was quantified with a seed-based approach. In addition, EEG networks capture connectivity among estimated electrophysiological

sources whereas fMRI connectivity depicts pair-wise correlation in hemodynamics. Furthermore, it is possible that a between-network interaction led to the relationship observed between connectivity in visual cortex and RSFC in inferior parietal cortex, which is distant from the visual area. Nevertheless, connectivity changes of both modalities showed similar trends with symptom changes (i.e., positive relationship between two modalities in **Fig. 3-1**). The brain connectivity was reduced in positive responders (in **Fig. 2-3C** and **2-4C**); this feature can be captured not only by fMRI but EEG independently as well. This finding is consistent with the previous discovery of a close link between EEG and fMRI from the point of view that they both are indicators of activity power regardless of the activity locations (Goldman et al., 2002; Laufs et al., 2003; Yuan et al., 2016).

The findings in the current study suggested a strategy of using multimodal neuroimaging data to guide rTMS. Our investigations have indicated that connectivity in the default mode network, measured in fMRI as well as EEG, can be an imaging-based, objective symptom biomarker. Thus, modulation of the biomarker can be informative in trials of brain stimulation methods, potentially not limited to rTMS. More importantly, though fMRI is capable of revealing symptom-related connectivity, an EEG-based network is still intriguing since it is compatible with TMS and thus, can provide instantaneous feedback in trials of stimulation protocols. Furthermore, biomarkers from the two modalities can be integrated to guide TMS targets. For example, fMRI can be used to capture a disease-modifying network involving deep cortical or subcortical structures while the connectivity involving superficial nodes of the network can be identified in EEG, potentially through a matching procedure with the fMRI-measured

network. Stimulation protocols could be adapted as networks are modulated in desired directions. Many neurological disorders are caused by abnormalities of brain networks instead of isolated hubs or from structural injury (Fox et al., 2012b). Integration of neuroimaging and neuromodulation protocols allow a broader platform of functional disorders to be investigated

3.2 fMRI acquisition in cTBS protocol

3.2.1 EEG-informed fMRI GLM

The acquisition of EEG and fMRI data in this chapter followed the same procedures as in **Chapter 3.1.1**.

fMRI preprocessing was performed as in **Chapter 3.1.1**. In the EEG analysis, we have identified the DMN subnetworks, and the visual network based on the spatial patterns of connectivity values. In addition, we evaluated the cross-model relationship between EEG networks and fMRI networks based on the simultaneous EEG and fMRI recordings. Since EEG networks were independently identified on EEG data alone, we compared the time course of each EEG network and its association with the dynamics of whole-brain fMRI time series, using an approach of EEG-network-informed analysis (Yuan et al., 2016; Yuan et al., 2018; Yuan et al., 2012). Firstly, to accommodate the dramatically different temporal scales of multimodal EEG and fMRI data, the time courses of the EEG networks were convolved with a canonical double-gamma hemodynamic response function (Friston et al., 1998) and then down-sampled to TR, resulting in EEG-network-informed regressors. Then we examined the temporal correlation between fMRI time series and EEG-network-informed regressors through a general linear model (GLM) analysis in AFNI, with separate GLM structed for each of

the four EEG network ROIs (i.e., left MFG, left IPL, right IPL and right FG). To examine the spatial extent of the correlation between fMRI time series and EEG-network-informed regressors, statistical maps were created by showing voxels where the time courses of BOLD signals co-varied with the time courses of EEG-network-informed regressors. The group-level significance of the association was evaluated using a mixed-effect model. GLM analysis in individuals yielded whole-brain maps of correlations, which were transformed to z-scores by a Fisher transform and then subject to the group-level voxel-wise t-test (df = 18, four out of the total twenty-three individuals were excluded because of insufficient data points after motion censoring). The significance criterion for detecting activation was set at $p_{corrected} < 0.05$ determined using the AFNI program 3dClustSim, i.e., thresholded at voxel $p < 0.005$ and cluster size > 30 voxels (Young et al., 2014).

3.2.2 Results

we assessed the cross-modal relationship between EEG networks and fMRI networks based on the simultaneous recordings of EEG and fMRI. Since EEG were acquired through electrodes over the scalp, its signals are concerned of limited sensitivity and specificity due to the volume conduction. Although we have taken the electrophysiological source imaging approach to tackle such issues, we further examined our simultaneous EEG and fMRI data for cross-modal validation. By performing a whole-brain analysis in the fMRI data, a number of regions were identified where the BOLD fMRI time courses co-varied with the regressors obtained from EEG network activities. Noteworthy, convolution with a canonical HRF was performed on the source activities of the EEG network to address its faster temporal scale than fMRI. Four EEG networks were investigated across, i.e., left MFG, left IPL, right IPL and right FG. Exemplar single-

session time courses of EEG (after convolution) and fMRI are plotted in **Fig. 3-2**, showing the regions where the temporal dynamics of BOLD signals positively correlated with the electrophysiological fluctuations derived from EEG networks (left MFG in **Fig. 3-2A**: r = 0.13, p = 0.76; left IPL in **Fig. 3-2B**: r = 0.17, p = 0.024). Results for the EEG-fMRI association as group-averaged maps are illustrated in **Fig. 3-2** and **Fig. 3-3**. Overall cross-modal association has been observed in multiple nodes of DMN. Interestingly, regarding EEG activities from left MFG (a key node of DMN), our analysis identified correlated BOLD activities in the right middle temporal gyrus, left cingulate gyrus and right culmen (shown in **Fig. 3-2A**). Meanwhile, the EEG activities from left IPL (also a key node of DMN), are shown to be correlated with BOLD activities in the left precuneus and Left cingulate gyrus (shown in **Fig. 3-2A**). On the contrary, the EEG activities from the right IPL only identified negative correlation in left posterior cingulate (**Fig. 3-3**). In addition, regarding the EEG visual network, extensive positive correlations were found in BOLD activities from a number of regions, including left precuneus, left IPL and right IPL, although not the primary visual cortex (shown **in Fig. 3-3**). Regions of significant EEG-fMRI association are tabulated in **Table 3-1**. Only results of post-TMS sessions are listed for the EEG-fMRI association, whereas results of pre- and post- sessions showed fewer regions with significance.

3.2.3 Discussion

We examined simultaneous EEG and fMRI data to seek cross-modal validation for the constructed EEG networks. The integrated analysis of simultaneous EEG-fMRI data has yielded results that strongly attest to the association between EEG and fMRI. Specifically, EEG activities have been found to correlate with fMRI activities from

multiple regions that make up the DMN and moreover, activities of different EEG networks appeared to engage two subsystems of DMN – the dorsal medial prefrontal cortex subsystem and the medial temporal lobe subsystem (Andrews-Hanna et al., 2010).

Table 3-1: Regions of significant correlations with activities from EEG resting-state networks in cTBS (Chen et al., Under Review).

Cluster size at q < 0.05	Peak-level T value	Peak MNI X (mm)	Y (mm)	Z (mm)	Region Description
EEG DMN / Left medial frontal gyrus					
196	3.7	-24	-34	32	Left cingulate gyrus
87	4.1	38	-60	-27	Right culmen
50	4.2	38	-45	6	Right middle temporal gyrus
EEG DMN / Left medial frontal gyrus					
66	3.8	-12	-14	45	Left cingulate gyrus
47	3.3	-1	-68	23	Left precuneus
EEG DMN / Right inferior parietal lobule					
41	-3.2	1	-40	16	Left posterior cingulate
EEG Visual Network / Right fusiform gyrus					
560	4.8	12	-30	40	Right cingulate gyrus
477	3.7	-14	-37	46	Left cingulate gyrus
302	3.7	-4	1	42	Left cingulate gyrus
296	3.3	-57	-32	18	Left insula
260	3.3	56	-31	38	Right inferior parietal lobule
129	3.9	11	-4	40	Right cingulate gyrus
89	3.7	-31	-21	-4	Left lentiform nucleus
80	3.3	41	-40	6	Right superior temporal gyrus
57	3.5	19	-66	26	Right precuneus
49	3.6	-14	-69	29	Left precuneus
47	3.2	-56	-25	32	Left inferior parietal lobule

For example, as shown in **Fig. 3-2A**, the activities of the EEG DMN network with hot-spot connectivity at the left MFG showed a significant, group-level correlation with BOLD fMRI dynamics in the right middle temporal gyrus (MTG). Both the MFG and MTG are known as key nodes belonging to the DMN (Buckner et al., 2008), and more specifically recognized as the dorsal medial prefrontal cortex subsystem of the DMN (Andrews-Hanna et al., 2010). In addition, the EEG activities derived from the left IPL network were shown to correlate with BOLD fMRI dynamics in the left precuneus (Brodmann Areas 23/31), which is also a key node of DMN (Buckner et al., 2008). Interestingly, the EEG activities from the right IPL were also found to correlate with BOLD signals in posterior cingulate cortex, but in anticorrelation. The left/right IPL together with the midline structures, including the precuneus (Brodmann Areas 23/31) and posterior cingulate cortex, are recognized as another subsystem of DMN, i.e., the medial temporal lobe subsystem (Andrews-Hanna et al., 2010). These results confirmed the association between the electrophysiological EEG and BOLD activities that belong to common DMN network system. The subsystems of DMN have been shown to exhibit normal, distinct functional contributions to cognition but can also be co-activated at the resting state (Andrews-Hanna et al., 2010; Shirer et al., 2012), while the subsystems can be altered differently in disorders (Jones et al., 2011; Miller et al., 2017; Tozzi et al., 2021). Our findings suggest that cTBS in MdDS may concurrently engage the subsystems of DMN.

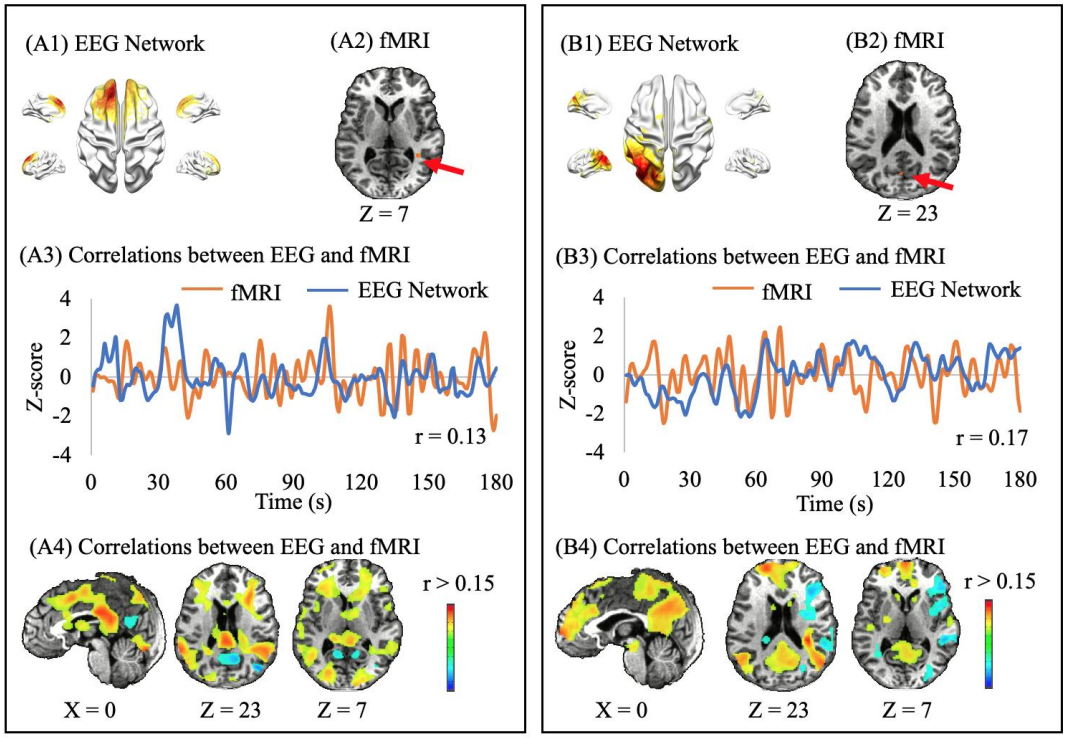

Figure 3-2: Cross-modal association between EEG and fMRI activities. (A1) the EEG network identified as best match to the Yeo template of DMN. (A2) the group-level region of significant correlation between fMRI signals and EEG network activities. (A3) shows a single-session example of the EEG network (after convolution with HRF) and the fMRI signals extracted from the group-level cluster at the right medial temporal gyrus, indicated by a red arrow in (A2). (A4) shows maps of correlations between the fMRI signals and EEG network activities in a representative subject, thresholded at r >0.15 for display. (B1) the EEG network identified as the left IPL network. (B2) the group-level region of significant correlation between fMRI signals and EEG network activities. (B3) shows a single-session example of the EEG network (after convolution with HRF) and the fMRI signals extracted from the group-level cluster at left precuneus, indicated by a red arrow in (B2). (B4) shows maps of correlations between the fMRI signals and EEG network activities in a representative subject, thresholded at r > 0.15 for display (Chen et al., Under Review).

However, the locations where EEG and fMRI activities were found to correlate did not completely overlap in space, at least at a group level. Interestingly, the EEG derived from left MFG and left IPL appear to engage two subnetworks of DMN, the ventral DMN and dorsal DMN, respectively (Shirer et al., 2012). Likewise, our previous work and other studies have also documented that the EEG activities can be linked to

BOLD fMRI activities that extends well beyond the origins of EEG (Goldman et al., 2002; Laufs et al., 2003; Yuan et al., 2016). It is possible that different sensitivity and specificity of sensing in EEG and fMRI modalities have contributed to the disparity in space. It is also possible that a network-level interaction has led to the relationship observed between activities in left MFG and right MTG, and between left IPL and precuneus, which are all nodes of the DMN. Furthermore, associations with EEG activities from the visual cortex, specifically the right fusiform gyrus, were observed in a number of regions beyond visual cortex, including left precuneus, left IPL and right IPL. Only in some individuals, EEG-fMRI association was observed in the primary visual cortex, but not significant at a group level. This finding is consistent with a few previous EEG-fMRI studies that have reported fMRI signals in regions of the default mode network are correlated to EEG activities from visual area (Laufs et al., 2003; Sadaghiani et al., 2010; Yuan et al., 2012), although EEG activities in different frequency ranges and electrodes/regions may result in positive or negative correlations. Therefore, future study is warranted to further unravel the complexity of the association between electrophysiological and BOLD signals.

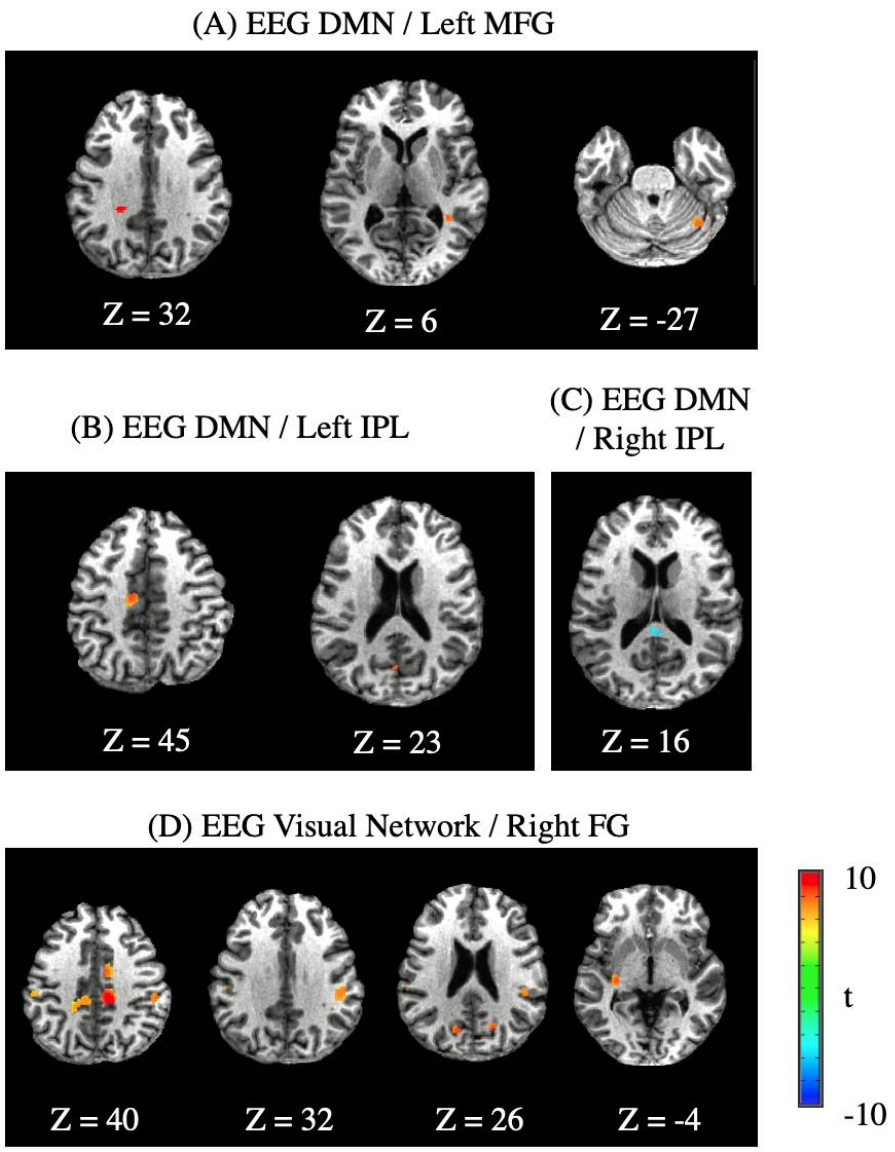

Figure 3-3: The group-level maps show regions where fMRI activities are significantly correlated to EEG network activities derived from (A) left medial frontal gyrus (MFG), (B) left inferior parietal lobule (IPL), (C) right inferior parietal lobule (IPL) and right fusiform gyrus (FG) (Chen et al., Under Review).

3.3 fMRI acquisition in tACS protocol

3.3.1 EEG-informed fMRI GLM

The acquisition of EEG and fMRI data in this chapter followed the same procedures as those described in **Chapter 3.1.1**.

Two patients were excluded from our analysis due to their left-handed condition, which could result in mirrored nervous system lateralization and further complicated our analysis. Four more datasets were affected by excessive motion artifacts during data recording. fMRI preprocessing was performed in AFNI (Analysis of Functional NeuroImages, https://afni.nimh.nih.gov/). The following steps were implemented: discard first five volumes to allow T1 equilibration, reduction of respiration- and pulse-associated noise, slice timing and rigid-body motion correction, spatial smoothing, and temporal filtering with a bandpass filter (0.005 - 0.1 Hz). Regression was utilized to remove low-frequency changes in respiration volume, six affine motion parameters, signal from a ventricular ROI, and signals from the white matter region. We also censored out data points with excessive motion in regression analyses (i.e. >= 0.3 mm between successive time points).

The implementation of GLM followed same procedures in **Chapter 3.2.1**. Briefly, 3 EEG networks (visual, default mode and parietal networks) derived from ICA were convolved with HRF and down-sampled to match the temporal resolution of BOLD signals. Resulted EEG regressors were fed into GLM with fMRI time courses.

3.3.2 Results

The covariation between EEG-derived regressors in tACS and fMRI was not as spatially specific as we observed in cTBS. As shown in **Table 3-2**, between EEG and fMRI were mostly anti-correlation which added difficulty to our interpretation of the results. From the anterior DMN, the EEG were able to identify fMRI activations at the precentral gyrus and posterior cingulate. For the EEG visual regressor, we observed the

association at precentral gyrus and cingulate gyrus. Lastly, in the parietal network, we observed more negative correlation featured the EEG in fMRI as tabulated in **Table 3-2**.

Table 3-2: Regions of significant correlations with activities from EEG resting-state networks in tACS (Chen et al., In preparation).

Cluster size at $q < 0.05$	Peak t	Peak MNI x	y	z	Anatomical structure
EEG anterior DMN/right Medial Frontal Gyrus					
155	5.07	60	-8	30	right precentral gyrus
80	-3.68	-57	-41	35	left supramarginal gyrus
58	-4.72	-44	-10	-13	left insula
43	3.23	-54	-13	33	left postcentral gyrus
41	4.2	-12	-55	26	left posterior cingulate
37	-3.5	-31	-1	40	left middle frontal gyrus
33	-4.36	-19	-37	24	left cingulate gyrus
32	-4.05	56	-45	43	right inferior parietal lobule
EEG Visual Network/left Cuneus					
859	-5.97	60	-10	33	right precentral gyrus
404	-4.39	-57	-7	27	left precentral gyrus
222	4.68	-21	-32	24	left cingulate gyrus
43	3.84	-34	-41	8	Left superior temporal gyrus
EEG Parietal Network/right Cuneus					
122	-3.73	51	15	18	right inferior frontal gyrus
113	4.3	6	15	17	right caudate
70	-3.84	-61	-39	35	left inferior parietal lobule
55	-3.63	33	-73	31	right middle temporal gyrus
42	-4.04	-27	-54	39	left precuneus
41	4.29	18	36	22	right anterior cingulate
41	-4.17	-31	-71	27	left middle temporal gyrus
40	3.44	51	-8	35	right precentral gyrus
40	4.21	16	-34	70	right postcentral gyrus
37	4.3	-14	-54	28	left posterior cingulate

34	-3.38	31	-48	41	right supramarginal gyrus
30	-3.63	43	5	43	right precentral gyrus

3.3.3 Discussion

In this section, we investigated the cross-modal association using GLM approach. Simultaneously acquired EEG data were used as regressors to compare with the BOLD signals. As a result, we found both activation and deactivation in multiple fMRI regions with regard to each EEG network. Notably, the identified regions where EEG and fMRI were positively correlated failed to show a strong spatial specificity in comparison to where EEG networks encompassed as a surface measure. For example, the precentral gyrus was picked as the largest cluster displaying strong covariation between fMRI and anterior DMN. But it was not the priority region connected to DMN in the literature (Raichle et al., 2001b; van den Heuvel et al., 2008). This was also different than our analysis of cTBS in **Chapter 3.2** which has identified overlapping locations between two modalities despite a few regions showing discrepancy in space. Also, deactivation dominated our identified brain regions in this covariation analysis, which might be attributed to intrinsic brain rhythms. As reported in other studies, the theta activity was negatively correlated with resting state fMRI DMN (Scheeringa et al., 2008) and different frequency of neuronal dynamics might contribute differently to the BOLD signals (Scheeringa et al., 2011). Besides, the direct impact tACS on the brain oscillations might be the reason for the significantly different brain organization afterwards compared to cTBS.

4. Chapter 4: Noninvasive Brain Stimulation Modifies Abnormal Entorhinal Connectivity in MdDS: A Comparison with Healthy Controls

In this chapter, I specifically examined the entorhinal cortex as the seed for resting state fMRI connectivity in tACS protocol, because EC was a critical region from our previous PET and fMRI investigations (Cha et al., 2012; Yuan et al., 2017). This analysis was conducted also because EC is located in the deep limbic region and its electric activities are not directly detectable by scalp EEG. To this end, fMRI is a volumetric measure with direct sensitivity to deep structures and offers a better approach to examine the role of entorhinal cortex in modifying clinical symptoms after noninvasive brain stimulations. Furthermore, we included the healthy controls in the ROI analysis to further probe the working mechanism of tACS in improving the symptoms of MdDS.

4.1 Resting state fMRI acquisition

The fMRI acquisition procedures were the same as in **Chapter 3.1**. Healthy participants were instructed to close their eyes and not think of anything specific for six minutes during recording.

4.2 EC-seeded fMRI connectivity

The EC has shown hyper-metabolism compared to the healthy control in our previous PET study (Cha et al., 2012) therefore a critical region in our fMRI imaging analysis to explore the mechanism of treatment protocols as well as the pathological cause of the disorder. To centralize our imaging analysis regarding the EC, we circled the region of interest at EC with a radius of 2.5 mm. Specifically, we identified EC coordinates in Talairach space for each individual patient and normal participants to address the

heterogeneity in brain morphology across individuals which was the issue when the group coordinates were applied. Averaged time series from that sphere were then compared with fMRI voxels brain-wide and their association was quantified as the temporal Pearson's correlation. These individual EC-based connectivity maps from MdDS in both pre- and post-treatment sessions were paired and subject of a t-test (3dttest in AFNI) with symptom changes as the covariate. Statistical maps illustrating changes in brain activation after the treatment were created and significant clusters on the map were defined as the number of voxels > 30 with original $p<0.005$ (Young et al., 2014). Through the resulting clusters which show strong association with clinical responses, the healthy data from these ROIs were extracted and benchmarked with patients' data for evaluating these specific contrasts. Two sample t-test were used to compare imaging responses in patients and healthy controls so that we could learn if the beneficial imaging response moved towards healthy baseline or not.

Table 4-1: Clinically relevant clusters at lEC seeded analysis (Chen et al., In preparation).

lEC seeded				MNI Coordinates (mm)		
Cluster#	Anatomical structure	#Voxels	Peak t	x	y	z
1	left thalamus	94	-4.19	-11	-28	21
2	right insula	81	-5.8	29	0	22
3	left superior temporal gyrus	72	3.29	-56	-21	-3
4	right precentral gyrus	72	-4.18	34	-10	33
5	left superior frontal gyrus	60	-4.28	-12	21	66
6	left precuneus	59	4.28	-29	-72	49
7	right inferior parietal lobule	54	3.56	62	-26	36

8	left middle temporal gyrus	53	3.46	-48	-64	-1
9	right inferior parietal lobule	53	4.33	34	-55	46
10	right superior temporal gyrus	50	-3.53	33	-57	14
11	right caudate	45	-4.17	16	11	19
12	left cingulate gyrus	39	-3.5	-26	-24	36
13	right precuneus	37	3.33	31	-69	56
14	Left cingulate gyrus	36	-4.06	-16	-4	30

4.3 Results

A total of 18 right-handed healthy participants were recruited and 4 were excluded due to excessive motion artifacts. The mean age of healthy controls at the time of this study was 48.57 +/-7.84 and a range of 36 to 65 years. The mean age of tACS cohort at the time of this study was 52.27 +/-11.67 and a range of 22 to 66 years. The duration of illness was of mean 39.32 +/- 54.45 and a range of 6 to 240 months. The inclusion and exclusion criteria were implemented the same as in **Chapter 2.1.1**.

Table 4-2: Clinically relevant clusters at rEC seeded analysis (Chen et al., In preparation).

rEC seeded				MNI Coordinates (mm)		
Cluster #	Anatomical structure	#Voxels	Peak t	x	y	z
1	left precuneus	244	3.93	-29	-70	47
2	left precuneus	137	4.31	-4	-62	48
3	left middle temporal gyrus	124	3.86	-69	-37	-3
4	right middle frontal gyrus	67	3.37	51	28	30
5	right angular gyrus	52	3.79	34	-55	44

6	left cingulate gyrus	50	-4.7	1	-20	23
7	right cingulate gyrus	50	-3.41	19	12	31
8	left middle temporal gyrus	40	3.33	-56	-41	3
9	left superior temporal gyrus	37	5.35	-67	-4	-4
10	right precuneus	35	3.53	31	-75	49
11	right cerebellar tonsil	34	-3.86	11	-51	-38
12	right cingulate gyrus	33	3.43	3	-46	43
13	left cingulate gyrus	31	-3.42	-16	-15	31
14	left cerebellar tonsil	30	-4.16	-6	-59	-40

During the analysis of EC seeded statistical maps from before and after treatment, we identified a few clusters which survived the multiple comparison distributed in several brain regions. A positive association between this local connectivity changes versus VAS changes could essentially be interpreted as positive responders having more reduction or less increase of brain connectivity at these specific regions. The clinically relevant clusters seeded at lEC enclosed key sites: left precuneus, left superior temporal gyrus, right inferior parietal lobule, left cingulate gyrus and right precuneus (**Table 4-1**); the rEC enclosed the following: left precuneus, right precuneus, left middle temporal gyrus, left cingulate gyrus, and right angular gyrus (**Table 4-2**). Notably, we have found subcortical sites (left thalamus, left insula and left cingulate gyrus) persistently showing negative association with VAS changes, which was opposite to what cortical clusters indicated

(left and right precuneus, left and right parietal lobule shown in **Table 4-1 and Table 4-2**).

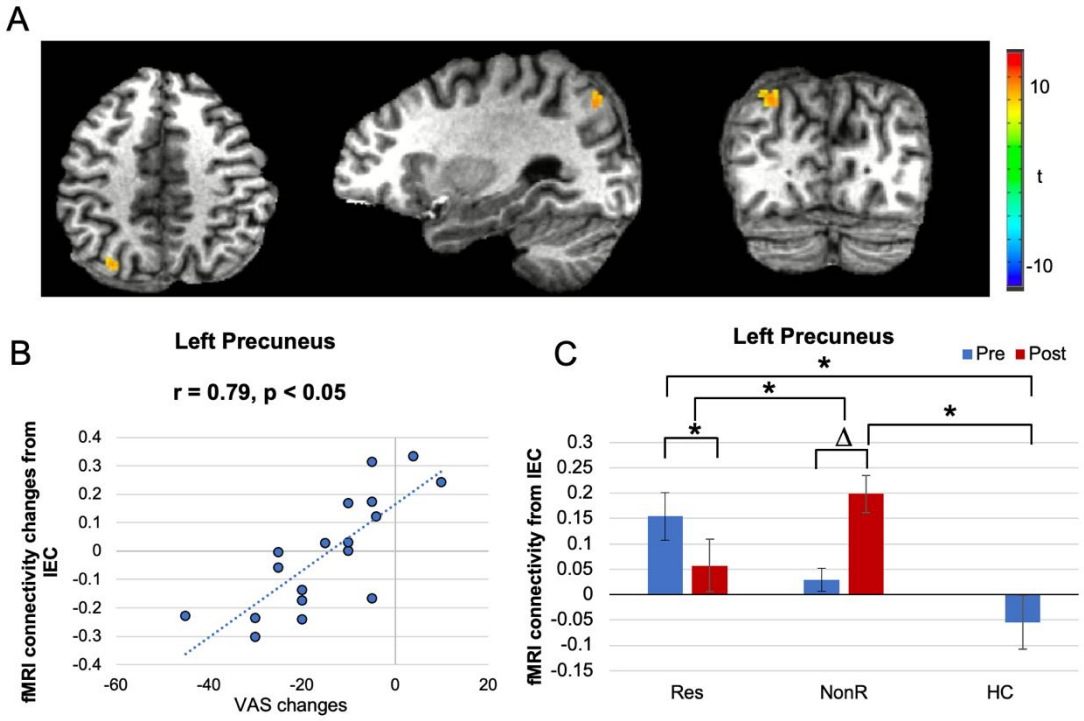

Figure 4-1: Connectivity at left precuneus regarding lEC was positively associated with clinical responses. (A) the scatterplot between fMRI changes and VAS changes. (B) the scatterplot between fMRI changes and VAS changes. (C) connectivity level among positive responders before-, after- tACS, and Healthy Control. * Indicates $p < 0.05$, Δ indicates $p < 0.1$. Res: Responders; NonR: Non Responders (Chen et al., In preparation).

For both lEC and rEC, the left precuneus was identified as a strong clinically relevant brain site. ROI analysis from the left precuneus was illustrated as the scatter plot (**Fig. 4-1B and 4-3B)** in which EEG changes covary with VAS changes. Furthermore, to explore how this region manifested in the healthy brains, we included healthy data from this specific ROI and all three conditions shown together as in a bar plot (**Fig. 4-1C and 4-3C)**. Specifically, we focused our attention on the positive responder subgroup (VAS reduction greater than 10 points, 12 patients) as this was the most relevant to the purpose

of featuring the responsive brain using EEG as a response biomarker. Through t-test, we found the significant difference in pre-tACS imaging compared with healthy was suppressed in after-tACS at left precuneus (**Fig. 4-1C**).

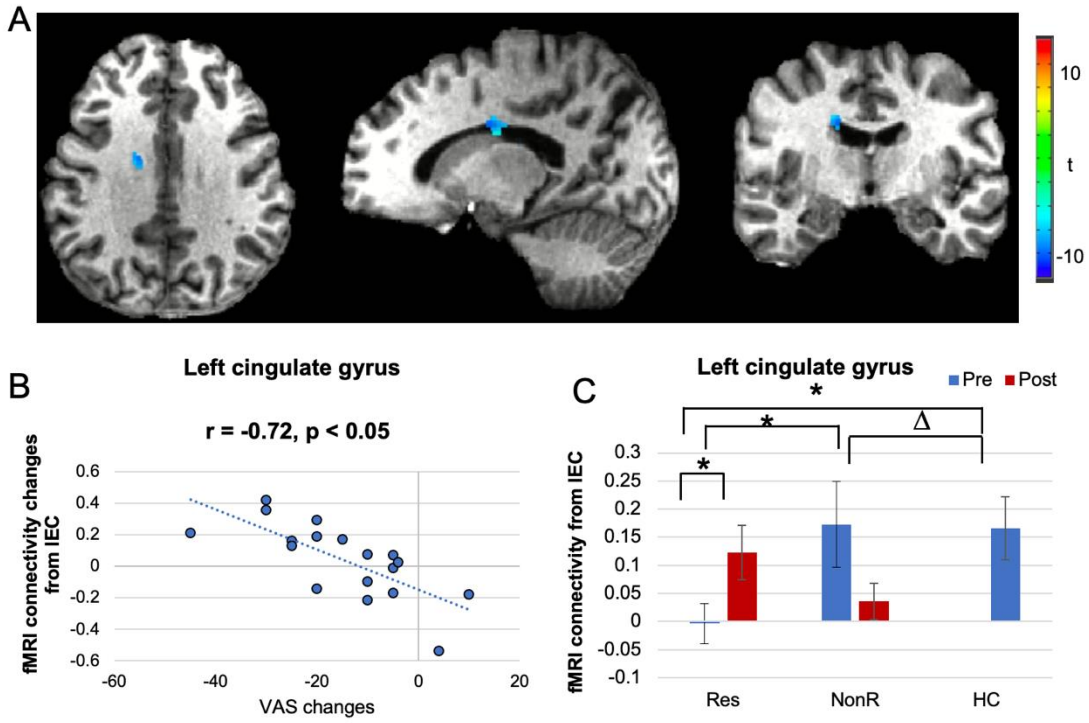

Figure 4-2: Connectivity at the left cingulate gyrus regarding lEC was negatively associated with clinical responses. (A) topography of the left cingulate gyrus. (B) the scatterplot between fMRI changes and VAS changes. (C) connectivity level among positive responders before-, after- tACS and Healthy Control. * Indicates $p < 0.05$, Δ indicates $p < 0.1$. Res: Responders; NonR: Non Responders (Chen et al., In preparation).

In contrast, in the connectivity between left cingulate gyrus with lEC (**Fig. 4-2A**), there was an opposite trend, which indicated an increase in the connectivity following tACS and also a higher connectivity in the HC group (**Fig. 4-2C**). The scatter plot between clinical responses and fMRI connectivity changes was illustrated in **Fig. 4-2B**.

4.4 Discussion

In this chapter, we specifically investigated EC-based fMRI connectivity in MdDS patients in order to find the imaging alterations that could link to positive clinical responses. We used EC as the seed as it played a critical role in distinguishing healthy versus MdDS in our previous PET study (Cha et al., 2012). Furthermore, by including healthy data into our ROI analysis, we aimed to examine how the therapy drove the MdDS brain with regard to the healthy brain so to provide further insight into the therapeutic mechanism of tACS.

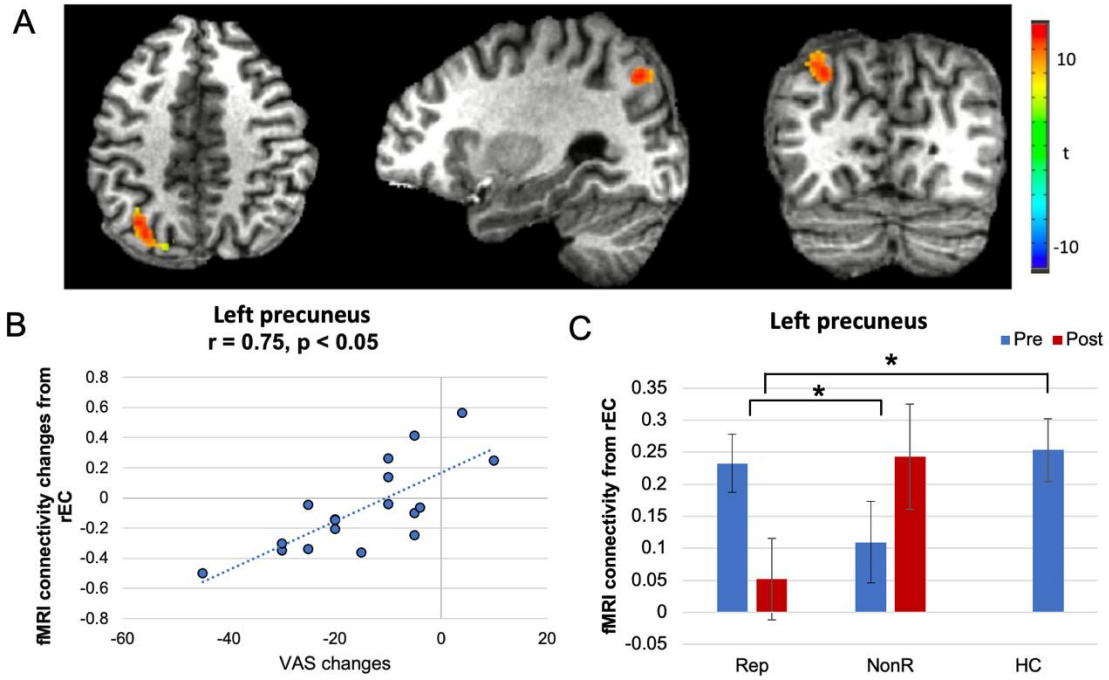

Figure 4-3: Connectivity at the left precuneus regarding rEC was positively associated with clinical responses. (A) topography of the left precuneus. (B) the scatterplot between fMRI changes and VAS changes. (C) connectivity level among positive responders before-, after- tACS and Healthy Control. * Indicates $p < 0.05$ (Chen et al., In preparation).

The EC located in the medial temporal lobe is closely coupled with DMN (Kahn et al., 2008) and has been associated with extensive cognitive function performance

(Braak and Del Tredici, 2011; Das et al., 2013; Tisserand et al., 2000). Indeed, we identified mostly DMN regions that showed clinical relevance, including left and right precuneus, left and right parietal lobule, multiple temporal regions as well as the cingulate gyrus. However, their associations with the clinical changes were not uniformly positive. Instead, the covariation features were highly dependent on which layer of the brain they were located in. For example, most of the cortical regions such as precuneus and temporal gyrus exhibited decrease or less increase of connectivity in positive responders (**Fig. 4-1 and Fig. 4-3**), while the cingulate gyrus in the subcortical brain primarily exhibited opposite trends in positive responders (**Fig. 4-2**).

We also integrated healthy data into the ROI analysis. We have seen psychiatric disorders such as depression, report normalization of the dysconnectivity of brain networks towards healthy brain after rTMS administrations (DeGiorgio et al., 2014). Similarly, in this study, we observed a correction at the left precuneus and cingulate gyrus prevalent in positive responders. However, the direction of imaging responses compared with healthy were less uniform than we expected, and partly different than our previous rTMS study (Yuan et al., 2017), which has found a positive correlation between resting state fMRI connectivity changes within DMN regarding lEC and clinical improvement. In fact, the versatility of the normalization effect has already been revealed by depression related investigations (Liston et al., 2014; Philip et al., 2018) and in a comprehensive meta-analysis (Kaiser et al., 2015), depression was considered as a result of combined hyper- and hypoconnectivity across various brain networks. To this end, MdDS could potentially be caused by a combination of dysfunctional networks and therefore the therapeutic impact revealed by fMRI appeared to be mixed. One factor that could account

for the discrepancy between two MdDS studies was the difference of administration protocols (Yuan et al., 2017). In this regard, tACS might be more powerful in augmenting brain connectivity than rTMS (Eldaief et al., 2011; Oliviero et al., 2003) in which attenuation of brain connectivity was easily achieved and consequently discovered. Finally, an intriguing question to ask is whether this rectification of brain connectivity is causally related to the symptoms improvement or just represents an association. Answering this demands a more sophisticated experiment design including measures to eliminate potential interferences, such as a sham group to control the placebo effect and the effect of peripheral nerve stimulations during the treatment, et cetera.

To conclude, the therapeutic role of tACS was preliminarily defined as suppressing EC-based fMRI connectivity at left precuneus and augmenting that of certain subcortical regions. Lack of a sham control is the major limitation of this study. Also, the relatively small sample size (22 patients, 14 healthy) limits the interpretation range of this study. Methodologically, the normalization across individual subjects was not perfect, especially when EC is far away from the normalization center (anterior commissure and posterior commissure) which could invisibly impact the alignment of statistical maps in the group-level analysis.

5. Chapter 5: Customizing Stimulation Parameters Based on Individual Imaging Features

In this Chapter, I have investigated the transient effect associated with a single administration of noninvasive brain stimulation, as opposed to the lasting effect of repetitive stimulations that was studied in **Chapters 2, 3 and 4.** The rationale for studying the transient effect was to seek a try-out design in the treatment protocol, such that a patient could have a test session with brief stimulations in various parameters, for example different targets or frequencies, prior to a fixed stimulation being repetitively performed. This is analogous to the process of patients trying out different medications, but at a much-accelerated timeline of within a single session rather than after a few days or weeks. This design is also motived by a paradigm shift towards closed-loop brain stimulation in a number studies of brain disorders (Bouthour et al., 2019; Kokkinos et al., 2019; Scangos et al., 2021; Widge et al., 2017). Based on the individual feedback at the try-out session, a favorable stimulation parameter could be selected among various options that are tested, then a single stimulation setting as selected will be repetitively administered in a protocol that could last for multiple days. We hypothesize that neuroimaging data could inform the selection of an optimal stimulation at the try-out stage, in conjunction with or replacing the patient's self-report. Therefore, in this chapter, I have analyzed the EEG data before and immediately after single, try-out stimulations of cTBS at three different targets. My analysis has determined that the EEG signatures can differentiate the optimal and non-optimal targets as indicated by subjects' self-report.

5.1 Introduction of transient EEG in cTBS

Our cTBS study included a try-out session at the beginning of the protocol administration: each participant initially received single administration of simulation at three targets, i.e., occipital cortex, cerebellar vermis, and lateral cerebellar hemisphere. Since changes in the connectivity of the DMN and the visual network were closely related to symptoms in MdDS (Cha, 2009; Chen et al., 2019; Ding et al., 2014; Yuan et al., 2017), the target regions of stimulation were in the dorsal occipital cortex and cerebellar vermis, which are functionally connected to the fronto-parietal regions. Continuous TBS was employed in this study because of the higher pain inducing effects of stimulation over the neck area that required a more time-limited protocol. Since cTBS is a much shorter protocol than standard 1Hz or 10Hz sessions, we were able to provide a more tolerable therapy as well as to provide back-to-back sessions of treatment on the same day. Then an optimal target was determined based on the assessment of acute changes after each single administration, followed by repetitive cTBS delivered on 3 consecutive days with the chosen optimal targets. However, another key remaining question is whether any symptom related changes in neural circuits were induced by cTBS, immediately after single administration. An indicator or biomarker that signals immediate effect independent of patient's self-report is informative for target selection, especially when patients were unable to perceive or report any responses.

We extended our investigation of networks to the concurrent EEG recording during the try-out sessions of cTBS, for the purpose of identifying early changes in the brain network connectivity. The transient effect measured by EEG can be used to inform

the determination of optimal targets, thereby enabling an imaging-based, closed-loop stimulation paradigm that is independent of patients' behavioral report.

5.1.1 Concurrent cTBS-EEG acquisition

In our 5 days cTBS treatment, simultaneous EEG and fMRI were collected on Day 1 before the cTBS administration and Day 5 after the cTBS administration. To examine EEG as a potential predictive biomarker in guiding cTBS parameters, on Day 2, we included a concurrent cTBS-EEG session which targeted three feasible sites and had the patient pick the best protocol to go on based on their direct response report that day. Participants received 600 pulses of testing cTBS at three locations in a randomized order between participants, including occipital, cerebellar vermis, and lateral cerebellar hemispheres. Concurrently with cTBS, 32-channel EEG data were recorded by a BrainAmp MR Plus amplifier (Brain Products GmbH, Munich, Germany) with sintered Ag/AgCl ring electrodes following the standard 10-20 system. Ten KΩ was the impedance upper limit for all 32 EEG electrodes. Sampling rate was 5000 Hz. A 5-min EEG resting state recording was acquired immediately before and after the cTBS stimulation at each location. In one participant, one of the post-stimulation EEG data was not available due to technical failure and therefore excluded from the Day 2 analyses. The best protocol from Day 2 was adopted for Day 3-5 for each individual patient.

5.1.2 Analysis of EEG on 2nd day in cTBS

On the 2nd day of the study protocol, a try-out session of cTBS was performed when stimulations at three different sites (i.e., occipital, cerebellar vermis, and lateral cerebellar hemispheres) were given to each patient; only one site was chosen as the optimal target for repetitive stimulation afterwards. We employed EEG network analysis

to examine the transient modulation on EEG connectivity immediately after a try-out stimulation at occipital, cerebellar vermis, and lateral cerebellar hemispheres, for the long-term purpose of establishing a closed-loop stimulation paradigm based on the EEG network analysis. From the concurrent TMS-EEG recordings at cTBS session, only the resting-state data immediately before and after stimulation were analyzed, without any TMS-induced artifacts. Firstly, EEG data were down-sampled to 250 Hz and independent component analysis was applied to remove artifacts related to eye movements, muscular and cardiac activities. Bad channels with excessive artifacts were discarded via visual check and replaced by an average of its nearby four channels. High-pass filtering at 0.5 Hz and low-pass filtering at 70 Hz was applied. Then all channels were re-referenced to the common average reference. After preprocessing, source images were calculated following the steps described above for the simultaneous MR-EEG signals. Because only 31 channels of EEG were acquired on the 2nd day TMS-EEG setting, the lead field was selected from a subset of the model built for the 126-channel EEG.

Then we investigated the transient effect of EEG connectivity changes on the 2nd day associated with cTBS stimulations at each location. We utilized the projecting matrix that was derived from the high-density EEG recordings before and after the entire cTBS protocol and applied the projecting matrix to obtain the connectivity maps immediately before and after cTBS to each location. In particular, the projecting matrix for the selected network was applied to every patient's continuous source time courses to calculate the time course of the network. Then, the Pearson correlation coefficient between the time course of each network and the time courses of source dipoles on the cortical surface area for each participant was calculated, resulting in a map of correlation coefficients as the

EEG connectivity map. Similarly, Fisher's transform and spatial smoothing were applied. Then "Post-minus-pre-connectivity" maps represent the connectivity changes after cTBS, which were calculated by subtracting the pre-cTBS map from the post-cTBS map for each participant and to each location on the 2nd day.

In our current cTBS protocol, at the Day 2 test sessions, the optimal and non-optimal targets were determined by each participant's self-report of symptoms. We determined whether connectivity metrics that became apparent after a full stimulation battery by Day 5 could have some signatures that were detectable on the test sessions on Day 2. Initially, the optimal target was determined subjectively as the one leading to the greatest reduction in VAS within 60 minutes after stimulation. In our investigations, we explored linear discriminant analyses to classify the optimal vs. nonoptimal targets based on the network connectivity changes from EEG data immediately before and after stimulating test targets, for the purpose of determining whether the EEG recordings only could predict optimal target selection. We chose linear discriminant analysis because it is a robust classifier commonly reported to out-perform many nonlinear classifiers in brain-computer interface studies (He et al., 2020), especially considering the relatively small sample size of our study.

Specifically, the EEG connectivity changes that were calculated in ROIs were used as features in the discriminant analysis. Only data that were labeled with optimal target or non-optimal target were used for training classifiers. Then we adopted a leave-one-out-cross-validation strategy for training the classifier: one target was selected as the test data while all others served as the training data, which repeated until all targets were exhausted as test data. The coefficients of a linear classifier were calculated according to

the Fisher criteria (Fisher, 1936). The performance of the classifier was evaluated based on the leave-one-out data from all repetitions. Based on classification outcomes of test data, we calculated the percentage of true positive (optimal target classified as optimal target), true negative (non-optimal target as non-optimal target), false positive (non-optimal target as optimal target) and false negative (optimal target as non-optimal target).

Furthermore, in those participants who were not able to perceive any favorable target associated with reduction of symptoms (5 out of 23), their targets were considered as undecided targets in our analyses. Therefore, we applied a trained discriminant classifier from all labeled data to the recordings with undecided targets in order to explore whether the neural signatures in those undecided targets are different from those of favorable targets.

5.1.3 Results

We analyzed EEG data test sessions of cTBS on Day 2, when single-administrations of cTBS were delivered at three different targets in a sequential and randomized order. In 18 out of 23 participates, optimal targets were chosen by the participants because of the greatest reductions of scores on the VAS after stimulation, while the other two targets were deemed as non-optimal targets. Five participants did not choose any target and all targets in these patients were considered as undecided targets. Three were randomly assigned to each of the three targets; one worsened with all targets and was treated over the precuneus, and one did not complete the study but had Day 2 data available. On Day 2, after single-administration of cTBS, the VAS changes for the optimal targets were -6.23 ± 1.55 (range -20 to 10), the VAS changes for the non-optimal

targets were 0.89 ± 1.83 (range -15 to 40), and VAS changes for the undecided targets were 2.63 ± 1.08 (range -5 to 10).

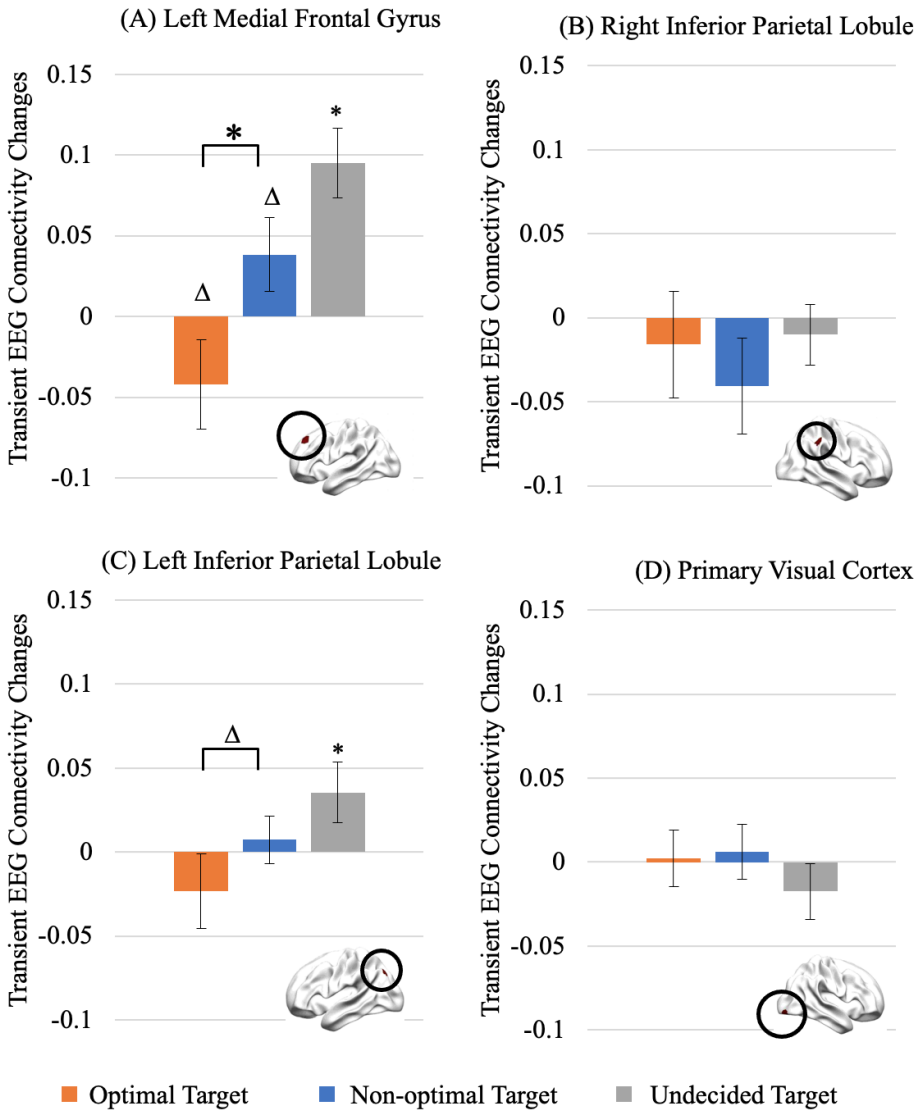

Figure 5-1: Transient changes in EEG network connectivity at try-out sessions. Connectivity changes immediately after single administration of cTBS are derived from left medial frontal gyrus (A), right inferior parietal lobule (B), left inferior parietal lobule (C), and primary visual cortex (D). The activities are grouped by whether the targets were selected as optimal targets, non-optimal targets, or considered as undecided targets. * Indicates significance at $p < 0.05$. D Indicates approaching significance at $p < 0.1$ (Chen et al., Under Review).

Our analysis examined whether transient changes could be detected in the EEG networks following single test sessions of cTBS. Specifically, we took a retrospective approach to quantifying the transient EEG network changes on Day 2 data by using ROIs defined in the Day 5 analyses, i.e., the regions that showed modulations that correlated with symptom changes after completion of the protocol. We analyzed in each category (optimal or non-optimal target), whether differences exist in the EEG network connectivity immediately after the test stimulation sessions relative to the baseline. Additionally, we also compared the transient changes between categories (i.e., optimal vs. non-optimal targets). **Figure 5-1** shows the results in ROIs corresponding to four EEG networks – the right IOG, the left MFG, the left IPL and right IPL. In the ROI at the left MFG (**Fig. 5-1B**), the transient EEG changes after single administration of cTBS were significantly different between the optimal and non-optimal targets ($p = 0.02$), while the decrease for the optimal targets and the increase for the non-optimal targets respectively approached significance ($p = 0.1$). In addition, in the ROI of the left IPL network (**Fig. 5-1C)**, the transient EEG changes after single session stimulation showed a difference approaching significance between the optimal and non-optimal targets ($p = 0.06$). Meanwhile, no significant transient changes were observed in the ROIs at the right IOG or the right IPL.

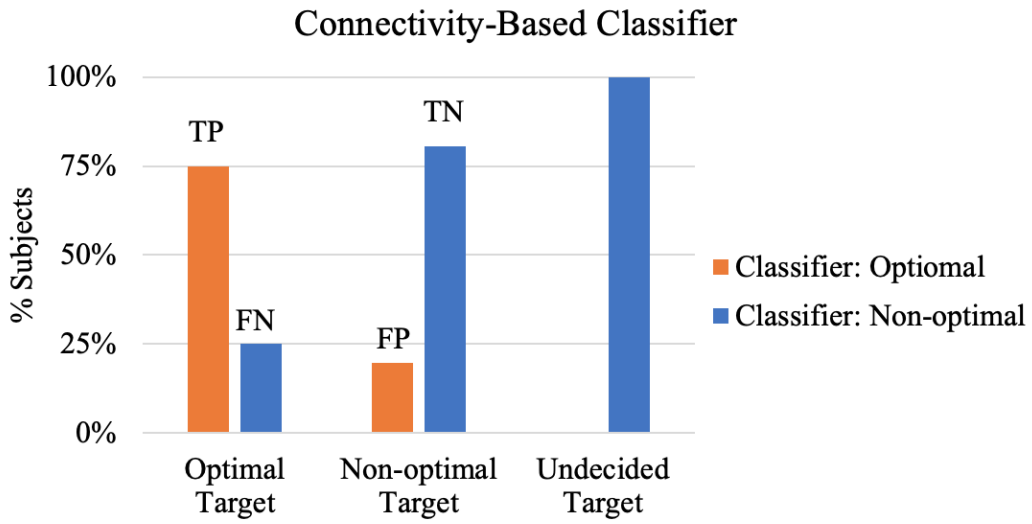

Figure 5-2: Transient changes in EEG network can predict the optimal vs. non-optimal targets. True positive, false negative, true negative and false negative are displayed for the classification results of a linear discriminate classifier (LDA) with leave-one-out cross validation (LOOCV). Based on the connectivity features, all undecided targets were automatically classified as non-optimal targets (Chen et al., Under Review).

In the other 5 participants, no optimal targets with favorable reduction of symptom were chosen, therefore all their targets were considered as undecided targets. The transient EEG connectivity changes are also plotted in **Fig. 5-1**. In the ROI at the left MFG, the undecided targets exhibited a strong increase in connectivity ($p = 0.03$), which appeared in the same direction as nonoptimal targets and opposite to the optimal target in the patients that had decided targets. Likewise, in the ROI at left IPL, an increase in EEG connectivity was observed after stimulating undecided targets ($p = 0.03$), which also appeared in the opposite direction as optimal targets.

We explored whether the EEG transient connectivity changes could be used to distinguish optimal targets from non-optimal targets. By using an LDA classifier and a leave-one-out cross validation strategy, the overall accuracy of prediction was 79.3%. As shown in **Fig. 5-2**, the classifier yielded 75% accuracy in predicting optimal targets (i.e., TP = 75%), whereas a slightly higher accuracy of 80% was obtained in predicting non-

optimal targets (i.e., TN = 80%). The false negative rate (FN = 25%) was slightly higher than the false positive rate (FP = 20%). Importantly, when applying the classifier that was trained by all optimal and non-optimal targets to the data in undecided targets, all targets of the undecided category were automatically classified as non-optimal targets.

5.1.4 Discussion

This current study for the first time has revealed the transient changes of network connectivity after single administration of cTBS, when multiple targets were tried out before an optimal target was selected to continue repetitive stimulations. Our analysis of using a ROI approach demonstrated that regions of symptom-associated modulation at completion of protocol also exhibited early transient changes at single administration of stimulation. Particularly, the left medial frontal gyrus showed a significantly greater decrease in connectivity when the optimal targets were stimulated compared with the non-optimal targets. Likewise, the left inferior parietal lobule exhibited larger decrease of connectivity which approached significance for the optimal targets, whereas the right inferior showed some modulation in an opposite trend. By combing the three nodes of the DMN, we have developed an LDA classifier that was built on the transient changes as features to classify the optimal vs. non-optimal targets. Leave-one-out-cross-validation has demonstrated that the classifier achieved an overall accuracy of 79.31%. More interestingly, we further applied the trained classifier to those undecided targets when self-reports indicated no favorable targets, and all of the undecided targets were classified to be non-optimal targets. Our results suggest a possible closed-loop paradigm that is based on the early, transient network changes, such that optimal target can be determined

by a try-and-choose approach. Notably, the imaging-based biomarker is objective and independent of self-reports, which can facilitate physicians in deciding optimal targets.

5.2 tACS parameters

Table 5-1: tACS parameters regarding phase and frequency in 22 patients (Chen et al., In preparation).

Subject ID	Phase conditions	Stimulation frequency (Hz)	Stimulation relative to IAF (Hz)
S1	in-phase	10	-0.4
S2	anti-phase	10	-0.4
S3	anti-phase	8.6	0
S4	anti-phase	10.1	0
S5	anti-phase	11.2	0
S6	in-phase	11.4	0
S7	in-phase	11.4	0
S8	anti-phase	10.5	0.1
S9	in-phase	8.5	0.2
S10	anti-phase	9	0.4
S11	anti-phase	10	0.4
S12	anti-phase	10	0.4
S13	anti-phase	10	0.7
S14	in-phase	10	1.2
S15	anti-phase	10	1.2
S16	anti-phase	10	1.3
S17	anti-phase	10	1.3
S18	in-phase	10	2.1
S19	anti-phase 40Hz	40	30.3
S20	anti-phase 40Hz	40	31

S21	anti-phase 40Hz	40	31.1
S22	anti-phase 40Hz	40	31.9

tACS is a promising neuromodulation tool which can directly modulate the brain oscillations and therefore facilitates probing the causal link between brain oscillations and its cognitive functions (Feurra et al., 2011). The precise knowledge of neurophysiological alterations when tACS is applied is not yet clear (Thut et al., 2011). More specifically, tACS using individual alpha frequency as the reference achieved a strong neural synchrony (Vossen et al., 2015; Zaehle et al., 2010). Thus, in our current study, we used the individual alpha frequency (IAF) to customize the stimulation frequency with aim of exerting strong external oscillations to intervene the current disturbance of neural signals (potential disconnection of DMN and the visual network). To this end, the phase of tACS was also under serious consideration as 0^o (in-phase) might potentiate neural synchrony while 180^o (anti-phase) could offset or impair the underlying synchrony between segregated regions (Polanía et al., 2012; Strüber et al., 2014). We randomized the in-phase and anti-phase conditions among 22 patients and **Table 5-1** tabulated the mixed phase and frequency parameters for individual patients.

5.2.1 patients grouped by phase conditions in tACS

In this protocol, tACS EEG data were collected as described in **Chapter 2.3.2**. The phase conditions were randomized among the patient pool, 6 patients of in-phase, 12 of anti-phase, and 4 of 40 Hz. The phase condition was an important factor to take into account as tACS has been shown to disrupt the brain oscillations between remotely linked regions with anti-phase (Polanía et al., 2012) but strengthen the brain synchronizations in in-phase set ups. To look into the clinical changes and EEG connectivity changes across

3 conditions, one-way ANOVA was used and post-hoc test afterwards. We used anti-phase 40 Hz as a control and expected the anti-phase at around IAF achieved better clinical responses and corresponding neural oscillation alterations revealed.

5.2.2 patients grouped by IAF frequencies in tACS

The strategy of setting up stimulation frequency was based on the individual alpha frequency (IAF) from the prior EEG recording. Patients were grouped as 7 patients at IAF (two were slightly lower than IAF), 10 patients at IAF+ (0.1-1.3Hz above IAF), and 5 patients at IAF++ (frequency greater than IAF+1.3Hz). The IAF has been reported as an important assisting parameter as tACS responses of the brain might be state-dependent (endogenous brain oscillations) (Neuling et al., 2013; Ruhnau et al., 2016) (Feurra et al., 2011). Thus, using the IAF to guide the tACS would potentially give the most robust modulation as the tACS may resonate with the intrinsic brain oscillation and interact with it directly under certain stimulation phases. In this tACS study of combined stimulation frequencies and phase conditions, we expected a combination of IAF guided stimulation and anti-phase condition could give more optimal clinical benefits than other alternatives. To look into the clinical changes and EEG changes across 3 conditions, one-way ANOVA was used and post-hoc test afterwards.

5.2.3 Results

In the first categorization by phase conditions, the anti-phase condition displayed significant improvement after treatment (paired t-test, $p < 0.05$), but none of the 3 subgroups showed significant clinical improvement greater than other two (ANOVA, $p > 0.005$) **(Fig. 5-3A**). We did observe significant EEG connectivity changes at the right cuneus that could differentiate the stimulation phases (**Fig. 5-6A**). The anti-phase 40Hz

protocol was able to reduce the EEG connectivity at the right cuneus while both in-phase and anti-phase failed to do so. No significant EEG connectivity changes were observed at the right medial frontal gyrus and the left cuneus (**Fig. 5-4A and 5-5A**).

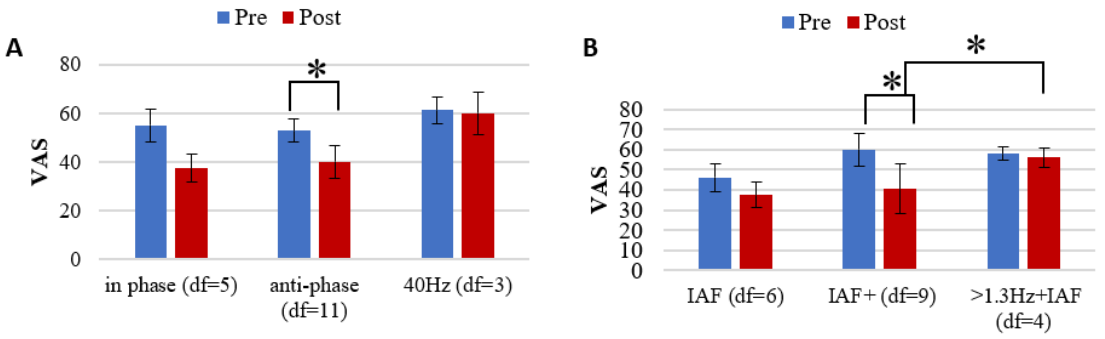

Figure 5-3: VAS across three subgroups. (A) is subgrouping patients by phase conditions and (B) is by stimulation frequencies. * indicates $p < 0.05$ (Chen et al., In preparation).

In the second categorization by stimulation frequencies, the IAF+ (0-1.3 Hz above IAF) significantly improved the symptoms than IAF++ (greater than 1.3 Hz + IAF) (**Fig. 5-3B**). The EEG network connectivity at the right cuneus significantly increased in the IAF+ than the other two groups (**Fig. 5-6B**). The left cuneus connectivity decreased within the IAF++ group (**Fig. 5-5B),** but not between subgroups (ANOVA $p > 0.05$). No significant EEG connectivity changes occurred at the right medial frontal gyrus (**Fig. 5-4B**).

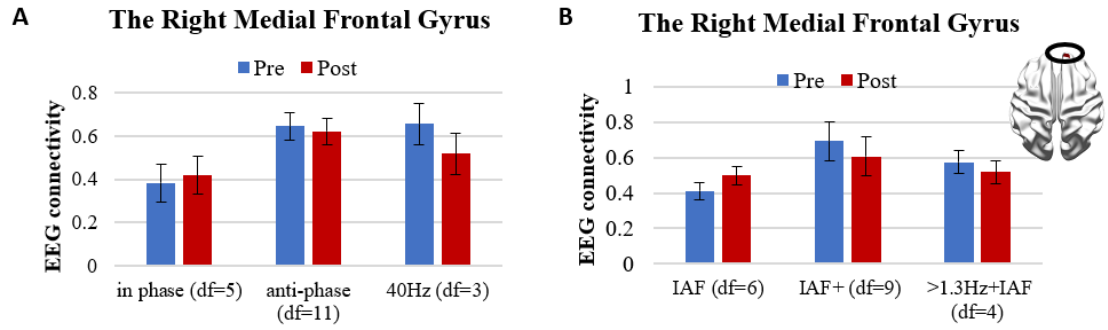

Figure 5-4: EEG changes across three subgroups at the right medial frontal gyrus. (A) is subgrouping patients by phase conditions and (B) is by stimulation frequencies. IAF:

stimulation frequency right at IAF or slightly lower; IAF+: 0-1.3Hz above IAF; >1.3Hz+IAF: greater than IAF+1.3Hz. * indicates $p < 0.05$ (Chen et al., In preparation).

5.2.4 Discussion

Previous studies have identified that the pre-stimulation state of the individual brain oscillation dictates the ensuing tACS effect and therefore encouraged the customized stimulation paradigms (Meier et al., 2019). A meta-analysis found individually tailored stimulations benefited the cognitive performance more than a standardized approach (Schutter and Wischnewski, 2016). Thus, in this section, we explored how different stimulation parameters might impact the brain responses.

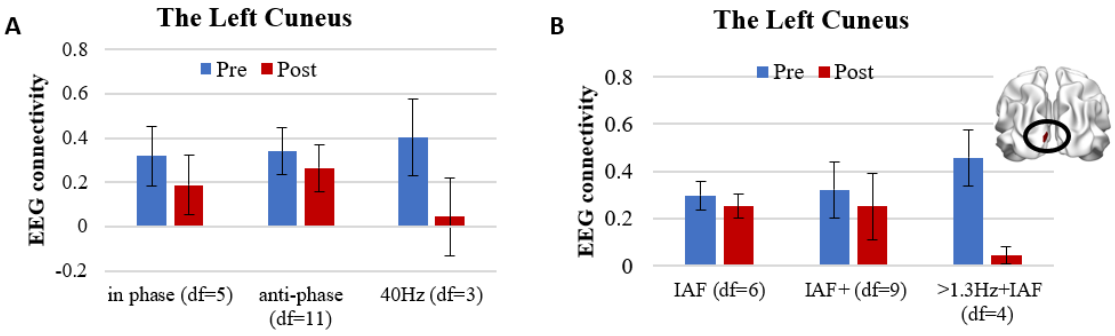

Figure 5-5: EEG changes across three subgroups at the left cuneus. (A) is subgrouping patients by phase conditions and (B) is by stimulation frequencies. IAF: stimulation frequency right at IAF or slightly lower; IAF+: 0-1.3 Hz above IAF; >1.3Hz+IAF: greater than IAF + 1.3 Hz. * indicates $p < 0.05$ (Chen et al., In preparation).

In our analysis grouping patients by tACS phase conditions, we investigated the EEG after tACS and the clinical improvement in each subgroup. We did not observe a significant clinical improvement between subgroups by phase conditions, but the EEG at the right cuneus was significant reduced by anti-phase 40 Hz than the in-phase. 40Hz is within the range of gamma frequency, which was used as a control in several tACS experiments (Alexander et al., 2019; Grabner et al., 2018), but in our study, it displayed strong disrupting effects in the parietal regions. In fact the gamma frequency was reported

to impact the brain in previous studies (Tseng et al., 2016), where in-phase gamma oscillations showed no faciliatory or inhibitory effect but behavioral impact manifested from the anti-phase gamma stimulation. This imaging phenomenon might also be attributed to cross-frequency effects, as reported previously, 40Hz tACS might interfere with the power at 10Hz in an antagonistic manner (Helfrich et al., 2014a). Lastly, we did not set up any phase condition between 0^{o} (in-phase) and 180^{o} (anti-phase) to explore the optimal tACS phase for MdDS. Because the neural signals require time (at the millisecond level) to travel through axons and synapses, the consequent time lag between any connected regions could be a potential factor that affects the responses to different phase conditions of tACS (Gregoriou et al., 2009).

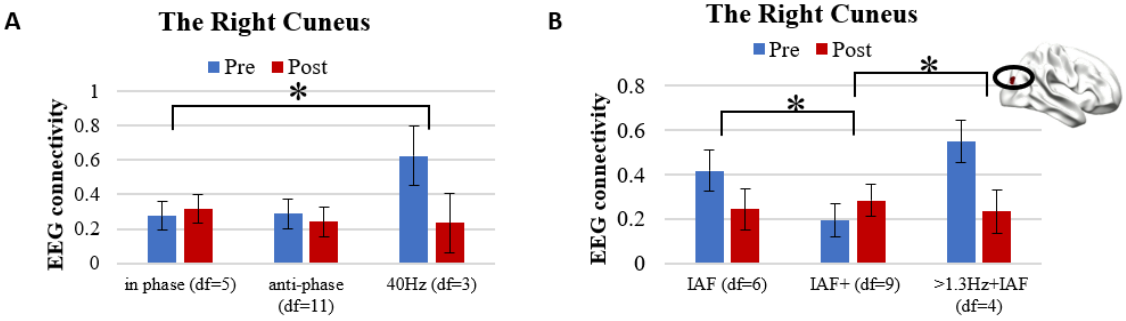

Figure 5-6: EEG changes across three subgroups at the right cuneus. (A) is subgrouping patients by phase conditions and (B) is by stimulation frequencies. IAF: stimulation frequency right at IAF or slightly lower; IAF+: 0-1.3 Hz above IAF; >1.3Hz+IAF: greater than IAF + 1.3 Hz. * Indicates $p < 0.05$ (Chen et al., In preparation).

In our frequencies grouped results, we used IAF to guide the tACS stimulation and found significant clinical improvement within IAF+ (**Fig. 5-3B**) which was significantly improved than IAF++. Corresponding to the clinical improvement, the EEG connectivity at the right cuneus in IAF+ was significantly different than other two groups, which indicated IAF+ as the most effective in inducing clinically relevant changes. Slower IAF (-2Hz) or faster IAF (+2Hz) were reported to modulate the brain differently

(Mioni et al., 2020). Indeed, we noted the slightly above IAF stimulation was therapeutically more effective instead of exactly matching the IAF or largely above the IAF (**Fig. 5-3B**). However, we did not see any significant changes in imaging within IAF+ group. Taken together with what we found in **Chapter 2.3**, this might suggest that the oscillatory network was not the primary target of tACS and a more direct way of looking at tACS impact could be the brain oscillations in different frequencies.

6. Chapter 6: Summary

Overall, this dissertation has investigated neuroimaging biomarkers in MdDS for noninvasive brain stimulation tools. By collaborating with a neurologist, I have analyzed the multimodal EEG and fMRI data in cohorts of patients receiving three different noninvasive brain stimulations as experimental treatment (rTMS, cTBS and tACS). I have utilized a suite of computational methods for EEG and fMRI. Especially, I have developed a data-driven method to extract and quantify the functional connectivity of resting-state brain networks as biomarkers.

The first key outcome of my investigation was the development of the response and predictive biomarkers in EEG data by evaluating the network-level activities with the clinical symptom changes after brain stimulations in MdDS. The rTMS has been seen to reduce the connectivity of positive responders more than that of negative ones (in the medial frontal gyrus, a key node of DMN), which indicates reducing brain connectivity is a promising treatment option for choosing brain stimulation protocols. In addition, I have found that a higher baseline connectivity is shown to relate to better rTMS efficacy, which indicates that individuals with higher baseline connectivity may be more receptive of the protocol with benefits. The biomarkers are observed close to stimulation sites, stemming from the medial frontal region for the DLPFC with rTMS and inferior parietal regions for the occipital cTBS. The imaging biomarkers from the visual network in conventional rTMS and cTBS originate from a consistent anatomical structure: the right occipital gyrus. However, the tACS EEG has revealed a reversed, negative association with clinical responses in parietal regions that is different from rTMS or cTBS, showing increased connectivity corresponds to symptom improvement.

In addition, my investigation of the cross-modal relationship has found that fMRI supports EEG in certain ways. The results indicate that fMRI changes in the region corresponding to the EEG biomarker (the DMN) show a strong association with EEG signal alterations after rTMS on DLPFC, but a weaker association in cTBS. The EEG-informed fMRI GLM in cTBS contains the key regions of EEG network (the precuneus in DMN) and also involves other regions that are not directly linked to the symptom-correlated EEG network activities. Despite the cross-modal consistency observed in rTMS and cTBS, EEG-informed fMRI in tACS exhibits different findings from rTMS or cTBS, showing mostly anti-correlations using EEG as the electrophysiological correlates in fMRI BOLD signals.

Furthermore, I have investigated the mechanism of noninvasive brain stimulation by comparing the fMRI resting state functional connectivity in post- vs. pre-stimulation of MdDS and healthy controls. In the positive responders of MdDS receiving stimulations, the connectivity between the left EC with regard to the left precuneus was significantly decreases after stimulation, while such connectivity in pre-stimulation MdDS was abnormally higher than that in HC. In addition, in the positive responders, the connectivity between the left EC and the left cingulate gyrus was increased after stimulation, being closer to the higher level of connectivity in HC. Nonetheless, the connectivity between right EC and left precuneus was significantly decreased by stimulation in the positive responders, although the connectivity of the pre-stimulation MdDS was at a par level with that in HC. These findings indicated the effect of stimulation as modifying the connectivity in symptom-relevant networks. The modifications in part have rectified the abnormal hyper- or hypo-connectivity in MdDS,

especially in regions connecting the entorhinal cortex and parts of the default mode network. Noteworthy, however, the stimulation also affects other regions in different directions of modulations.

Based on the imaging biomarkers that are consistently discovered across protocols, the feasibility of using real-time EEG features to guide noninvasive brain stimulation application has been tested and demonstrated. There are significant imaging-based differences in our cTBS protocol between optimal versus non-optimal stimulation sites when all were administered as a single, try-out setting to patients, which hints that the imaging features could be used to tailor the stimulation protocol to individual patients before a repetitive and full protocol being performed to achieve optimal therapeutic effects. Additionally, individual EEG features (i.e., individual alpha frequency) that were utilized to guide the tACS protocol parameters have demonstrated an increased efficacy.

Limitations

Notably, several factors limit the interpretation of my dissertation work. First, we did not arrange any sham arms in the investigation of noninvasive brain stimulation effects. Thus, placebo effects could not be ruled out as a contributing factor to the clinical improvement. Nevertheless, across three protocols, individuals were medically refractory, having failed two medication trials and physical therapy. Placebo effects are generally minor in medically refractory groups (Li et al., 2018; Liston et al., 2014), but cannot be completely ruled out. Second, the sample size was relatively small due to MdDS being a rare disorder (Cha, 2015; Cha, 2009). Future work should seek to increase the sample size in a single stimulation protocol. In the meantime, integrating imaging analysis in a combined responsive group across different protocols could also be

investigated in order to increase the sample size, since my work here has suggested certain homogenous biomarker between protocols (such as rTMS and cTBS).

Outlook

My dissertation work has suggested that, in future clinics, patients could go through brief, try-out sessions before settling into a fixed protocol for repetitive treatment stimulations. With the acquired information on the brain imaging responses to the try-out protocols, we can then take advantage of the imaging biomarkers described in my dissertation to guide the clinicians in customizing the protocol parameters for each individual patient, in order to achieve optimal and long-lasting therapeutic effect. For example, the baseline brain state - in the form of the functional connectivity in resting state brain networks - is an important indicator for certain beneficial TMS protocol. Also, individual alpha frequency of baseline EEG can be referred to when choosing stimulation frequencies. Furthermore, the modification of network connectivity seen in transient EEG after a try-out stimulation can facilitate the determination of an optimal target.

7. Products of This Dissertation

Peer-Review Publications

1. [Under Review] **Chen Y**, Cha YH, Gleghorn D, Doudican B, Shou G, Ding L, Yuan H*: Brain Network Effects by Continuous Theta Burst Stimulation in Mal de Débarquement Syndrome: Simultaneous EEG and fMRI Study.
2. [In Preparation] **Chen Y**, Cha YH, Gleghorn D, Doudican B, Ding L, Yuan H*: Modulation of Brain Networks by Transcranial Alternating Current Stimulation in Mal de Débarquement Syndrome.
3. Shou G, Yuan H, Li C, **Chen Y**, Chen Y, Ding L. Whole-brain electrophysiological functional connectivity dynamics in resting-state EEG. *Journal of Neural Engineering, 2020*. DOI: 10.1088/1741-2552/ab7ad3.
4. Chen Y, Tang J, **Chen Y**, Farrand J, **Yuan H***: Amplitude of fNIRS Resting-State Global Signal is related to EEG Vigilance Measures at Different Body Positions: A Simultaneous fNIRS and EEG Study. *Front. Neurosci.,* 2020. DOI: 10.3389/fnins.2020.560878.
5. **Chen Y,** Cha YH, Li C, Shou G, Gleghorn D, Ding L, Yuan H: Multimodal Imaging of rTMS Effect on Brain Network: A Combined EEG and fMRI Study. *Brain Connectivity,* 2019. DOI: 10.1089/brain.2018.0647.
6. **Chen Y**, Tang J, Li C, Shou G, Gleghorn D, Doudican B, Cha YH, Ding L, Yuan H*: Effect of Body Positions on EEG signals in Mal de Débarquement Syndrome. *Annu Int Conf IEEE Eng Med Biol Soc. 2018 Jul; 2018:1931-1934.* DOI: 10.1109/EMBC.2018.8512699.

7. **Chen Y**, Li C, Shou G, Urbano D, Cha YH, Ding L, Yuan H*: Assessing rTMS Effects in MdDS: Cross-modal Comparison between Resting State EEG and fMRI Connectivity. *Annu Int Conf IEEE Eng Med Biol Soc. 2017 Jul; 2017:1950-1953*. DOI: 10.1109/EMBC.2017.8037231 **(Won Open Finalist among more than 200 submissions in the Student Paper Competition)**.
8. Chen Y, Farrand J, Tang J, **Chen Y**, O'Keeffe J, Shou G, Ding L, Yuan H*: Relationship between Amplitude of Resting-State fNIRS Global Signal and EEG Vigilance Measures. *Annu Int Conf IEEE Eng Med Biol Soc. 2017 Jul; 2017:537-540*. DOI: 10.1109/EMBC.2017.8036880.

Published Conference Abstracts

1. **Chen Y**, Gleghorn D, Doudican B, Cha YH, Ding L, Yuan H: Modulation of Brain Networks by Repetitive Theta Burst Stimulation in Mal de Débarquement Syndrome. *Society for Neuroscience Annual Meeting, Chicago, IL, US, 2019.*
2. **Chen Y**, Gleghorn D, Doudican B, Cha YH, Ding L, Yuan H: Modulation of Brain Networks by Continuous Theta Burst Stimulation in Mal de Débarquement Syndrome. *41st International IEEE EMBC, Berlin, Germany, 2019*.
3. **Chen Y**, Li C, Shou G, Urbano D, Cha YH, Ding L, Yuan H: Effect of Repetitive Theta Burst Stimulation in Mal de Débarquement Syndrome: an fMRI Study. *3rd OU-OUHSC Biomedical Engineering Symposium, Oklahoma City, OK, 2019.*
4. **Chen Y**, Li C, Shou G, Urbano D, Cha YH, Ding L, Yuan H: Assessing rTMS Effects in MdDS: Cross-modal Comparison between Resting State EEG and fMRI Connectivity. *2nd OU-OUHSC Biomedical Engineering Symposium, Oklahoma City, OK, 2018.*

5. **Chen Y**, Li C, Shou G, Urbano D, Cha YH, Ding L, Yuan H: Assessing rTMS Effects in MdDS: Cross-modal Comparison between Resting State EEG and fMRI Connectivity. *8th International IEEE EMBS Neural Engineering Conference, Shang Hai, China, 2017.*
6. Chen Y, Farrand J, Tang J, **Chen Y**, O'Keeffe J, Shou G, Ding L, Yuan H: Amplitude of Resting-State fNIRS Global Signal is related to EEG Vigilance Measures. *8th International IEEE EMBS Neural Engineering Conference, Shang Hai, China, 2017.*
7. **Chen Y**, Li C, Shou G, Urbano D, Cha YH, Ding L, Yuan H: Assessing rTMS Effects in MdDS: Cross-modal Comparison between Resting State EEG and fMRI Connectivity. *1st OU-OUHSC Biomedical Engineering Symposium, Oklahoma City, OK, 2017*.
8. Chen Y, Farrand J, Tang J, **Chen Y**, O'Keeffe J, Shou G, Ding L, Yuan H: Amplitude of Resting-State fNIRS Global Signal is related to EEG Vigilance Measures. *1st OU-OUHSC Biomedical Engineering Symposium, Oklahoma City, OK, 2017.*
9. Farrand J, Chen Y, Tang J, **Chen Y**, O'Keeffe J, Shou G, Ding L, Yuan H: Multimodal Imaging of Human Brain Auditory Responses Using Simultaneous EEG and fNIRS. *1st OU-OUHSC Biomedical Engineering Symposium, Oklahoma City, OK, 2017.*

Poster Presentations

1. **Chen Y**, Li C, Shou G, Gleghorn D, Cha YH, Ding L, Yuan H: Modulation of Brain Networks by Repetitive Theta Burst Stimulation in Mal de Débarquement Syndrome. *OCNS Research Retreat, Oklahoma City, Oklahoma, 2020.*
2. **Chen Y**, Li C, Shou G, Gleghorn D, Cha YH, Ding L, Yuan H: Modulation of Brain Networks by Repetitive Theta Burst Stimulation in Mal de Débarquement Syndrome. *Society for Neuroscience, Chicago, Illinois, 2019 (***awarded Robberson Conference Presentation & Creative Exhibition Travel Grant from OU Graduate College***).*
3. **Chen Y**, Li C, Shou G, Gleghorn D, Cha YH, Ding L, Yuan H: Effect of Repetitive Theta Burst Stimulation in Mal de Débarquement Syndrome: an fMRI Study. *3rd OU-OUHSC Biomedical Engineering Symposium, Oklahoma City, OK, 2019.*
4. **Chen Y**, Tang J, Li C, Shou G, Gleghorn D, Doudican B, Cha YH, Ding L, Yuan H: Effect of Body Positions on EEG signals in Mal de Débarquement Syndrome. *IEEE EMBC in Honolulu, HI, 2018.*
5. **Chen Y**, Li C, Shou G, Urbano D, Cha YH, Ding L, Yuan H: Assessing rTMS Effects in MdDS: Cross-modal Comparison between Resting State EEG and fMRI Connectivity. *2nd OU-OUHSC Biomedical Engineering Symposium, Oklahoma City, OK, 2018.*
6. **Chen Y**, Li C, Shou G, Urbano D, Cha YH, Ding L, Yuan H: Assessing rTMS Effects in MdDS: Cross-modal Comparison between Resting State EEG and fMRI Connectivity. *Artificial Intelligence / Machine Learning Symposium at The*

*University of Oklahoma, Norman, OK, 2018 (***won 2nd place and finalist at the Student Poster Competition***).*

7. **Chen Y**, Li C, Shou G, Urbano D, Cha YH, Ding L, Yuan H: Assessing rTMS Effects in MdDS: Cross-modal Comparison between Resting State EEG and fMRI Connectivity. *8th International IEEE EMBS Neural Engineering Conference, Shang Hai, China, 2017*.
8. **Chen Y**, Li C, Shou G, Urbano D, Cha YH, Ding L, Yuan H: Assessing rTMS effects in MdDS: cross-modal comparison between resting state EEG and fMRI connectivity. *1st OU-OUHSC Biomedical Engineering Symposium, Oklahoma City, OK, 2017 (***won Finalist at the Student Poster Competition***).*

Oral Presentations

1. **Chen Y**, Li C, Shou G, Gleghorn D, Cha YH, Ding L, Yuan H: Assessing rTMS effects in MdDS: cross-modal comparison between resting state EEG and fMRI connectivity. *Oral presentation for the OCNS Research Retreat, 2019.*
2. **Chen Y**, Li C, Shou G, Urbano D, Cha YH, Ding L, Yuan H: Assessing rTMS effects in MdDS: cross-modal comparison between resting state EEG and fMRI connectivity. *Graduate Student Research & Creativity Day, OU-Norman campus, 2018.*
3. **Chen Y**, Li C, Shou G, Urbano D, Cha YH, Ding L, Yuan H: Assessing rTMS effects in MdDS: cross-modal comparison between resting state EEG and fMRI connectivity. *IEEE EMBC in Jeju island, Korea, 2017* (**awarded Graduate Travel Fellowship from OU Institute for Biomedical Engineering, Science, and Technology**).

8. References

Abreu, R., Leal, A., Figueiredo, P., 2018. EEG-Informed fMRI: A Review of Data Analysis Methods. Frontiers in Human Neuroscience 12.

Alexander, M.L., Alagapan, S., Lugo, C.E., Mellin, J.M., Lustenberger, C., Rubinow, D.R., Fröhlich, F., 2019. Double-blind, randomized pilot clinical trial targeting alpha oscillations with transcranial alternating current stimulation (tACS) for the treatment of major depressive disorder (MDD). Transl Psychiatry 9, 106.

Allen, P.J., Josephs, O., Turner, R., 2000. A method for removing imaging artifact from continuous EEG recorded during functional MRI. Neuroimage 12, 230-239.

Andrews-Hanna, J.R., Reidler, J.S., Sepulcre, J., Poulin, R., Buckner, R.L., 2010. Functional-anatomic fractionation of the brain's default network. Neuron 65, 550-562.

Avissar, M., Powell, F., Ilieva, I., Respino, M., Gunning, F.M., Liston, C., Dubin, M.J., 2017. Functional connectivity of the left DLPFC to striatum predicts treatment response of depression to TMS. Brain Stimul 10, 919-925.

Baeken, C., Duprat, R., Wu, G.-R., De Raedt, R., van Heeringen, K., 2017. Subgenual Anterior Cingulate–Medial Orbitofrontal Functional Connectivity in Medication-Resistant Major Depression: A Neurobiological Marker for Accelerated Intermittent Theta Burst Stimulation Treatment? Biological Psychiatry: Cognitive Neuroscience and Neuroimaging 2, 556-565.

Benjamini, Y., Yekutieli, D., 2001. The control of the false discovery rate in multiple testing under dependency. Ann. Statist. 29, 1165-1188.

Billeci, L., Sicca, F., Maharatna, K., Apicella, F., Narzisi, A., Campatelli, G., Calderoni, S., Pioggia, G., Muratori, F., 2013. On the Application of Quantitative EEG for Characterizing Autistic Brain: A Systematic Review. Front Hum Neurosci 7.

Biswal, B., Yetkin, F.Z., Haughton, V.M., Hyde, J.S., 1995. Functional connectivity in the motor cortex of resting human brain using echo-planar MRI. Magn Reson Med 34, 537-541.

Bouthour, W., Mégevand, P., Donoghue, J., Lüscher, C., Birbaumer, N., Krack, P., 2019. Biomarkers for closed-loop deep brain stimulation in Parkinson disease and beyond. Nat Rev Neurol 15, 343-352.

Braak, H., Del Tredici, K., 2011. The pathological process underlying Alzheimer's disease in individuals under thirty. Acta Neuropathol 121, 171-181.

Brakowski, J., Spinelli, S., Dörig, N., Bosch, O.G., Manoliu, A., Holtforth, M.G., Seifritz, E., 2017. Resting state brain network function in major depression - Depression symptomatology, antidepressant treatment effects, future research. J Psychiatr Res 92, 147-159.

Britz, J., Van De Ville, D., Michel, C.M., 2010. BOLD correlates of EEG topography reveal rapid resting-state network dynamics. Neuroimage 52, 1162-1170.

Broyd, S.J., Demanuele, C., Debener, S., Helps, S.K., James, C.J., Sonuga-Barke, E.J.S., 2009. Default-mode brain dysfunction in mental disorders: A systematic review. Neuroscience & Biobehavioral Reviews 33, 279-296.

Buckner, R.L., Andrews-Hanna, J.R., Schacter, D.L., 2008. The brain's default network: anatomy, function, and relevance to disease. Ann N Y Acad Sci 1124, 1-38.

Cha, Y.-H., 2015. Mal de debarquement syndrome: new insights. Ann N Y Acad Sci 1343, 63-68.

Cha, Y.-H., Gleghorn, D., Doudican, B., 2019. Occipital and Cerebellar Theta Burst Stimulation for Mal De Debarquement Syndrome. Otology & neurotology: official publication of the American Otological Society, American Neurotology Society [and] European Academy of Otology and Neurotology.

Cha, Y.-H., Shou, G., Gleghorn, D., Doudican, B.C., Yuan, H., Ding, L., 2018. Electrophysiological Signatures of Intrinsic Functional Connectivity Related to rTMS Treatment for Mal de Debarquement Syndrome. Brain Topography.

Cha, Y.H., 2009. Mal de debarquement. Semin Neurol 29, 520-527.

Cha, Y.H., Chakrapani, S., Craig, A., Baloh, R.W., 2012. Metabolic and functional connectivity changes in mal de debarquement syndrome. PloS one 7, e49560.

Cha, Y.H., Cui, Y.Y., Baloh, R.W., 2013. Repetitive Transcranial Magnetic Stimulation for Mal de Debarquement Syndrome. Otology & Neurotology 34, 175-179.

Cha, Y.H., Deblieck, C., Wu, A.D., 2016a. Double-Blind Sham-Controlled Crossover Trial of Repetitive Transcranial Magnetic Stimulation for Mal de Debarquement Syndrome. Otol Neurotol 37, 805-812.

Cha, Y.H., Urbano, D., Pariseau, N., 2016b. Randomized Single Blind Sham Controlled Trial of Adjunctive Home-Based tDCS after rTMS for Mal De Debarquement Syndrome: Safety, Efficacy, and Participant Satisfaction Assessment. Brain Stimul 9, 537-544.

Chail, A., Saini, R.K., Bhat, P.S., Srivastava, K., Chauhan, V., 2018. Transcranial magnetic stimulation: A review of its evolution and current applications. Industrial psychiatry journal 27, 172-180.

Chen, Y., Cha, Y.-H., Gleghorn, D., Doudican, B.C., Shou, G., Ding, L., Yuan, H., In preparation. Modulation on Brain Network by Transcranial Alternating Current Stimulation in Mal de Debarquement Syndrome.

Chen, Y., Cha, Y.-H., Gleghorn, D., Doudican, B.C., Shou, G., Ding, L., Yuan, H., Under Review. Brain Network Effects by Continuous Theta Burst Stimulation in Mal de Débarquement Syndrome: Simultaneous EEG and fMRI Study.

Chen, Y., Cha, Y.-H., Li, C., Shou, G., Gleghorn, D., Ding, L., Yuan, H., 2019. Multimodal Imaging of Repetitive Transcranial Magnetic Stimulation Effect on Brain Network: A Combined Electroencephalogram and Functional Magnetic Resonance Imaging Study. Brain Connect 9, 311-321.

Dale, A.M., Sereno, M.I., 1993a. Improved Localizadon of Cortical Activity by Combining EEG and MEG with MRI Cortical Surface Reconstruction: A Linear Approach. J Cogn Neurosci 5, 162-176.

Dale, A.M., Sereno, M.I., 1993b. Improved Localization of Cortical Activity by Combining Eeg and Meg with Mri Cortical Surface Reconstruction - a Linear-Approach. Journal of Cognitive Neuroscience 5, 162-176.

Das, S.R., Pluta, J., Mancuso, L., Kliot, D., Orozco, S., Dickerson, B.C., Yushkevich, P.A., Wolk, D.A., 2013. Increased functional connectivity within medial temporal lobe in mild cognitive impairment. Hippocampus 23, 1-6.

DeGiorgio, M., Syring, J., Eckert, A.J., Liston, A., Cronn, R., Neale, D.B., Rosenberg, N.A., 2014. An empirical evaluation of two-stage species tree inference strategies using a multilocus dataset from North American pines. BMC Evol Biol 14, 67.

Dell'Osso, B., Mundo, E., D'Urso, N., Pozzoli, S., Buoli, M., Ciabatti, M., Rosanova, M., Massimini, M., Bellina, V., Mariotti, M., Altamura, A.C., 2009. Augmentative repetitive navigated transcranial magnetic stimulation (rTMS) in drug-resistant bipolar depression. Bipolar Disord 11, 76-81.

Dhami, P., Knyahnytska, Y., Atluri, S., Lee, J., Courtney, D.B., Croarkin, P.E., Blumberger, D.M., Daskalakis, Z.J., Farzan, F., 2019. Feasibility and clinical effects of theta burst stimulation in youth with major depressive disorders: An open-label trial. J Affect Disord 258, 66-73.

Di Lorenzo, F., Bonnì, S., Picazio, S., Motta, C., Caltagirone, C., Martorana, A., Koch, G., 2020. Effects of Cerebellar Theta Burst Stimulation on Contralateral Motor Cortex Excitability in Patients with Alzheimer's Disease. Brain Topogr 33, 613-617.

Ding, L., Shou, G.F., Yuan, H., Urbano, D., Cha, Y.H., 2014. Lasting Modulation Effects of rTMS on Neural Activity and Connectivity as Revealed by Resting-State EEG. Ieee Transactions on Biomedical Engineering 61, 2070-2080.

Drysdale, A.T., Grosenick, L., Downar, J., Dunlop, K., Mansouri, F., Meng, Y., Fetcho, R.N., Zebley, B., Oathes, D.J., Etkin, A., Schatzberg, A.F., Sudheimer, K., Keller, J., Mayberg, H.S., Gunning, F.M., Alexopoulos, G.S., Fox, M.D., Pascual-Leone, A., Voss, H.U., Casey, B.J., Dubin, M.J., Liston, C., 2017. Resting-state connectivity biomarkers define neurophysiological subtypes of depression. Nat Med 23, 28-38.

Eldaief, M.C., Halko, M.A., Buckner, R.L., Pascual-Leone, A., 2011. Transcranial magnetic stimulation modulates the brain's intrinsic activity in a frequency-dependent manner. Proceedings of the National Academy of Sciences 108, 21229-21234.

Feurra, M., Paulus, W., Walsh, V., Kanai, R., 2011. Frequency specific modulation of human somatosensory cortex. Frontiers in Psychology 2, 13-13.

Fischl, B., Sereno, M.I., Tootell, R.B.H., Dale, A.M., 1999. High-resolution intersubject averaging and a coordinate system for the cortical surface. Hum Brain Mapp 8, 272-284.

Fitzgerald, P.B., Hoy, K., McQueen, S., Maller, J.J., Herring, S., Segrave, R., Bailey, M., Been, G., Kulkarni, J., Daskalakis, Z.J., 2009. A randomized trial of rTMS targeted with MRI based neuro-navigation in treatment-resistant depression. Neuropsychopharmacology 34, 1255-1262.

Fox, M.D., Buckner, R.L., White, M.P., Greicius, M.D., Pascual-Leone, A., 2012a. Efficacy of transcranial magnetic stimulation targets for depression is related to intrinsic functional connectivity with the subgenual cingulate. Biol Psychiatry 72, 595-603.

Fox, M.D., Halko, M.A., Eldaief, M.C., Pascual-Leone, A., 2012b. Measuring and manipulating brain connectivity with resting state functional connectivity magnetic resonance imaging (fcMRI) and transcranial magnetic stimulation (TMS). Neuroimage 62, 2232-2243.

Fox, M.D., Raichle, M.E., 2007. Spontaneous fluctuations in brain activity observed with functional magnetic resonance imaging. Nat Rev Neurosci 8, 700-711.

Friston, K.J., Fletcher, P., Josephs, O., Holmes, A., Rugg, M.D., Turner, R., 1998. Event-related fMRI: characterizing differential responses. Neuroimage 7, 30-40.

Glover, G.H., 2011. Overview of functional magnetic resonance imaging. Neurosurgery clinics of North America 22, 133-vii.

Goldman, R.I., Stern, J.M., Engel, J., Jr., Cohen, M.S., 2002. Simultaneous EEG and fMRI of the alpha rhythm. Neuroreport 13, 2487-2492.

Grabner, R.H., Krenn, J., Fink, A., Arendasy, M., Benedek, M., 2018. Effects of alpha and gamma transcranial alternating current stimulation (tACS) on verbal creativity and intelligence test performance. Neuropsychologia 118, 91-98.

Grech, R., Cassar, T., Muscat, J., Camilleri, K.P., Fabri, S.G., Zervakis, M., Xanthopoulos, P., Sakkalis, V., Vanrumste, B., 2008. Review on solving the inverse problem in EEG source analysis. Journal of NeuroEngineering and Rehabilitation 5, 25.

Gregoriou, G.G., Gotts, S.J., Zhou, H., Desimone, R., 2009. High-frequency, long-range coupling between prefrontal and visual cortex during attention. science 324, 1207-1210.

Greicius, M., 2008. Resting-state functional connectivity in neuropsychiatric disorders. Curr Opin Neurol 21, 424-430.

Greicius, M.D., Krasnow, B., Reiss, A.L., Menon, V., 2003. Functional connectivity in the resting brain: a network analysis of the default mode hypothesis. Proc Natl Acad Sci U S A 100, 253-258.

Gudayol-Ferré, E., Peró-Cebollero, M., González-Garrido, A.A., Guàrdia-Olmos, J., 2015. Changes in brain connectivity related to the treatment of depression measured through fMRI: a systematic review. Front Hum Neurosci 9.

Hain, T.C., Hanna, P.A., Rheinberger, M.A., 1999. Mal de debarquement. Archives of Otolaryngology–Head & Neck Surgery 125, 615-620.

Hämäläinen, M.S., Ilmoniemi, R.J., 1994. Interpreting magnetic fields of the brain: minimum norm estimates. Medical & Biological Engineering & Computing 32, 35-42.

Helfrich, R.F., Knepper, H., Nolte, G., Strüber, D., Rach, S., Herrmann, C.S., Schneider, T.R., Engel, A.K., 2014a. Selective modulation of interhemispheric functional connectivity by HD-tACS shapes perception. PLoS Biol 12, e1002031.

Helfrich, Randolph F., Schneider, Till R., Rach, S., Trautmann-Lengsfeld, Sina A., Engel, Andreas K., Herrmann, Christoph S., 2014b. Entrainment of Brain Oscillations by Transcranial Alternating Current Stimulation. Current Biology 24, 333-339.

Herbsman, T., Avery, D., Ramsey, D., Holtzheimer, P., Wadjik, C., Hardaway, F., Haynor, D., George, M.S., Nahas, Z., 2009. More lateral and anterior prefrontal coil location is associated with better repetitive transcranial magnetic stimulation antidepressant response. Biol Psychiatry 66, 509-515.

Horn, A., Fox, M.D., 2020. Opportunities of connectomic neuromodulation. Neuroimage 221, 117180.

Huang, Y.-Z., Edwards, M.J., Rounis, E., Bhatia, K.P., Rothwell, J.C., 2005. Theta burst stimulation of the human motor cortex. Neuron 45, 201-206.

Hutchison, R.M., Womelsdorf, T., Allen, E.A., Bandettini, P.A., Calhoun, V.D., Corbetta, M., Della Penna, S., Duyn, J.H., Glover, G.H., Gonzalez-Castillo, J., Handwerker, D.A., Keilholz, S., Kiviniemi, V., Leopold, D.A., de Pasquale, F., Sporns, O., Walter, M., Chang, C., 2013. Dynamic functional connectivity: promise, issues, and interpretations. Neuroimage 80, 360-378.

Ilmoniemi, R.J., Kičić, D., 2009. Methodology for Combined TMS and EEG. Brain topography 22, 233.

Insausti, R., Juottonen, K., Soininen, H., Insausti, A.M., Partanen, K., Vainio, P., Laakso, M.P., Pitkänen, A., 1998. MR volumetric analysis of the human entorhinal, perirhinal, and temporopolar cortices. AJNR Am J Neuroradiol 19, 659-671.

Jones, D.T., Machulda, M.M., Vemuri, P., McDade, E.M., Zeng, G., Senjem, M.L., Gunter, J.L., Przybelski, S.A., Avula, R.T., Knopman, D.S., Boeve, B.F., Petersen, R.C.,

Jack, C.R., Jr., 2011. Age-related changes in the default mode network are more advanced in Alzheimer disease. Neurology 77, 1524-1531.

Kahn, I., Andrews-Hanna, J.R., Vincent, J.L., Snyder, A.Z., Buckner, R.L., 2008. Distinct cortical anatomy linked to subregions of the medial temporal lobe revealed by intrinsic functional connectivity. J Neurophysiol 100, 129-139.

Kaiser, R.H., Andrews-Hanna, J.R., Wager, T.D., Pizzagalli, D.A., 2015. Large-Scale Network Dysfunction in Major Depressive Disorder: A Meta-analysis of Resting-State Functional Connectivity. JAMA Psychiatry 72, 603-611.

Kar, S.K., 2019. Predictors of Response to Repetitive Transcranial Magnetic Stimulation in Depression: A Review of Recent Updates. Clin Psychopharmacol Neurosci 17, 25-33.

Keilholz, S.D., Silva, A.C., Raman, M., Merkle, H., Koretsky, A.P., 2004. Functional MRI of the rodent somatosensory pathway using multislice echo planar imaging. Magnetic Resonance in Medicine: An Official Journal of the International Society for Magnetic Resonance in Medicine 52, 89-99.

Kokkinos, V., Sisterson, N.D., Wozny, T.A., Richardson, R.M., 2019. Association of Closed-Loop Brain Stimulation Neurophysiological Features With Seizure Control Among Patients With Focal Epilepsy. JAMA Neurol 76, 800-808.

Kreuzer, M., 2017. EEG Based Monitoring of General Anesthesia: Taking the Next Steps. Frontiers in Computational Neuroscience 11.

Laufs, H., Krakow, K., Sterzer, P., Eger, E., Beyerle, A., Salek-Haddadi, A., Kleinschmidt, A., 2003. Electroencephalographic signatures of attentional and cognitive default modes in spontaneous brain activity fluctuations at rest. Proc Natl Acad Sci U S A 100, 11053-11058.

Lehmann, D., Ozaki, H., Pal, I., 1987. EEG alpha map series: brain micro-states by space-oriented adaptive segmentation. Electroencephalogr Clin Neurophysiol 67, 271-288.

Lei, X., Wu, T., Valdes-Sosa, P., 2015. Incorporating priors for EEG source imaging and connectivity analysis. Front Neurosci 9, 284.

Li, B., Liu, L., Friston, K.J., Shen, H., Wang, L., Zeng, L.-L., Hu, D., 2013. A Treatment-Resistant Default Mode Subnetwork in Major Depression. Biological psychiatry 74, 48-54.

Li, C.T., Chen, M.H., Juan, C.H., Liu, R.S., Lin, W.C., Bai, Y.M., Su, T.P., 2018. Effects of prefrontal theta-burst stimulation on brain function in treatment-resistant depression: A randomized sham-controlled neuroimaging study. Brain Stimul 11, 1054-1062.

Li, X., Guo, N., Li, Q., 2019. Functional Neuroimaging in the New Era of Big Data. Genomics, Proteomics & Bioinformatics 17, 393-401.

Lindquist, M.A., Meng Loh, J., Atlas, L.Y., Wager, T.D., 2009. Modeling the hemodynamic response function in fMRI: Efficiency, bias and mis-modeling. Neuroimage 45, S187-S198.

Liston, C., Chen, A.C., Zebley, B.D., Drysdale, A.T., Gordon, R., Leuchter, B., Voss, H.U., Casey, B.J., Etkin, A., Dubin, M.J., 2014. Default mode network mechanisms of transcranial magnetic stimulation in depression. Biol Psychiatry 76, 517-526.

Logothetis, N.K., 2008. What we can do and what we cannot do with fMRI. Nature 453, 869-878.

Logothetis, N.K., Pauls, J., Augath, M., Trinath, T., Oeltermann, A., 2001. Neurophysiological investigation of the basis of the fMRI signal. Nature 412, 150.

Macdonell, R.A.L., Donnan, G.A., Bladin, P.F., Berkovic, S.F., Wriedt, C.H.R., 1988. The Electroencephalogram and Acute Ischemic Stroke: Distinguishing Cortical From Lacunar Infarction. Archives of Neurology 45, 520-524.

Meier, J., Nolte, G., Schneider, T.R., Engel, A.K., Leicht, G., Mulert, C., 2019. Intrinsic 40Hz-phase asymmetries predict tACS effects during conscious auditory perception. PLoS One 14, e0213996.

Menon, V., 2015. Large-Scale Functional Brain Organization. Academic Press: Elsevier.

Miller, D.R., Hayes, S.M., Hayes, J.P., Spielberg, J.M., Lafleche, G., Verfaellie, M., 2017. Default Mode Network Subsystems are Differentially Disrupted in Posttraumatic Stress Disorder. Biol Psychiatry Cogn Neurosci Neuroimaging 2, 363-371.

Mioni, G., Shelp, A., Stanfield-Wiswell, C.T., Gladhill, K.A., Bader, F., Wiener, M., 2020. Modulation of Individual Alpha Frequency with tACS shifts Time Perception. Cerebral Cortex Communications 1.

Mulert, C., Jager, L., Schmitt, R., Bussfeld, P., Pogarell, O., Moller, H.J., Juckel, G., Hegerl, U., 2004. Integration of fMRI and simultaneous EEG: towards a comprehensive understanding of localization and time-course of brain activity in target detection. Neuroimage 22, 83-94.

Neuling, T., Rach, S., Herrmann, C.S., 2013. Orchestrating neuronal networks: sustained after-effects of transcranial alternating current stimulation depend upon brain states. Front Hum Neurosci 7, 161.

Noachtar, S., Rémi, J., 2009. The role of EEG in epilepsy: A critical review. Epilepsy & Behavior 15, 22-33.

Nunez, P.L., Srinivasan, R., 2006. Electric fields of the brain: the neurophysics of EEG. Oxford University Press, USA.

O'Reardon, J.P., Solvason, H.B., Janicak, P.G., Sampson, S., Isenberg, K.E., Nahas, Z., McDonald, W.M., Avery, D., Fitzgerald, P.B., Loo, C., Demitrack, M.A., George, M.S., Sackeim, H.A., 2007. Efficacy and safety of transcranial magnetic stimulation in the acute treatment of major depression: a multisite randomized controlled trial. Biol Psychiatry 62, 1208-1216.

Oliviero, A., Strens, L.H.A., Di Lazzaro, V., Tonali, P.A., Brown, P., 2003. Persistent effects of high frequency repetitive TMS on the coupling between motor areas in the human. Exp Brain Res 149, 107-113.

Paulus, W., 2011. Transcranial electrical stimulation (tES - tDCS; tRNS, tACS) methods. Neuropsychol Rehabil 21, 602-617.

Pelled, G., Chuang, K.-H., Dodd, S.J., Koretsky, A.P., 2007. Functional MRI detection of bilateral cortical reorganization in the rodent brain following peripheral nerve deafferentation. Neuroimage 37, 262-273.

Penny, W.D., Friston, K.J., Ashburner, J.T., Kiebel, S.J., Nichols, T.E., 2011. Statistical parametric mapping: the analysis of functional brain images. Elsevier.

Perry, A., Bentin, S., 2009. Mirror activity in the human brain while observing hand movements: a comparison between EEG desynchronization in the mu-range and previous fMRI results. Brain Res 1282, 126-132.

Philip, N.S., Barredo, J., van ’t Wout-Frank, M., Tyrka, A.R., Price, L.H., Carpenter, L.L., 2018. Network Mechanisms of Clinical Response to Transcranial Magnetic

Stimulation in Posttraumatic Stress Disorder and Major Depressive Disorder. Biological psychiatry 83, 263-272.

Polanía, R., Nitsche, M.A., Korman, C., Batsikadze, G., Paulus, W., 2012. The importance of timing in segregated theta phase-coupling for cognitive performance. Current Biology 22, 1314-1318.

Raichle, M.E., 2015. The brain's default mode network. Annu Rev Neurosci 38, 433-447.

Raichle, M.E., MacLeod, A.M., Snyder, A.Z., Powers, W.J., Gusnard, D.A., Shulman, G.L., 2001a. A default mode of brain function. Proceedings of the National Academy of Sciences 98, 676-682.

Raichle, M.E., MacLeod, A.M., Snyder, A.Z., Powers, W.J., Gusnard, D.A., Shulman, G.L., 2001b. A default mode of brain function. Proc Natl Acad Sci U S A 98, 676-682.

Ritter, P., Villringer, A., 2006. Simultaneous EEG–fMRI. Neuroscience & Biobehavioral Reviews 30, 823-838.

Ruhnau, P., Neuling, T., Fuscá, M., Herrmann, C.S., Demarchi, G., Weisz, N., 2016. Eyes wide shut: transcranial alternating current stimulation drives alpha rhythm in a state dependent manner. Sci Rep 6, 1-6.

Rusjan, P.M., Barr, M.S., Farzan, F., Arenovich, T., Maller, J.J., Fitzgerald, P.B., Daskalakis, Z.J., 2010. Optimal transcranial magnetic stimulation coil placement for targeting the dorsolateral prefrontal cortex using novel magnetic resonance image-guided neuronavigation. Hum Brain Mapp 31, 1643-1652.

Sadaghiani, S., Scheeringa, R., Lehongre, K., Morillon, B., Giraud, A.L., Kleinschmidt, A., 2010. Intrinsic connectivity networks, alpha oscillations, and tonic alertness: a

simultaneous electroencephalography/functional magnetic resonance imaging study. J Neurosci 30, 10243-10250.

Scangos, K.W., Makhoul, G.S., Sugrue, L.P., Chang, E.F., Krystal, A.D., 2021. State-dependent responses to intracranial brain stimulation in a patient with depression. Nat Med 27, 229-231.

Scheeringa, R., Bastiaansen, M.C., Petersson, K.M., Oostenveld, R., Norris, D.G., Hagoort, P., 2008. Frontal theta EEG activity correlates negatively with the default mode network in resting state. International journal of psychophysiology 67, 242-251.

Scheeringa, R., Fries, P., Petersson, K.-M., Oostenveld, R., Grothe, I., Norris, D.G., Hagoort, P., Bastiaansen, M.C., 2011. Neuronal dynamics underlying high-and low-frequency EEG oscillations contribute independently to the human BOLD signal. Neuron 69, 572-583.

Schutter, D.J.L.G., Wischnewski, M., 2016. A meta-analytic study of exogenous oscillatory electric potentials in neuroenhancement. Neuropsychologia 86, 110-118.

Schwab, S., Koenig, T., Morishima, Y., Dierks, T., Federspiel, A., Jann, K., 2015. Discovering frequency sensitive thalamic nuclei from EEG microstate informed resting state fMRI. Neuroimage 118, 368-375.

Schwippel, T., Schroeder, P.A., Fallgatter, A.J., Plewnia, C., 2019. Clinical review: The therapeutic use of theta-burst stimulation in mental disorders and tinnitus. Prog Neuropsychopharmacol Biol Psychiatry 92, 285-300.

Shirer, W.R., Ryali, S., Rykhlevskaia, E., Menon, V., Greicius, M.D., 2012. Decoding subject-driven cognitive states with whole-brain connectivity patterns. Cerebral cortex (New York, N.Y. : 1991) 22, 158-165.

Siddiqi, S.H., Taylor, S.F., Cooke, D., Pascual-Leone, A., George, M.S., Fox, M.D., 2020. Distinct Symptom-Specific Treatment Targets for Circuit-Based Neuromodulation. Am J Psychiatry 177, 435-446.

Sridharan, D., Levitin, D.J., Menon, V., 2008. A critical role for the right fronto-insular cortex in switching between central-executive and default-mode networks. Proc Natl Acad Sci U S A 105, 12569-12574.

Strüber, D., Rach, S., Trautmann-Lengsfeld, S.A., Engel, A.K., Herrmann, C.S., 2014. Antiphasic 40 Hz Oscillatory Current Stimulation Affects Bistable Motion Perception. Brain Topography 27, 158-171.

Thut, G., Veniero, D., Romei, V., Miniussi, C., Schyns, P., Gross, J., 2011. Rhythmic TMS causes local entrainment of natural oscillatory signatures. Current Biology 21, 1176-1185.

Tisserand, D.J., Visser, P.J., van Boxtel, M.P., Jolles, J., 2000. The relation between global and limbic brain volumes on MRI and cognitive performance in healthy individuals across the age range. Neurobiol Aging 21, 569-576.

Tozzi, L., Zhang, X., Chesnut, M., Holt-Gosselin, B., Ramirez, C.A., Williams, L.M., 2021. Reduced functional connectivity of default mode network subsystems in depression: Meta-analytic evidence and relationship with trait rumination. Neuroimage Clin 30, 102570.

Tseng, P., Chang, Y.-T., Chang, C.-F., Liang, W.-K., Juan, C.-H., 2016. The critical role of phase difference in gamma oscillation within the temporoparietal network for binding visual working memory. Scientific reports 6, 32138.

van den Heuvel, M., Mandl, R., Luigjes, J., Hulshoff Pol, H., 2008. Microstructural organization of the cingulum tract and the level of default mode functional connectivity. J Neurosci 28, 10844-10851.

Vidaurre, D., Smith, S.M., Woolrich, M.W., 2017. Brain network dynamics are hierarchically organized in time. Proceedings of the National Academy of Sciences 114, 12827-12832.

Vossen, A., Gross, J., Thut, G., 2015. Alpha Power Increase After Transcranial Alternating Current Stimulation at Alpha Frequency (α-tACS) Reflects Plastic Changes Rather Than Entrainment. Brain Stimul 8, 499-508.

Ward, A.M., Schultz, A.P., Huijbers, W., Van Dijk, K.R., Hedden, T., Sperling, R.A., 2014. The parahippocampal gyrus links the default-mode cortical network with the medial temporal lobe memory system. Hum Brain Mapp 35, 1061-1073.

Weigand, A., Horn, A., Caballero, R., Cooke, D., Stern, A.P., Taylor, S.F., Press, D., Pascual-Leone, A., Fox, M.D., 2018. Prospective Validation That Subgenual Connectivity Predicts Antidepressant Efficacy of Transcranial Magnetic Stimulation Sites. Biol Psychiatry 84, 28-37.

Whitton, A.E., Deccy, S., Ironside, M.L., Kumar, P., Beltzer, M., Pizzagalli, D.A., 2018. Electroencephalography Source Functional Connectivity Reveals Abnormal High-Frequency Communication Among Large-Scale Functional Networks in Depression. Biological Psychiatry: Cognitive Neuroscience and Neuroimaging 3, 50-58.

Widge, A.S., Ellard, K.K., Paulk, A.C., Basu, I., Yousefi, A., Zorowitz, S., Gilmour, A., Afzal, A., Deckersbach, T., Cash, S.S., Kramer, M.A., Eden, U.T., Dougherty, D.D., Eskandar, E.N., 2017. Treating refractory mental illness with closed-loop brain

stimulation: Progress towards a patient-specific transdiagnostic approach. Exp Neurol 287, 461-472.

Yeo, B.T., Krienen, F.M., Sepulcre, J., Sabuncu, M.R., Lashkari, D., Hollinshead, M., Roffman, J.L., Smoller, J.W., Zollei, L., Polimeni, J.R., Fischl, B., Liu, H., Buckner, R.L., 2011. The organization of the human cerebral cortex estimated by intrinsic functional connectivity. J Neurophysiol 106, 1125-1165.

Young, K.D., Zotev, V., Phillips, R., Misaki, M., Yuan, H., Drevets, W.C., Bodurka, J., 2014. Real-time FMRI neurofeedback training of amygdala activity in patients with major depressive disorder. PLoS One 9, e88785.

Yousry, T.A., Schmid, U.D., Alkadhi, H., Schmidt, D., Peraud, A., Buettner, A., Winkler, P., 1997. Localization of the motor hand area to a knob on the precentral gyrus. A new landmark. Brain 120 (Pt 1), 141-157.

Yu, X., Glen, D., Wang, S., Dodd, S., Hirano, Y., Saad, Z., Reynolds, R., Silva, A.C., Koretsky, A.P., 2012. Direct imaging of macrovascular and microvascular contributions to BOLD fMRI in layers IV–V of the rat whisker–barrel cortex. Neuroimage 59, 1451-1460.

Yuan, H., Ding, L., Zhu, M., Zotev, V., Phillips, R., Bodurka, J., 2016. Reconstructing Large-Scale Brain Resting-State Networks from High-Resolution EEG: Spatial and Temporal Comparisons with fMRI. Brain Connect 6, 122-135.

Yuan, H., Phillips, R., Wong, C.K., Zotev, V., Misaki, M., Wurfel, B., Krueger, F., Feldner, M., Bodurka, J., 2018. Tracking resting state connectivity dynamics in veterans with PTSD. Neuroimage Clin 19, 260-270.

Yuan, H., Shou, G., Gleghorn, D., Ding, L., Cha, Y.H., 2017. Resting State Functional Connectivity Signature of Treatment Effects of Repetitive Transcranial Magnetic Stimulation in Mal de Debarquement Syndrome. Brain Connect 7, 617-626.

Yuan, H., Zotev, V., Phillips, R., Drevets, W.C., Bodurka, J., 2012. Spatiotemporal dynamics of the brain at rest--exploring EEG microstates as electrophysiological signatures of BOLD resting state networks. Neuroimage 60, 2062-2072.

Zaehle, T., Rach, S., Herrmann, C.S., 2010. Transcranial Alternating Current Stimulation Enhances Individual Alpha Activity in Human EEG. PLoS One 5, e13766.

Zeidman, L.A., Stone, J., Kondziella, D., 2014. New revelations about Hans Berger, father of the electroencephalogram (EEG), and his ties to the Third Reich. J Child Neurol 29, 1002-1010.

Zhang, D., Raichle, M.E., 2010. Disease and the brain's dark energy. Nat Rev Neurol 6, 15-28.

Zhang, Y., van Drongelen, W., He, B., 2006. Estimation of in vivo brain-to-skull conductivity ratio in humans. Applied Physics Letters 89, 223903-2239033.

Zhao, D., Li, Y., Liu, T., Voon, V., Yuan, T.F., 2020. Twice-Daily Theta Burst Stimulation of the Dorsolateral Prefrontal Cortex Reduces Methamphetamine Craving: A Pilot Study. Front Neurosci 14, 208.